

Strongly-Interacting Fermi Gases with Population Imbalance

by

Mark Ku

B.Sc., The University of British Columbia, 2007

A THESIS SUBMITTED IN PARTIAL FULFILLMENT OF
THE REQUIREMENTS FOR THE DEGREE OF

MASTER OF SCIENCE

in

The Faculty of Graduate Studies

(Physics)

THE UNIVERSITY OF BRITISH COLUMBIA

(Vancouver)

August 2009

© Mark Ku 2009

Abstract

This thesis presents a theoretical study of strongly-interacting Fermi systems with population imbalance, which is motivated by some differences in cold atoms experiments. We calculate the energy of a single fermion interacting resonantly with a Fermi sea of different species fermions in anisotropic traps, and show that finite particle numbers and the trap geometry impact the phase structure and the critical polarization, the limit of resonance superfluidity in traps. Our findings contribute to understanding some experimental discrepancies as finite-size and confinement effects. For an imbalanced gas in the uniform system, we calculate the energy of adding an impurity, and construct the equation of state of the partially-polarized normal Fermi liquid. Finally, we study the properties of a spin-down polaron in a trapped gas containing arbitrary numbers of spin-up and spin-down fermions, and derive a self-consistent equation for the polaron energy.

Table of Contents

Abstract	ii
Table of Contents	iii
List of Tables	vi
List of Figures	vii
Acknowledgements	ix
Dedication	1
1 Introduction	2
1.1 Strongly-Interacting Fermi Gases	3
1.2 Condensates of Fermionic Atoms	3
1.3 Asymmetric Fermi Gases	6
1.4 Outline	8
2 Interactions in Cold Atoms	9
2.1 Two-Body Scattering	9
2.1.1 Scattering at Low Energies	10
2.1.2 The T -Matrix	12
2.2 Interactions in Cold Fermi Gases	14
2.3 Regularized Contact Interaction	15
2.4 Strongly-Interacting Regime in Cold Fermi Gases	18
2.4.1 Feshbach Resonances	18
2.4.2 Universal Regime	19
3 $N + 1$ Body Problem in the Uniform System	22
3.1 Symmetric Fermi Gases	23
3.1.1 Molecular BEC Regime	24
3.1.2 Weakly-Attractive BCS Regime	24
3.1.3 Crossover Regime at Unitarity	25

Table of Contents

3.2	Unitary Asymmetric Fermi Gases: Uniform System	26
3.2.1	Breakdown of the Fully-Paired Superfluid	26
3.2.2	Phases in Asymmetric Fermi Gases	27
3.3	$N + 1$ Body Problem in the Uniform System	29
3.3.1	Variational Calculation of the $N + 1$ Body Energy	29
3.3.2	BEC and BCS Limit of the Chevy Equation	32
3.3.3	$N + 1$ Body Energy at $\mathbf{p} = \mathbf{0}$	33
3.3.4	On the Existence of Partially-Polarized Phases	35
3.3.5	Effective Mass of the Fermi Polaron	35
3.4	Towards General Asymmetry: The $N + M$ Body System as a Landau Fermi Liquid	35
3.5	Application to Trapped Fermi Gases	38
3.5.1	Local Density Approximation	38
3.5.2	Phase Separation and Density Profile in Trapped Fermi Gases	38
3.5.3	Trapped Fermi Gases Containing Large Particle Num- bers	41
3.6	Experiments with Spin-Polarized Fermi Gases	41
4	$N + 1$ Body Problem in Trapped Fermi Gases	44
4.1	Evaluation of $N + 1$ Body Energy in Harmonic-Oscillator Traps	44
4.1.1	Interaction Matrix Elements in a Harmonic-Oscillator Basis	45
4.1.2	Variational Solution to the $N + 1$ Body Ground State Energy in Harmonic-Oscillator Traps	49
4.1.3	Evaluation of the Unrestricted Sum $M_u(\alpha, E + \varepsilon_{\mathbf{h}})_{\mathbf{S},\mathbf{L}}$	55
4.2	Polaron Energy in Traps	57
4.2.1	Generalized Energy Scaling in Traps	58
4.2.2	Results for the Polaron Energy	59
4.3	Phase Structure in Trapped Fermi Gases	62
4.4	Outlook: Towards the $N + M$ Body System	65
5	$N + M$ Body Problem	66
5.1	$N + M$ Body Problem in the Uniform System	66
5.1.1	Derivation of the $N + M$ Body Energy	66
5.1.2	Analytic Expression of the $N + M$ Body Energy in the Uniform System	72
5.1.3	Equation of State of the Normal Fermi Liquid	79
5.1.4	Results and Comparison	80

Table of Contents

5.1.5	Phase Structure of Trapped Fermi Gases with Large Particle Numbers	82
5.2	$N + M$ Body Problem in Traps	84
5.3	Outlook	92
6	Summary and Outlook	93
	Bibliography	95
 Appendices		
A	1 + 1 Body Problem in Harmonic-Oscillator Traps	101

List of Tables

- 2.1 Experimental and theoretical values of the universal parameter for the superfluid energy ξ 21
- 4.1 Polaron energy $\eta(1, N)$ for the five lowest closed-shell configurations, in comparison with the MC results of Ref. [5] 60
- 4.2 Fit results to the combined (odd and even n_F) results for $\eta(\alpha, N)$ using the Ansatz $a(\alpha)(1 + b(\alpha)N^{-c(\alpha)})$ 62
- 4.3 Critical polarization P_c and critical concentration x_c as a function of aspect ratio α and total particle numbers N_{tot} . . 65

List of Figures

1.1	Non-interacting systems of ultracold bosonic and fermionic atoms in a confining harmonic potential	4
1.2	The BEC-BCS Crossover	5
2.1	General scattering geometry	10
2.2	Momentum cutoff schemes	15
2.3	Complex contour used to evaluate Eq. (2.28)	16
2.4	Experimental realization of a Feshbach resonance	19
3.1	Proton and neutron densities in ^{100}Sn and ^{100}Zn	23
3.2	Phase diagram of unitary asymmetric Fermi gases	28
3.3	Graphical representation of the components of the trial wavefunction Eq. (3.11)	30
3.4	RF spectroscopy on polarons	34
3.5	Equation of state of the asymmetric Fermi gas based on the MC results of Ref. [38]	36
3.6	Equation of state of the asymmetric Fermi gas based on the MC results of Ref. [43]	37
3.7	Density profiles of spin-polarized Fermi gases obtained in the MIT and Rice experiments	42
4.1	Graphical representation of the components of the trial wavefunction Eq. (4.22) in traps	49
4.2	Examples of closed-shell configurations	58
4.3	Local Fermi energy	59
4.4	Polaron energy $\eta(1, N)$ for an isotropic trap	61
4.5	Polaron energy $\eta(\alpha, N)$ as a function of N for various aspect ratios α	62
4.6	Critical polarization P_c and critical concentration x_c as a function of aspect ratio α for $N_{\text{tot}} = 10^4$ and $N_{\text{tot}} = 10^5$. . .	64

List of Figures

5.1	Graphical representation of the components of the trial wave-function Eq. (5.1)	67
5.2	Geometries for the angular integral Eq. (5.27)	73
5.3	Graphical illustration of the angular integral $I_\theta(\gamma, k, v)$	74
5.4	The integration region of the angular integral $I_\theta(\gamma, v, k)$ for $v < 1 - \gamma$	75
5.5	The integration region of the angular integral $I_\theta(\gamma, v, k)$ for $1 - \gamma < v < 1 + \gamma$	76
5.6	$N + M$ body energy $\eta(x)$ for the uniform system.	81
5.7	Equation of state for the polarized normal Fermi liquid in the uniform system	82
5.8	Critical concentration $x_c(\xi)$ as a function of ξ for trapped Fermi gases with large particle numbers	83
5.9	Critical polarization $P_c(\xi)$ as a function of ξ for trapped Fermi gases with large particle numbers	83
5.10	Graphical representation of the components of the trial wave-function Eq. (5.45) in traps	84

Acknowledgements

This thesis documents the research I have undertaken during the two years of my M.Sc. program. In a way, the completion of this thesis represents a closure of these two years, a period of time that I will never forget. I have been tremendously blessed to encounter many people who have built into my life, and a few paragraphs cannot do justice to give all of them the gratitude they deserve. I count everyone I have come across in the last two years to be a blessing from God, and to each one of them is a sincere thank you that comes from the depth of my heart.

First of all, I would like to thank Achim Schwenk, my supervisor. He has trained me in the way of a physicist. His emphasis on the clarity of communication, insistence on being sure of what I say and what I write, and repeated reminders to think about the physics will always accompany me in my future endeavor. I am deeply indebted to this wonderful mentor.

I would also like to thank Jens Braun, a post doc at TRIUMF, with whom I had the pleasure to work. I have benefited tremendously from working with him. Jens has helped me with almost anything and everything, including programming, mathematical tricks, and LATEX techniques. His presence has made the project many times easier and enriching. To this co-mentor are my many thanks.

There are many people around the TRIUMF Theory Group corridor who have been of great help in the past, and I would like to thank them as well. Among them are Ian Allison, who has provided countless computer assistance before his departure from TRIUMF. In Jens' absence, Sonia Bacca has taught me many useful things, including poster making and using the Grace program. These people have made my time in the Theory Group much more enjoyable, and I am really thankful for their presence.

This thesis has led to one paper published in the Phys. Rev. Lett. [34], and one paper in preparation. I would like to thank Michael McNeil Forbes, Richard Furnstahl, Randall Hulet, Christopher Pethick, Thomas Schaefer, and Martin Zwierlein for useful discussions. I would also like to acknowledge the support of the Natural Sciences and Engineering Research Council of Canada and the University of British Columbia, which have been the sources

Acknowledgements

of my funding during my M.Sc. study.

I cannot express my thanks enough in words to my brothers and sisters from the UBC Campus for Christ community. Through them, God has built up my faith tremendously, and has taught me the way of a man, a leader, and a Christian. Their passion for God is infectious, and I count myself very blessed to know this group of brothers and sisters. I am extremely thankful to them, and I pray that they will continue to be a community of faithful believers and a beacon of light at the UBC campus.

Lastly, I would like to thank my family. I cannot express my gratitude enough to my parents, Mark Sr. and Marie, who have taught me valuable wisdom in life, who have provided me a stable environment during the course of my growing up and education, and who have given me unconditional support in my pursuit of a career in physics. I must also thank my brothers, Martin and Matthew, who have given me tremendous inspiration, who have accompanied me through both fun and tough times, and who have been my best friends in the course of my life. To them are my many thanks and prayers.

Dedication

*To Mark Sr., Marie, Martin, and Matthew, my family,
Esther, the girl I love,
and my Lord and Savior, Jesus Christ, the way, the truth, and the life,
for whom I live.*

Chapter 1

Introduction

Over the past ten years, there has been an impressive progress in the study of ultracold atoms. The ability to achieve low temperatures is necessary to bring dilute atomic gases into quantum degeneracy, where the matter wavelength $\lambda = \hbar/p$ is comparable to the typical separation distance. The first realization of Bose-Einstein condensates in 1995 for rubidium [1], lithium [8], and sodium [23] demonstrated that atomic gases have a strong potential to study quantum phenomena on a macroscopic scale. Quantum degeneracy in Fermi gases was first obtained in 1999 for ^{40}K atoms [25]. Since then, the field of ultracold Fermi gases has been rapidly expanding. A typical experiment with Fermi gases studies $N \sim 10^6$ atoms at a temperature $T \sim 100$ nK, with density $10^{13} - 10^{14}$ atoms/cm³ [32]. Such dilute, ultracold atoms provide an accessible and controllable system where quantum many-body phenomena can be studied experimentally.

In a cold Fermi gas, the populations in different hyperfine states can be controlled experimentally, with nearly complete freedom. Therefore, it is possible to study phenomena in two-component Fermi systems, similar to those in spin-1/2 electrons and nucleons. Each of the two hyperfine states can be labeled as the spin-up or spin-down component. Recently, experiments with spin-polarized Fermi gases [40, 41, 51, 52, 54, 55, 58, 59] open up the frontier in exploring superfluidity and universal properties in strongly-interacting asymmetric Fermi systems, and provide insights to problems in condensed matter, nuclear and particle physics. A great deal of theoretical effort has also been devoted to understanding asymmetric Fermi gases¹, and this effort is still ongoing to fully elucidate the physics behind the experimental results. In this thesis, I will present our work on strongly-interacting Fermi gases with population imbalance. In the introduction, I will first briefly discuss strongly-interacting fermions and condensates of fermionic atoms. A motivation to study asymmetric Fermi gases will follow. In the end of the introduction, I will give an outline of the thesis.

¹Ref. [29] reviews the theory of Fermi gases, and provides an introductory discussion on the current theory of asymmetric Fermi gases.

1.1 Strongly-Interacting Fermi Gases

In a two-component Fermi gas at low temperatures, interactions are restricted to atoms in different spin-states due to Pauli exclusion. In the regime of low energies and long wavelengths, atomic interactions can be described by S -wave scattering. The S -wave scattering length a characterizes the two-body low-energy collision process. In cold Fermi gases, the scattering length a can be tuned by making use of Feshbach resonances [26, 27]. In particular, one can achieve large scattering lengths, $|a| \rightarrow \infty$, by tuning an external magnetic field to a resonant value $B = B_0$. The resulting Fermi gas with large scattering length is strongly interacting.

Consider a dilute, strongly-interacting Fermi gas, where the effective interaction range r_e is much smaller than the Fermi wavelength $k_F^{-1} \sim n^{-1/3}$, and whose scattering length diverges. The only remaining length scale is the Fermi wavelength. Therefore, only the Fermi momentum or the density sets the scale, and the physics is independent of interaction details. In this unitary or universal regime, the physics is said to be universal [4]. For example, consider a two-component Fermi gas with equal populations in the unitary regime. As we will see in Section 3.1.3, it is a resonant superfluid for low temperatures. At $T = 0$, the internal energy of the gas must be proportional to the Fermi energy up to a universal constant, $E/N = 3/5 \xi E_F$, and the superfluid gap must also be set by the Fermi energy, $\Delta \sim E_F$. These universal proportionality constants must be the same across different unitary systems regardless of densities. An example of such universality is demonstrated in the experimental measurement of the average energy [3, 33, 40, 56, 57], which is found to be $\xi \sim 0.4$, independent of the atomic species used (see, e.g., Table 2.1).

Large scattering lengths are found in many fields of physics. For example, nuclear matter is strongly interacting, and dilute neutron matter in nuclei or the crust of neutron stars is expected to have universal properties. Experiments with cold atoms provide a clean and controllable system to investigate the universal regime of strongly-interacting Fermi systems, and thus provide insights to problems in condensed matter, nuclear and particle physics.

1.2 Condensates of Fermionic Atoms

Particles are classified as either bosons or fermions. Fermions are particles with half-integer spin and obey the Pauli exclusion principle, which states

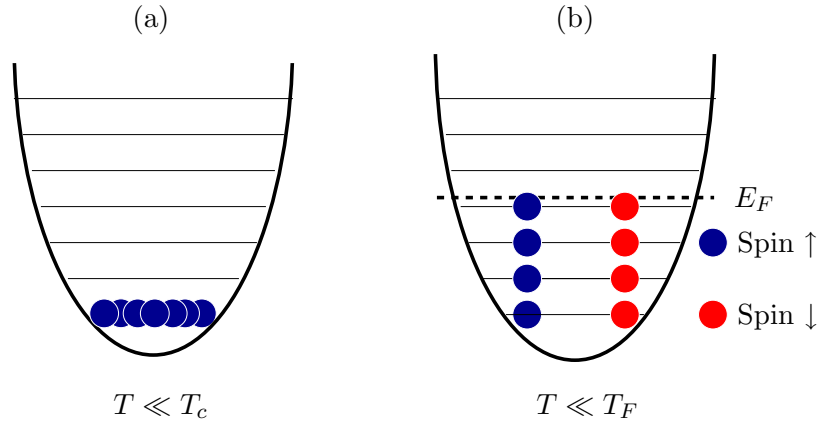


Figure 1.1: Non-interacting systems of ultracold bosonic and fermionic atoms in a confining harmonic potential. (a) Below a critical temperature T_c , bosonic particles occupy the lowest-energy state and form a Bose-Einstein condensate (BEC). The BEC is a superfluid, and is described by a many-body wave function in which all the particles occupy the same single-particle state. (b) Fermionic atoms obey the Pauli exclusion principle. At low temperatures, $T \ll T_F = E_F/k_B$, they fill up the lowest-energy single-particle states up to the Fermi energy E_F , forming the Fermi sea.

that two indistinguishable fermions cannot occupy the same quantum state. Bosons, which have integer spin, are able to occupy the same state. For neutral atoms, the number of neutrons determines whether it is a fermion or boson. An example of a bosonic atom is ${}^7\text{Li}$, while ${}^6\text{Li}$ is a fermionic atom.

At low temperatures, the distinction between bosons and fermions becomes important, see Fig. 1.1. Because bosons are not constrained by the Pauli exclusion principle, below a critical temperature, a large number of bosons occupies the ground state. This forms a Bose-Einstein condensate (BEC), which is a superfluid state. On the other hand, due to the Pauli exclusion principle, non-interacting fermions will simply fill the lowest-energy single-particle levels at low temperatures, with one fermion in each level, up to the Fermi energy $E_F = k_F^2/2m$, where k_F is the Fermi momentum. This is the arrangement known as the Fermi sea. Since spin is also a degree of freedom, in a two-spin component system, each energy level can accommodate two fermions, with one in each spin state.

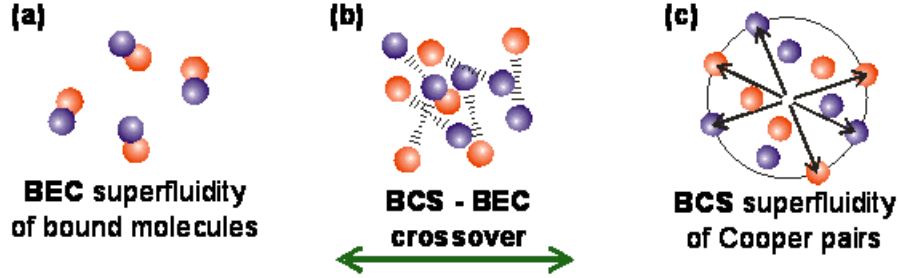


Figure 1.2: The BEC-BCS Crossover (Figure taken from Ref. [32]). The effective interatomic interaction can be controlled with a magnetic Feshbach resonance. The scattering length diverges, $a = \pm\infty$, at a resonant field $B = B_0$. Away from the resonance, the scattering length can take on either positive or negative values. (a) In the regime where $a > 0$, the strongly-attractive interaction causes one spin-up and one spin-down atom to form a bound molecule in free space with binding energy $E_b = \hbar^2/ma^2$. These molecules are bosons, and will condense to form a Bose-Einstein condensate (BEC). Therefore, this is known as the BEC regime. (c) On the side where $a < 0$, the interaction is not strong enough to bind atoms into molecules. However, since the Fermi surface is unstable to any attractive interaction, two atoms near the Fermi surface with back-to-back momenta will pair up to form a Cooper pair. The pairs are localized in momentum space and thus delocalized in coordinate space. The bosonic Cooper pairs also condense to form a superfluid, and this is the BCS mechanism through which conventional superconductivity occurs. Therefore, this side is referred to as the BCS regime. (b) In the unitary regime (large scattering length), resonant pairs and resonance superfluidity occur in the BEC-BCS crossover regime.

Interparticle interactions change this picture considerably. As discussed previously, the effective interaction can be controlled by a magnetic Feshbach resonance, which enables cold atoms to access different regimes of interaction strength. The effective interaction is characterized by the scattering length a . At a resonant external field, $B = B_0$, the scattering length diverges, $a = \pm\infty$. Away from resonance, the scattering length takes on either positive or negative values, and decreases in magnitude as the magnetic field moves away from B_0 . Here, we will briefly discuss the $T = 0$ ground states of a symmetric two-component Fermi gas ($N_\uparrow = N_\downarrow$) in the different regimes of interactions.

In the regime away from $B = B_0$, where a is positive and small, the interaction is strongly attractive, so two atoms in free space with opposite spins will form a bound, bosonic molecule with binding energy $E_b = \hbar^2/ma^2$. The effective interaction between these molecules is repulsive. In this regime, molecules form in a many-body Fermi system with two spin states. These bosonic molecules condense to form a BEC at low temperatures, and therefore, this is called the BEC regime, see Fig. 1.2 (a).

On the other side, where a is negative and small in magnitude, the fermionic atoms attract weakly. The interaction is not strong enough to bind a pair of atoms into a molecule in free space. However, as Bardeen, Cooper, and Schrieffer (BCS) have shown, the Fermi surface is unstable to pairing in the presence of an attractive interaction [2]. Therefore, in a many-body system, a pair of spin-up and spin-down fermions near the Fermi surface with back-to-back momenta form a large (delocalized in coordinate space) bound-state known as Cooper pair. These Cooper pairs are bosonic, and condense to form a superfluid at low temperatures. This is the same mechanism through which conventional superconductivity occurs. This is called the BCS regime, see Fig. 1.2 (c).

The scattering length diverges at the Feshbach resonance, $B = B_0$. Here, resonant pairs of spin-up and spin-down fermions form, at the crossover between a molecule and a Cooper pair, see Fig. 1.2 (b). These resonant Cooper pairs are highly delocalized molecules with free-space binding energy $E_b = 0$. In an equal two-component mixture, the crossover is smooth, and superfluidity persists for all regimes of interaction at low temperatures.

1.3 Asymmetric Fermi Gases

Naturally, one can ask what are the effects of population asymmetry, with $N_\uparrow > N_\downarrow$. Asymmetric Fermi systems are a recurring theme in nature. In magnetized superconductors, an external magnetic field can imbalance the spin densities [28, 36, 50]. Cold neutron matter in neutron stars contains a highly imbalanced population of neutrons and protons. Most stable nuclei also contain a higher number of neutrons than protons. Therefore, asymmetric Fermi systems are a highly relevant subject in many fields of physics.

Spin-polarized ultracold Fermi gases provide a novel tool to study strongly-interacting asymmetric Fermi systems. There are exciting experimental results from the MIT [54, 58, 59] and the Rice University [40, 41] groups. The two groups found differences in the observed phase structure and critical polarization at which superfluidity ceases to exist. The MIT experi-

ment [54, 58, 59] observed phase separation in the trap, which contains an equal-density core, surrounded by a partially-polarized shell and an outer region of majority atoms. The equal-density core is confirmed to be superfluid by the presence of vortices [58], and exists up to a critical polarization $P_c = (N_\uparrow - N_\downarrow)/N_{\text{tot}} = 0.70(3)$ [54, 58, 59]. The Rice experiment [40, 41] also observed phase separation, with a fully-paired core surrounded by normal majority fermions, but with an extremely thin partially-polarized shell, and a high critical polarization $P_c \gtrsim 0.9$. The two experiments employed harmonic traps with cylindrical symmetry ($\omega_x = \omega_y = \alpha\omega$, $\omega_z = \omega$). The MIT experiment has an aspect ratio $\alpha \sim 5$ and total particle numbers $N_{\text{tot}} = N_\uparrow + N_\downarrow \sim 10^6 - 10^7$. The Rice experiment was in a highly elongated trap, with $\alpha \sim 35 - 45$ and for lower $N_{\text{tot}} \sim 10^5$.

These experiments have led to a number of theoretical investigations (see Ref. [29] and references within). The critical polarization is influenced by the energies of the superfluid and the polarized normal gas. The universal superfluid energy parameter $\xi = 0.42$ [13, 43] has been determined using Monte Carlo (MC) calculations. For large asymmetries, the energy of the polarized normal state is governed by the energy of a spin-down fermion interacting resonantly with a spin-up Fermi sea. In the uniform system, the energy $E = \eta E_F$ of this Fermi polaron has been calculated variationally including one-particle–one-hole excitations, with $\eta = -0.607$ [17, 18]. This agrees very well with the Monte Carlo results [13, 38, 43, 45, 46], and $2p2h$ contributions were shown to be small [21].

The variational value of $\eta = -0.607$ requires the existence of at least one partially-polarized phase in the uniform system². With the local-density approximation (LDA), the polaron energy can be used to estimate the critical concentration $x_c = n_\downarrow/n_\uparrow$ and the critical polarization P_c in traps with large particle numbers. The variational value $\eta = -0.607$ leads to $P_c = 0.74$ and $x_c = 0.47$ [47]. These results are in good agreement with $P_c = 0.70(3)$ of the MIT experiment [54, 58, 59] and with a tomography measurement $x_c \approx 0.47$ [55].

In summary, the results in the uniform system agree well with the MIT experiment, whose trap contained a larger number of particles. Understanding how finite-size and confinement effects influence the polaron energy, as well as the equation of state for the normal phase, can contribute to understanding the MIT-Rice differences. This forms the motivation behind our work described in this thesis.

²For a detailed discussion, we refer to Chapter 3, see also Refs. [9, 17].

1.4 Outline

In this thesis, I will summarize our work on strongly-interacting Fermi gases with population imbalance. This work was done in collaboration with Jens Braun, who is now at the Friedrich Schiller University, Jena, Germany, and with Achim Schwenk. This work has led to a paper in Phys. Rev. Lett. [34], and another paper is in preparation.

In Chapter 2, I will provide an overview of interactions in cold atoms. A brief review of low-energy scattering will be provided, and its application to atomic interactions will be discussed. I will then introduce the concept of regularized contact interactions, and review the renormalization of the coupling constant, an important result for the later chapters. Lastly, the strongly-interacting regime will be discussed.

In Chapter 3, I will review the theory of unitary asymmetric Fermi gases in the uniform system. I will begin with a review on the condensates of fermionic atoms. Next, a discussion on the theory of unitary asymmetric Fermi gases in the uniform system will be provided. I will then introduce Chevy's variational solution to the $N + 1$ body problem. Application to trapped gases will then be discussed. Lastly, I will review the experimental work on spin-polarized Fermi gases in greater detail.

In Chapter 4, I will present our work on the $N + 1$ body problem in trapped Fermi gases. The variational calculation of the polaron energy in anisotropic traps will be described, and the numerical results will be presented. I will then discuss the impact of the polaron energy on the critical polarization and the critical concentration, and show that the MIT-Rice differences can be understood partially based on our microscopic results.

In Chapter 5, I will present our study on the $N + M$ body problem, which is the natural next step towards general asymmetry. I will describe the variational calculation of the $N + M$ body energy in the uniform system, and show the numerical results. The equation of state of the normal Fermi liquid is constructed based on the variational $N + M$ body energy, and applied to traps with large particle numbers to compute the critical polarization and the critical concentration. Lastly, I will describe the derivation of the $N + M$ body energy in trapped Fermi gases. The numerical evaluation of this energy in traps is to be left for future work.

Finally, in Chapter 6, I will summarize our work, and present an outlook.

Chapter 2

Interactions in Cold Atoms

Interactions give rise to the rich phenomena observed in cold atoms. Effects of interactions in quantum degenerate, dilute Fermi gases with two components can be accurately described by the physics of two-body scattering. The goal of this chapter is to provide an overview of interactions in cold atoms, and to present results that will be essential to the later chapters. We will begin with a brief review of the scattering problem. For a detailed treatment, we refer to standard textbooks on quantum mechanics, such as Refs. [35, 49]. Next, we will apply two-body scattering to atomic interactions, and discuss the regularized contact interaction, which serves as the standard low-energy Hamiltonian in dilute Fermi gases. Lastly, we will review the strongly-interacting regime of cold Fermi gases with discussions on Feshbach resonances and the universal regime.

Throughout this work, we will be working with the following units

$$\hbar = c = k_B = 1, \quad (2.1)$$

and the normalization

$$\begin{aligned} \langle \mathbf{x} | \mathbf{x}' \rangle &= \delta^3(\mathbf{x} - \mathbf{x}'), \\ \langle \mathbf{x} | \mathbf{k} \rangle &= e^{i\mathbf{k} \cdot \mathbf{x}}, \\ \langle \mathbf{k} | \mathbf{k}' \rangle &= (2\pi)^3 \delta^3(\mathbf{k} - \mathbf{k}'). \end{aligned} \quad (2.2)$$

2.1 Two-Body Scattering

In the non-relativistic limit, the quantum mechanical two-body process can be decomposed into center-of-mass and relative components, just as in the case of the classical two-body problem. The center-of-mass momentum is conserved, and the problem reduces to the solution of Schrödinger equation for the relative motion. In the relative frame, two-body scattering is equivalent to a free particle of relative momentum \mathbf{k} and reduced mass $m_r = m_1 m_2 / (m_1 + m_2)$ incident upon a scattering potential $V(r)$, where r is the interparticle distance, and m_1, m_2 are the masses of the two particles.

2.1. Two-Body Scattering

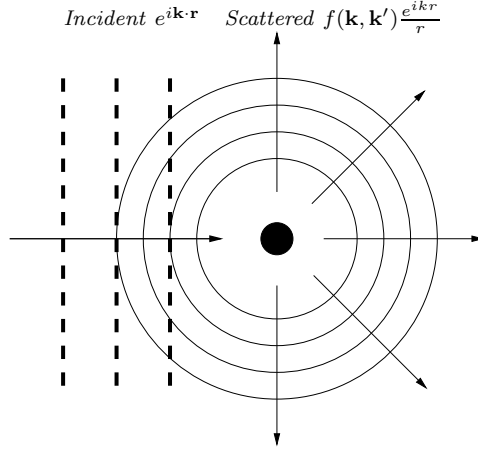


Figure 2.1: General scattering geometry. An incident plane wave, $e^{i\mathbf{k}\cdot\mathbf{r}}$, scatters off a potential, $V(r)$, located at the origin. The asymptotic scattered wavefunction is a spherical wave $\frac{e^{i\mathbf{k}r}}{r}$, with scattering amplitude $f(\mathbf{k}, \mathbf{k}')$.

The qualitative picture describing potential scattering is illustrated in Fig. 2.1. A plane wave $\psi_0 = e^{i\mathbf{k}\cdot\mathbf{r}}$ is incident upon a scattering potential, $V(r)$, located at the origin. We assume the potential is spherically symmetric. In the far field limit $r \gg R_0$, where R_0 is the range of the potential, the scattered wavefunction looks like a spherical wave, which is a function of the incident momentum \mathbf{k} and direction $\hat{\mathbf{r}}$ only. In other words, the total wavefunction, in the asymptotic limit, has the form

$$\psi(\mathbf{r}) = e^{i\mathbf{k}\cdot\mathbf{r}} + f(\mathbf{k}, \mathbf{k}') \frac{e^{i\mathbf{k}r}}{r}, \quad (2.3)$$

where $f(\mathbf{k}, \mathbf{k}')$ is the scattering amplitude, and $\mathbf{k}' = k\hat{\mathbf{r}}$.

In this section, we will review two-body scattering at low energies, relevant to cold dilute atomic gases, and the T -matrix.

2.1.1 Scattering at Low Energies

The scattering amplitude can be expanded in terms of partial waves, which are labeled by angular momentum quantum numbers $l = 0, 1, 2, \dots$. These partial waves are eigenstates of \mathbf{L}^2 , where $\mathbf{L} = \mathbf{r} \times \mathbf{k}$ is the angular momentum operator, with eigenvalues $l(l+1)$. At low collisional energies $E = k^2/2m_r \sim 0$, the main contribution to the scattered wavefunction comes from S -wave

2.1. Two-Body Scattering

states, which have an $l = 0$ component. In the absence of scattering, the total wavefunction of Eq. (2.3) is $\psi(\mathbf{r}) = e^{i\mathbf{k}\cdot\mathbf{r}}$, whose S -wave component is

$$\int \frac{d\Omega}{4\pi} e^{i\mathbf{k}\cdot\mathbf{r}} = \frac{1}{kr} \left(\frac{e^{ikr}}{2i} - \frac{e^{-ikr}}{2i} \right), \quad (2.4)$$

consisting of an inward and an outward propagating spherical wave. Scattering only affects the outward propagating wave. In addition, since particles are conserved, at large distance, the only possible change to the outgoing wave due to scattering is a change of phase, $e^{ikr} \rightarrow e^{i(kr+2\delta_0(k))}$. The quantity $\delta_0(k)$ is the S -wave phase shift (the factor of 2 is a convention). This results in an additional term $\frac{e^{i(kr+\delta_0(k))}}{kr} \sin \delta_0(k)$ in Eq. (2.4) due to scattering. Therefore, in the presence of scattering at low energies, the total wavefunction is

$$\psi(\mathbf{r}) = e^{i\mathbf{k}\cdot\mathbf{r}} + \frac{e^{i\delta_0(k)} \sin \delta_0(k)}{k} \frac{e^{ikr}}{r}. \quad (2.5)$$

Thus, the S -wave scattering amplitude is given by

$$f_0(k) = \frac{1}{k \cot \delta_0(k) - ik}. \quad (2.6)$$

At low momenta, the S -wave phase shift has the scaling $\delta_0(k) \sim k$ (see, e.g., Ref. [49]). Therefore, in the $k \rightarrow 0$ limit, the S -wave scattering amplitude tends to a constant value, and we define the S -wave scattering length a by $f_0(k \rightarrow 0) = -a$. The S -wave scattering length plays an important role in low-energy scattering. For positive scattering lengths $a > 0$, bound states form with the binding energy

$$E_b = \frac{1}{2m_r a^2}. \quad (2.7)$$

Expanding $\cot \delta_0(k)$ up to $O((R_0 k)^2)$ terms, we obtain the S -wave scattering amplitude at low energies,

$$f_0(k) = -\frac{1}{\frac{1}{a} - \frac{r_e}{2} k^2 + ik}. \quad (2.8)$$

This relation defines the effective range r_e of the interaction. Typically, one has $r_e \sim R_0$; however, in some cases, e.g., close to a narrow Feshbach resonance, r_e can become much larger than R_0 , and thus provides a new length scale [29].

2.1.2 The T -Matrix

The previous section dealt with scattering at low energies. A useful tool to study scattering theory in general is the transition matrix, or the T -matrix. To begin, we define our problem with the Hamiltonian

$$H = H_0 + V, \quad (2.9)$$

where $H_0 = \frac{p^2}{2m_r}$ is the non-interacting Hamiltonian. Let E be an energy eigenvalue of H , $|\psi\rangle$ be the corresponding eigenstate of H , and $|\psi_0\rangle$ be a free-particle eigenstate of H_0 with the same energy. This choice is possible because both H_0 and H exhibit continuous energy spectra. Then, one can check that the following solution,

$$|\psi\rangle = |\psi_0\rangle + \frac{1}{E - H_0 \pm i\epsilon} V |\psi\rangle, \quad (2.10)$$

where $\epsilon \rightarrow 0^+$, satisfies the Schrödinger equation $(H_0 + V - E)|\psi\rangle = 0$. The $\pm i\epsilon$ is necessary to ensure convergence. The physical meaning of \pm will become explicit shortly. By applying Eq. (2.10) to the right-hand side iteratively, one obtains

$$|\psi\rangle = \left(1 + \frac{1}{E - H_0 \pm i\epsilon} V + \frac{1}{E - H_0 \pm i\epsilon} V \frac{1}{E - H_0 \pm i\epsilon} V + \dots \right) |\psi_0\rangle. \quad (2.11)$$

This expression can be written as

$$|\psi\rangle = |\psi_0\rangle + \frac{1}{E - H_0 \pm i\epsilon} T |\psi_0\rangle, \quad (2.12)$$

where the T -matrix is defined by

$$T = V \sum_{n=0}^{\infty} \left(\frac{1}{E - H_0 \pm i\epsilon} V \right)^n. \quad (2.13)$$

The T -matrix has the property

$$V |\psi\rangle = T |\psi_0\rangle, \quad (2.14)$$

and hence its name, the transition matrix.

To relate the T -matrix to the scattering amplitude, let us turn to Eq. (2.10). Choosing the plane wave $|\psi_0\rangle = |\mathbf{k}\rangle$ as the incident free-particle, and making the use of the normalization Eq. (2.2), we can write Eq. (2.10) in the following form,

$$\psi(\mathbf{r}) = e^{i\mathbf{k}\cdot\mathbf{r}} - \frac{m_r}{2\pi} \int d^3r' \frac{e^{\pm ik|\mathbf{r}-\mathbf{r}'|}}{|\mathbf{r}-\mathbf{r}'|} \langle \mathbf{r}' | V | \psi \rangle, \quad (2.15)$$

2.1. Two-Body Scattering

where the \pm corresponds to the choice of $\pm i\epsilon$ in Eq. (2.10).

In the asymptotic limit $r \gg R_0$, one can expand $|\mathbf{r} - \mathbf{r}'| \simeq |\mathbf{r}| - \hat{\mathbf{r}} \cdot \mathbf{r}'$ for $r \gg r'$. With the help of Eq. (2.14), Eq. (2.15) becomes

$$\psi(\mathbf{r}) = e^{i\mathbf{k} \cdot \mathbf{r}} - \frac{m_r}{2\pi} \frac{e^{\pm ikr}}{r} \langle \pm \mathbf{k} \hat{\mathbf{r}} | T | \mathbf{k} \rangle. \quad (2.16)$$

At this point, the physical meaning of $\pm i\epsilon$ in Eq. (2.10) becomes clear. The solution with $+i\epsilon$ corresponds to an incident plane wave plus an outgoing spherical wave. On the other hand, the solution with $-i\epsilon$ consists of a plane wave plus an incoming spherical wave. Therefore, the physical choice is $+i\epsilon$.

Eq. (2.16) gives the following relation of the scattering amplitude to the T -matrix:

$$f(\mathbf{k}, \mathbf{k}') = -\frac{m_r}{2\pi} \langle \mathbf{k}' | T | \mathbf{k} \rangle. \quad (2.17)$$

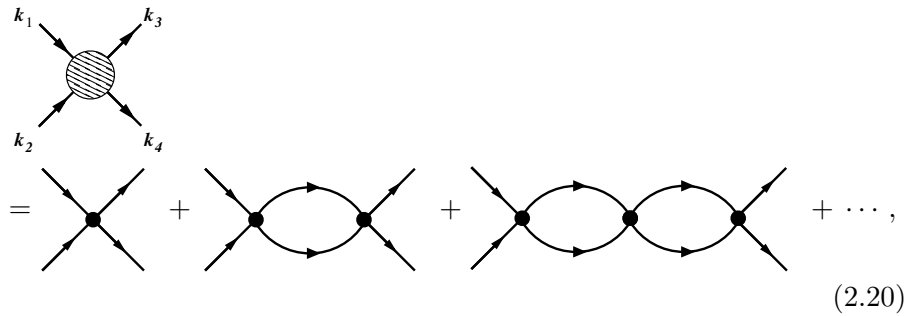
One way to understand the structure of the T -matrix is to look at its momentum-space representation. Recall that the free-particle Green's function is

$$\langle \mathbf{k}' | \frac{1}{E - H_0 + i\epsilon} | \mathbf{k} \rangle = (2\pi)^3 \delta^3(\mathbf{k} - \mathbf{k}') \frac{1}{E - \frac{k^2}{2m_r} + i\epsilon}. \quad (2.18)$$

For $n = 1, 2, \dots$, each of the terms in Eq. (2.13) has the following form in momentum space:

$$\begin{aligned} & \langle \mathbf{k}' | V \left(\frac{1}{E - H_0 + i\epsilon} V \right)^n | \mathbf{k} \rangle \\ &= \int V_{\mathbf{k}', \mathbf{q}_1} \left(\prod_{i=1}^n \frac{d^3 q_i}{(2\pi)^3} G_0(E, \mathbf{q}_i) V_{\mathbf{q}_i, \mathbf{q}_{i+1}} \right) \Big|_{\mathbf{q}_{n+1} = \mathbf{k}}, \end{aligned} \quad (2.19)$$

where $V_{\mathbf{q}', \mathbf{q}} = \langle \mathbf{q}' | V | \mathbf{q} \rangle$, and $G_0(\omega, \mathbf{q}) = \left(\omega - \frac{q^2}{2m_r} + i\epsilon \right)^{-1}$. Therefore, the T -matrix in momentum space can be written as the following series of Feynman diagrams,



$$= \text{[Diagram 1]} + \text{[Diagram 2]} + \text{[Diagram 3]} + \dots, \quad (2.20)$$

where $\mathbf{k}_1, \mathbf{k}_2$ ($\mathbf{k}_3, \mathbf{k}_4$) are the momenta of the incident (outgoing) particles pair, and \mathbf{k} (\mathbf{k}') is the corresponding relative momentum. By momentum conservation, $\mathbf{k}_1 + \mathbf{k}_2 = \mathbf{k}_3 + \mathbf{k}_4$. The interpretation of Eq. (2.20) is as follow: the incident particles can interact with each other for an arbitrary number of times, and the scattering amplitude is the sum of all such contributions.

In the next section, we will apply scattering theory to describe interactions in cold atoms.

2.2 Interactions in Cold Fermi Gases

In this section, we will apply the theory of two-body scattering to experiments with cold Fermi gases. In the relevant regime of low densities and low temperatures, the range R_0 of the interatomic potential is much smaller than both the thermal wavelength $\lambda_T = \sqrt{\frac{2\pi}{mk_B T}}$ and the Fermi wavelength $k_F^{-1} \sim n^{-1/3}$,

$$R_0 \ll \lambda_T, \quad R_0 \ll k_F^{-1}. \quad (2.21)$$

As discussed above, in such a regime where the typical collisional energy is low, the dominant contribution to the collisional process is S -wave scattering. Since we will be working in the $T = 0$ limit, only the S -wave scattering will be considered in this work. Furthermore, the antisymmetry of the wavefunction of identical fermions exclude S -wave scattering between particles of the same species. In another word, only atoms in different hyperfine states will interact.

In the study of many-body physics, it is often convenient to use an effective potential instead of a more complicated atomic potential. In dilute Fermi gases, where the Fermi wavelength is much larger than the effective range, $k_F^{-1} \gg r_e$, the particles do not probe the internal structure of the interaction. Therefore, one can model atomic interactions with an effective potential in dilute Fermi gases. Different effective potentials can be considered, as the low-energy process is independent of the short-range details. One model potential is the attractive square-well:

$$V(r) = \begin{cases} -V_0 & r < R_0, \\ 0 & r > R_0. \end{cases} \quad (2.22)$$

This potential is sometimes used in Monte Carlo simulations [38].

Another important effective potential is the regularized contact interaction,

$$V(\mathbf{r}) = g(\Lambda)\delta_\Lambda^3(\mathbf{r}), \quad (2.23)$$

2.3. Regularized Contact Interaction

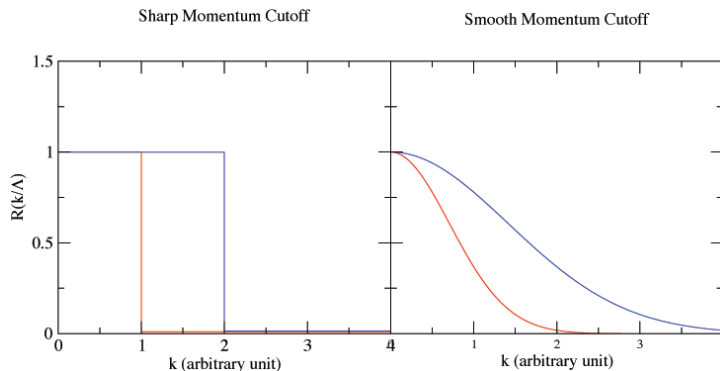


Figure 2.2: Momentum cutoff schemes. *Left*: Sharp momentum cutoff given by $R(k/\Lambda) = \Theta(1 - k/\Lambda)$. *Right*: Smooth momentum cutoff given by $R(k/\Lambda) = e^{-k^2/\Lambda^2}$. Plots are shown for increasing Λ , with the blue curves having a larger value of Λ .

where $g(\Lambda)$ is the coupling constant, and Λ is a momentum cutoff necessary to regularize the potential. This is the interaction we will consider in the subsequent chapters.

2.3 Regularized Contact Interaction

The contact interaction introduced in Eq. (2.23) is given by a constant in momentum space and requires regularization. We use a momentum cutoff Λ to avoid divergences at large momenta. This is called regularization. Once a regularization scheme has been introduced, one proceeds to calculate the scattering amplitude using the T -matrix. This scattering amplitude is then compared to the low-energy form, Eq. (2.8), and we match the coupling constant, $g(\Lambda)$, to the physical scattering length for arbitrary cutoff. The renormalized coupling constant consequently absorbs the cutoff dependency, and physical observables are independent of the regularization scheme and cutoff for large Λ .

In the rest of this section, we will match the renormalized coupling constant $g(\Lambda)$ of the contact interaction, Eq. (2.23), to the physical scattering length. We will consider a general cutoff scheme of the form

$$\langle \mathbf{k}' | V | \mathbf{k} \rangle = g(\Lambda) R(k/\Lambda) R(k'/\Lambda), \quad (2.24)$$

where the function $R(u)$ has the property $R(0) = 1$ and $\lim_{u \rightarrow \infty} R(u) =$

2.3. Regularized Contact Interaction

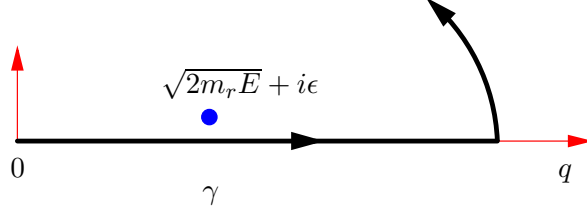


Figure 2.3: Contour used to evaluate Eq. (2.28). The contour is counter-clockwise and encloses the pole at $q = \sqrt{2m_r E} + i\epsilon$.

0, and $g(\Lambda)$ is the renormalized coupling constant. There are two cutoff schemes that we will consider. One is the sharp cutoff, given by

$$\langle \mathbf{k}' | V | \mathbf{k} \rangle = g(\Lambda) \Theta(1 - k/\Lambda) \Theta(1 - k'/\Lambda), \quad (2.25)$$

with $R(u) = \Theta(1 - u)$, where $\Theta(x > 0) = 1$, and $\Theta(x < 0) = 0$. This cutoff scheme is useful when one considers uniform systems. For Fermi gases in harmonic oscillator traps, it is more convenient to use a smooth Gaussian cutoff

$$\langle \mathbf{k}' | V | \mathbf{k} \rangle = g(\Lambda) e^{-k^2/\Lambda} e^{-k'^2/\Lambda}, \quad (2.26)$$

with $R(u) = e^{-u^2}$. These two cutoff schemes are depicted in Fig. 2.2.

To renormalize the coupling constant, we first calculate the scattering amplitude, and then define the coupling constant so it absorbs the divergent contribution due to the cutoff. Therefore, we proceed to evaluate the T -matrix element in momentum space, which is given by Eq. (2.20). The n^{th} term, where $n = 0, 1, 2, \dots$, is given by

$$\begin{aligned} & \langle \mathbf{k}' | V \left(\frac{1}{E - H_0 + i\epsilon} V \right)^n | \mathbf{k} \rangle \\ &= (g(\Lambda))^{n+1} R(k/\Lambda) R(k'/\Lambda) \left(\int \frac{d^3 q}{(2\pi)^3} \frac{R^2(q/\Lambda)}{E - \frac{q^2}{2m_r} + i\epsilon} \right)^n. \end{aligned} \quad (2.27)$$

The integral in the above equation can be evaluated using the contour

2.3. Regularized Contact Interaction

shown in Fig. 2.3:

$$\begin{aligned} & \int \frac{d^3q}{(2\pi)^3} \frac{R^2(q/\Lambda)}{E - \frac{q^2}{2m_r} + i\epsilon} \\ &= \frac{1}{2\pi^2} \left(\int_0^\infty dq \frac{q^2 R^2(q/\Lambda)}{E - \frac{q^2}{2m_r}} + \frac{1}{2} 2\pi i \operatorname{Res} \left[\frac{q^2 R^2(q/\Lambda)}{E - \frac{q^2}{2m_r}}, \sqrt{2m_r E} + i\epsilon \right] \right), \end{aligned} \quad (2.28)$$

where $\operatorname{Res}[f(z), z_0]$ is the residue of the function $f(z)$ at $z = z_0$. The residue in Eq. (2.28) is given by

$$\begin{aligned} & \frac{1}{2} 2\pi i \operatorname{Res} \left[\frac{q^2 R^2(q/\Lambda)}{E - \frac{q^2}{2m_r}}, \sqrt{2m_r E} + i\epsilon \right] \\ &= -i\pi m_r \sqrt{2m_r E} R^2 \left(\frac{\sqrt{2m_r E}}{\Lambda} \right) \xrightarrow{\Lambda \rightarrow \infty} -i\pi m_r \sqrt{2m_r E}. \end{aligned} \quad (2.29)$$

Because we are only interested in the leading E terms, we expand the integrand as a geometric series for small E . After a change of variable $q/\Lambda \rightarrow u$, we obtain

$$\int_0^\infty dq \frac{q^2 R^2(q/\Lambda)}{E - \frac{q^2}{2m_r}} = -2m_r \Lambda \int_0^\infty du R^2(u) + O(E). \quad (2.30)$$

Combining the results of Eqs. (2.27)-(2.30), we obtain

$$\begin{aligned} & \langle \mathbf{k}' | V \left(\frac{1}{E - H_0 + i\epsilon} V \right)^n | \mathbf{k} \rangle \\ &= (g(\Lambda))^{n+1} R(k/\Lambda) R(k'/\Lambda) \left(-\frac{m_r}{\pi^2} \Lambda \int_0^\infty du R^2(u) - i \frac{m_r}{2\pi} \sqrt{2m_r E} \right)^n. \end{aligned} \quad (2.31)$$

Summing the series and taking $R(k/\Lambda) \xrightarrow{\Lambda \rightarrow \infty} 1$ give us $\langle \mathbf{k}' | T | \mathbf{k} \rangle$. By conservation of energy, the scattered wave carries the energy $E = k^2/2m_r$. Therefore, we have

$$\langle \mathbf{k}' | T | \mathbf{k} \rangle = \frac{1}{\frac{1}{g(\Lambda)} + \frac{m_r}{\pi^2} \Lambda \int_0^\infty du R^2(u) + i \frac{m_r}{2\pi} k}, \quad (2.32)$$

and according to Eq. (2.17), the scattering amplitude is

$$f(\mathbf{k}, \mathbf{k}') = -\frac{1}{\frac{2\pi}{m_r g(\Lambda)} + \frac{2}{\pi} \Lambda \int_0^\infty du R^2(u) + ik}. \quad (2.33)$$

Recall that the low-energy scattering amplitude is given by Eq. (2.8). We see that in this case, the scattering amplitude of Eq. (2.33) indeed has the form $f(\mathbf{k}, \mathbf{k}') = -\frac{1}{a^{-1} + ik}$, with an effective range $r_e \sim O(1/\Lambda) \rightarrow 0$ for the contact interaction, which is expected. The scattering length and the renormalized coupling constant are therefore matched by

$$g(\Lambda) = \frac{2\pi}{m_r} \frac{1}{\frac{1}{a} - \frac{2}{\pi}\Lambda \int_0^\infty du R^2(u)}. \quad (2.34)$$

With the sharp cutoff scheme of Eq. (2.25), $R(u) = \Theta(1 - u)$, one finds

$$g(\Lambda) = \frac{2\pi}{m_r} \frac{1}{\frac{1}{a} - \frac{2}{\pi}\Lambda}. \quad (2.35)$$

With the smooth cutoff given by Eq. (2.26), $R(u) = e^{-u^2}$, the renormalized coupling constant is

$$C(\Lambda) = \frac{2\pi}{m_r} \frac{1}{\frac{1}{a} - \frac{\Lambda}{\sqrt{2\pi}}}, \quad (2.36)$$

where we use $C(\Lambda)$ to distinguish this from the case of sharp cutoff.

2.4 Strongly-Interacting Regime in Cold Fermi Gases

The ability to tune the scattering length a is an important experimental tool that enables the study of strongly-interacting Fermi gases. In this section, we will briefly discuss Feshbach resonances, a phenomenon that enables experimental control of the scattering length. We will also describe the universal regime, in which low density, strongly-interacting Fermi systems share universal properties, independent of interaction details.

2.4.1 Feshbach Resonances

The possibility to tune the scattering length a enables much of the recent experimental progress with cold Fermi gases. In particular, the ability to achieve large scattering lengths, $|a| \gg 1/k_F$ by making the use of Feshbach resonances [26, 27], allows experiments with Fermi gases to explore the strongly-interacting regime.

Due to the hyperfine interaction, two colliding atoms can form a bound state whose magnetic moment is different from the total magnetic moment of the pair. Consequently, the bound state (referred to as the closed channel)

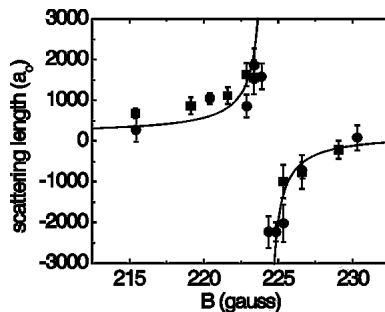


Figure 2.4: Experimental measurement of the scattering length vs. B by measuring a mean-field energy shift with radio frequency (RF) spectroscopy [48]. The measurement was taken for $T/T_F = 0.4$ and two different densities: $n = 1.8 \times 10^{14} \text{cm}^{-3}$ (circles) and $n = 5.8 \times 10^{13} \text{cm}^{-3}$ (squares). The cold gas consisted of about 10^5 atoms of ^{40}K . The characteristic diverging scattering length near the resonance is observed.

and the scattering state (the open channel) can have different Zeeman shift in the presence of an external magnetic field. In the absence of coupling between the two channels, the closed channel has no effect on scattering in the open channel. However, in cold atoms the channels are coupled, and the scattering length becomes large when the bound state energy of the closed channel and the scattering energy of the open channel are close to each other. This resonance occurs at a magnetic field B_0 , and one can parametrize the scattering length as

$$a = a_{bg} \left(1 - \frac{\Delta_B}{B - B_0} \right), \quad (2.37)$$

where a_{bg} is a background scattering length away from the resonance, and Δ_B is the width of the resonance. Fig. 2.4 shows an experimental realization for ^{40}K atoms, with a resonance at $B_0 \simeq 224$ G.

2.4.2 Universal Regime

Consider the regime of large scattering lengths, $|a| \rightarrow \infty$, and low densities, where the Fermi wavelength is much larger than the range of the interaction

2.4. Strongly-Interacting Regime in Cold Fermi Gases

and the effective range³:

$$r_e, R_0 \ll k_F^{-1} \sim n^{-1/3} \ll a \rightarrow \infty. \quad (2.38)$$

In this limit, Eq. (2.6) becomes $f_0(k) = -i/k$. This is called the unitary or the universal regime, where the scattering amplitude is at the unitary limit, independent of the interaction [4].

In the unitary regime, the Fermi wavelength k_F^{-1} is the only length scale, and the only energy scale is the Fermi energy $E_F = (6\pi^2 n)^{2/3}/2m$ set by the density. All other thermodynamic quantities are proportional to the Fermi energy up to a universal constant. For example, consider a $T = 0$ unitary two-component Fermi gas containing spin up (\uparrow) and spin down (\downarrow) fermions with equal densities, $n_\uparrow = n_\downarrow$. In Section 3.1.3, we will see that this is a crossover superfluid. The chemical potential $\mu = \mu_\uparrow = \mu_\downarrow$ at unitarity has the scaling relation

$$\mu = \xi E_F, \quad (2.39)$$

where ξ is a universal parameter. This parameter is also related to the energy per particle and the pressure. Using the relation $\mu_\sigma = (\partial E / \partial N_\sigma)_{S,V}$, where $\sigma = \uparrow, \downarrow$, one has $\mu = \frac{1}{2} \left(\frac{\partial N}{\partial N_\uparrow} \frac{\partial}{\partial N} + \frac{\partial N}{\partial N_\downarrow} \frac{\partial}{\partial N} \right)_{S,V} E = \left(\frac{\partial E}{\partial N} \right)_{S,V}$. Integrating over the density, one finds $\frac{E}{N} = \frac{1}{n} \int \mu dn$. Therefore, the universal scaling for the energy per particle is

$$\frac{E}{N} = \xi \frac{3}{5} E_F. \quad (2.40)$$

Similarly, using the thermodynamic relation $E = TS - PV + \sum_\sigma \mu_\sigma N_\sigma$, one finds the pressure at $T = 0$ to obey the scaling law

$$P = \xi \frac{2}{5} n E_F. \quad (2.41)$$

Presently, there is no analytic solution to the many-body problem of two-components Fermi gases with equal-densities in the unitary regime, because the large scattering length $k_F |a| \gg 1$ prevents any known systematic expansion. Instead, numerical simulations with fixed-node Monte Carlo (MC) methods are used to study the unitary regime, leading to the universal $\xi = 0.42(1)$ [13, 43]. The most recent calculation gives $\xi = 0.40(1)$ [14].

³Typically, experiments with cold Fermi gases achieve large scattering lengths near *broad* Feshbach resonances, where $r_e \sim R_0$, and $k_F r_e \ll 1$. However, near a *narrow* resonance, the effective range is large and negative, so that $|k_F r_e| \gg 1$.

2.4. Strongly-Interacting Regime in Cold Fermi Gases

		ξ
${}^6\text{Li}$	Innsbruck (2005) [3]	$0.27^{+0.09}_{-0.12}$
	Duke (2005) [33]	0.51(4)
	Rice (2006) [40]	0.46(5)
	ENS (2007) [57]	0.41(15)
${}^{40}\text{K}$	JILA (2006) [56]	$0.46^{+0.12}_{-0.05}$
Theory	QMC [13, 43]	0.42(1)

Table 2.1: Experimental and theoretical values of the universal parameter for the superfluid energy ξ .

The MC value of $\xi = 0.42(1)$ is consistent with experimental measurements [3, 33, 40, 56, 57], given in Table. 2.1. The recent experiments with ${}^6\text{Li}$ [40, 57] and ${}^{40}\text{K}$ [56] give $\xi \sim 0.4$. The fact that the value of ξ does not depend on the atomic species demonstrates the universal behavior of these unitary systems.

Large scattering lengths play a prominent role in many fields of physics. For example, the neutron-neutron scattering length is $a_{nn} = -18.5 \pm 0.3$ fm ($1 \text{ fm} = 10^{-15} \text{ m}$), which is about 20 times larger than the interaction range $R_0 \approx 1.4$ fm. Therefore, the universal regime, characterized by Eq. (2.38), is relevant to dilute neutron matter in nuclei or the crust of neutron stars. Experiments with cold Fermi gases provide a clean and controllable system to investigate the physics of the universal regime, and thus give insights into condensed matter, nuclear and particle physics.

Chapter 3

$N + 1$ Body Problem in the Uniform System

In the absence of interactions, the ground state of a Fermi system is simply the Fermi sea. With tunable interactions in two-component Fermi gases, it is possible to form bosonic bound states of different-species fermions. These bound states may be molecular dimers in the $a > 0$ regime, or Cooper pairs in the $a < 0$ regime. In a symmetric gas with equal populations, the ground state at $T = 0$ is a superfluid condensate of these bosonic pairs. Superfluidity is a remarkable phenomenon found in many different fields of physics, and the ability to study fermionic superfluidity in a controllable manner makes cold Fermi gases a highly valuable experimental tool.

The key to fermionic superfluidity is pairing. Naturally, one can ask what happens to superfluidity in a gas with imbalanced spin populations, $N_{\uparrow} \neq N_{\downarrow}$, where not every particle can find a partner. The ability to freely choose the populations in different hyperfine states allows cold Fermi gases to explore such asymmetric Fermi systems, and to provide insights in many different fields of physics where the problem of population imbalance arises. For example, an external magnetic field can, in principle, change the spin densities in superconductors⁴ [28, 36, 50]. Another example are neutron stars, which are composed of mostly neutrons, with proton fractions typically of the order 10% [15]. Most stable nuclei also contain an asymmetric population of protons and neutrons. In neutron-rich nuclei, neutrons leak out to form neutron skins. Examples of nucleon densities are shown in Fig. 3.1, and they show striking similarities to the spin densities in resonantly-interacting cold atoms (see Fig 3.7).

The purpose of this chapter is to provide a background to our studies of trapped asymmetric Fermi gases in the next chapter. We will begin with a review of condensates of fermionic atoms. Next, we will discuss the theory

⁴In a typical superconductor, imbalancing spin densities by a magnetic field is hindered by the Meissner effect. Below a critical field, the magnetic field is either expelled from the superconductor, or enters in the form of quantized flux. Above this critical field, equal-density superconductivity breaks down [16, 19]

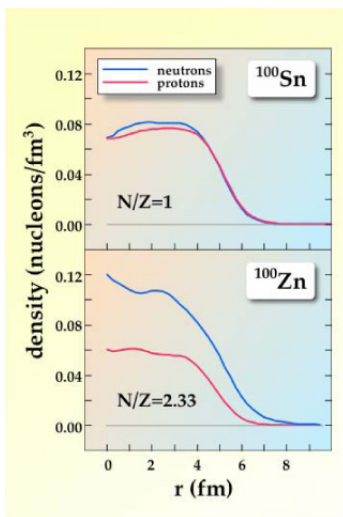


Figure 3.1: Calculated densities of protons and neutrons in ^{100}Sn ($Z = N = 50$, top) and ^{100}Zn ($Z = 30$, $N = 70$, bottom). This figure is taken from Ref. [7]. The neutron density extends much further out in ^{100}Zn (neutron skin). The calculations were done in the framework of density functional theory.

of unitary asymmetric Fermi gases in the uniform system, and introduce Chevy's variational solution to the $N+1$ body problem. We will then discuss the application to trapped gases. Finally, we will review the experimental work on spin-polarized Fermi gases.

Throughout this chapter, we will refer to the atoms in different hyperfine states as spin-up (\uparrow) and spin-down (\downarrow) atoms. N_σ denotes the particle number of the $\sigma = \uparrow, \downarrow$ species, and n_σ denotes the density. In the case of asymmetric systems, we assume $N_\uparrow > N_\downarrow$, and define the concentration $x = n_\downarrow/n_\uparrow$. The polarization is defined as $P = (N_\uparrow - N_\downarrow)/(N_\uparrow + N_\downarrow)$, and it measures the asymmetry of the system.

3.1 Symmetric Fermi Gases

The ability to control the scattering length with Feshbach resonances allows cold Fermi gases to probe different regimes of superfluidity. In this section, we will review the theory of two-component Fermi gases with equal population. We will briefly describe fermionic superfluidity in the molecular BEC

($k_F a \ll 1$) and the weakly attractive BCS ($-k_F a \ll 1$) regimes, and then discuss superfluidity in the unitary limit ($|a| \rightarrow \infty$).

3.1.1 Molecular BEC Regime

As discussed in the previous chapter, across Feshbach resonance, a positive scattering length $a > 0$ is associated with the formation of a bound state in low-energy two-body collisions. Therefore, in a two-component Fermi gas on the $a > 0$ side of the resonance, two atoms with opposite spins will form a bound, bosonic molecule⁵. The size of these molecules is given by the scattering length a . Since they are bosonic in nature, these molecules condense to form a Bose-Einstein condensate (BEC) at low temperatures. Therefore, the limit $k_F a \ll 1$ is called the molecular BEC regime.

The theory of a non-interacting BEC in the uniform system is well established, and can be found in standard many-body physics textbooks, such as Ref. [39]. For bosons of density n and mass M , the critical temperature is given by $T_c = (2\pi/(k_B M)) (n/\zeta(3/2))^{2/3}$, where $\zeta(3/2) \simeq 2.612$. In the case of symmetric Fermi gases, $n = n_\uparrow = n_\downarrow$, and $M = 2m$, so in terms of the Fermi temperature $T_F = E_F$, one has

$$T_c = 0.218 T_F. \quad (3.1)$$

Below this temperature, a superfluid BEC forms, and the condensate fraction is given by [39]:

$$\frac{N_C}{N_0} = \begin{cases} 1 - (T/T_c)^3 & \text{for } T \leq T_c, \\ 0 & \text{for } T > T_c. \end{cases} \quad (3.2)$$

3.1.2 Weakly-Attractive BCS Regime

In the regime of weak attraction, $-k_F a \ll 1$, the interaction is not strong enough to bind a pair of atoms into a molecule. However, as Bardeen, Cooper, and Schrieffer (BCS) have shown, the Fermi surface is unstable to

⁵Experimentally, two different regimes can be achieved with positive scattering lengths, representing two different branches of the many-body problem for $a > 0$ [44]. If one starts from $a = 0$, and adiabatically ramps up the scattering length, the configuration of a weakly repulsive gas is achieved [6], provided that one stays far away from the resonance. On the other hand, if one starts from a negative scattering length $a < 0$, and crosses the resonance adiabatically to the side $a > 0$, conversion of atomic pairs into molecules is ensured. Alternatively, molecular formation can be achieved by cooling down a gas with a fixed $a > 0$. In this work, the molecular regime will be assumed for $a > 0$.

3.1. Symmetric Fermi Gases

pairing in the presence of an arbitrarily weak attraction [2]. Therefore, spin-up and spin-down atoms near the Fermi surface with back-to-back momenta form bosonic bound states, known as Cooper pairs. The Cooper pairs are localized in momentum space, and thus delocalized in coordinate space, in contrast to the tightly bound molecules on the BEC side. Due to back-to-back pairing near the Fermi surface, Cooper pairs have zero center-of-mass momentum.

At low temperatures, these Cooper pairs condense to form a superfluid. This is the same mechanism through which conventional BCS superconductivity occurs. Therefore, the regime of negative scattering lengths, $-k_F a \ll 1$, away from resonance is called the BCS regime. Condensation occurs below a critical temperature T_c , and fermionic superfluid excitations display a gap in the spectrum $\sqrt{(\epsilon_{\mathbf{p}} - \mu)^2 + \Delta^2}$, where $\epsilon_{\mathbf{p}}$ is the free-particle dispersion, and Δ the superfluid gap. The critical temperature and superfluid gap for a BCS superfluid in the weakly-interacting limit have been calculated perturbatively [30]. The critical temperature is given by

$$T_c = \left(\frac{2}{e}\right)^{7/3} \frac{e^\gamma}{\pi} T_F \pi^{2k_F a} \approx 0.28 T_F e^{\pi/2k_F a}, \quad (3.3)$$

where $\gamma \approx 0.577$ is the Euler-Mascheroni constant. Note that the critical temperature grows exponentially with $1/k_F a$. Due to the exponential suppression and low densities, the ability to obtain large scattering lengths with Feshbach resonances is crucial to achieving superfluidity in fermionic atoms away from the BEC regime.

The gap in the BCS theory at $T = 0$ is given by

$$\Delta = \frac{\pi}{e^\gamma} T_c \approx 1.76 T_c. \quad (3.4)$$

The gap can be thought of as the energy necessary to break a Cooper pair.

3.1.3 Crossover Regime at Unitarity

As the magnetic field is tuned towards the resonance from either side, $B \rightarrow B_0$, the scattering length diverges, $|a| \rightarrow \infty$, and the Fermi gas enters the unitary regime. If one begins from the BCS side, as the Fermi gas approaches the resonance, the spin-up and spin-down atoms feel an increasingly strong attraction that bind them into Cooper pairs. If one approaches the resonance from the BEC side, the molecules formed by atoms of opposite spins increase in size, with a decreasing binding energy $E_b \rightarrow 0$. The transition between the BEC and BCS superfluids is smooth. Resonant pairs of spin-up and

spin-down fermions form, which are a crossover between a molecule (with the binding energy $E_b = 0$) and a delocalized BCS Cooper pair.

The physics of the crossover superfluid is universal. As discussed in Section 2.4.2, the energy per particle is $E/N = \xi 3/5 E_F$, where E_F is the non-interacting Fermi energy. The universal parameter $\xi = 0.42(1)$ has been calculated by Monte Carlo (MC) methods [13, 43], and an improved value of $\xi = 0.40(1)$ has been obtained [14]. This is in good agreement with experimental values [3, 33, 40, 56, 57]. The superfluid gap at unitarity has also been calculated using MC methods [13], and is found to be

$$\frac{\Delta}{E_F} = 0.50(2). \quad (3.5)$$

3.2 Unitary Asymmetric Fermi Gases: Uniform System

The fully-paired superfluid is the ground state of a unitary Fermi gas with $N_\uparrow = N_\downarrow$. An imbalance in the spin population, e.g. $N_\uparrow > N_\downarrow$, is created by a mismatch in the chemical potentials, $\mu_\uparrow > \mu_\downarrow$. When an asymmetry in the population is introduced, it may result in the breakdown of the Cooper pairs that form the condensate, and other phases can be energetically favoured. Therefore, the phase diagram of unitary asymmetric Fermi gases can be very rich. This section will discuss the effects of asymmetry on the phases in the uniform system. We will begin by discussing a maximal extent of the fully-paired superfluid in the presence of mismatched chemical potentials. Next, we will discuss the phase diagram of unitary asymmetric Fermi gases in the uniform system. The discussion of this section serves to motivate Chevy's $N + 1$ body problem, which we will describe in the next section.

3.2.1 Breakdown of the Fully-Paired Superfluid

In an asymmetric gas, the presence of a chemical potential difference, $\mu_\uparrow > \mu_\downarrow$, creates stress on pairing. Due to the pairing gap, Cooper pairs are robust to a certain extent of the mismatch. The maximal possible extent of fully-paired superfluidity corresponds to the point where the mismatch is large enough to destroy the Cooper pairs:

$$\mu_\uparrow - \mu_\downarrow \geq 2\Delta. \quad (3.6)$$

This is a more conservative limit than the Clogston-Chandrasekhar result in the weakly-interacting BCS regime $k_F|a| \ll 1$, which has the critical condition $\mu_\uparrow - \mu_\downarrow \geq \sqrt{2}\Delta$ [16, 19].

3.2. Unitary Asymmetric Fermi Gases: Uniform System

Dividing both sides of Eq. (3.6) by $\mu_\uparrow + \mu_\downarrow$, and using the relation $(\mu_\uparrow + \mu_\downarrow)/2 = \xi E_F$, Eq. (3.6) becomes $(1 - \mu_\downarrow/\mu_\uparrow)/(1 + \mu_\downarrow/\mu_\uparrow) \geq \Delta/\xi E_F$. Solving the inequality for $\mu_\downarrow/\mu_\uparrow$ with $\xi = 0.42(1)$ and Eq. (3.5), one finds that the fully-paired superfluid is has to cease for [9, 20]

$$\frac{\mu_\downarrow}{\mu_\uparrow} \leq \eta_c \equiv \frac{\xi - \Delta/E_F}{\xi + \Delta E_F} = -0.09(3). \quad (3.7)$$

The condition of Eq. (3.6) sets the most conservative limit for the superfluid. It is purely based on energetics consideration, without taking interactions into account. The actual limit on the right hand side of Eq. (3.6) may be less than 2Δ . As a result, the actual extent of the superfluid phase may be limited to larger $\mu_\downarrow/\mu_\uparrow$. Therefore, the range of the fully paired superfluid is

$$\eta_c \leq \eta_\alpha < \frac{\mu_\downarrow}{\mu_\uparrow} \leq 1, \quad (3.8)$$

where η_α is the actual phase boundary for the superfluid, see Fig. 3.2.

3.2.2 Phases in Asymmetric Fermi Gases

Despite the lack of analytic solution, it is possible to investigate the $T = 0$ phase diagram of unitary asymmetric Fermi gases based on very general arguments. The most general phase diagram possible for unitary asymmetric Fermi gases is given by Fig. 3.2 a). It consists of the following three regions: a fully-polarized region (FP) extending for $\mu_\downarrow/\mu_\uparrow < \eta_\beta$, a partially-polarized region (PP) for $\eta_\beta < \mu_\downarrow/\mu_\uparrow < \eta_\alpha$, in which different partially-polarized phases may be realized, and a fully-paired region (SF) for $\eta_\beta < \mu_\downarrow/\mu_\uparrow \leq 1$. If the true phase diagram would have an empty PP region, then one has $\eta_\beta = \eta_\alpha$.

At $T = 0$, the ground state of a fully-polarized gas is simply the spin-up Fermi sea. In the fully-paired case, the ground state is the crossover superfluid. Therefore, each of these two regions consists of a single phase.

Multiple partially-polarized phases and phase transitions may be present in the PP region. At any given $\eta_\beta < \mu_\downarrow/\mu_\uparrow < \eta_\alpha$, the gas is in the configuration with the minimal energy. One of the most natural configurations for consideration is the partially-polarized Fermi liquid, in which the minority species interact resonantly with the majority species without forming pairs. Polarized superfluid states have also been proposed, such as the Fulde-Ferrell-Larkin-Ovchinnikov (FFLO or LOFF) state [28, 36]. The FFLO state possesses Cooper pairs with nonzero center-of-mass momenta, and it

3.2. Unitary Asymmetric Fermi Gases: Uniform System

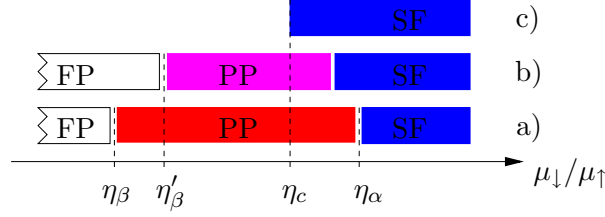


Figure 3.2: Phase Diagram of Unitary Fermi Gases. a) The most generic phase diagram, which consists of a fully-polarized normal phase (FP), for $\mu_{\downarrow}/\mu_{\uparrow} < \eta_{\beta}$, a partially-polarized region with one or more phases (PP) across $\eta_{\beta} < \mu_{\downarrow}/\mu_{\uparrow} < \eta_{\alpha}$, and a fully-paired superfluid phase (SF) for $\eta_{\alpha} < \mu_{\downarrow}/\mu_{\uparrow}$. b) An approximation that assumes the PP region consists of only the partially-polarized normal Fermi liquid. In this approximation, the PP region extends to a smaller range of $\mu_{\downarrow}/\mu_{\uparrow}$, and the FP-PP phase boundary η'_{β} is larger, $\eta'_{\beta} \geq \eta_{\beta}$. c) The superfluid phase has a maximal range $-0.09 \approx \eta_c < \mu_{\downarrow}/\mu_{\uparrow}$, which is the conservative limit of Eq. (3.8).

has also been suggested that a supersolid FFLO phase may be found in unitary Fermi gases [10]. Other proposals include the breached pair or Sarma state [37, 50], states with a deformed Fermi surface [53], and an induced intraspecies p -wave superfluid [11].

An important question is whether the phase diagram Fig. 3.2 a) contains an empty PP region. The lack of knowledge of the PP region hinders us from knowing the exact values of η_{α} and η_{β} . However, if one can establish bounds on these values, then it is possible to determine whether the phase diagram contains partially-polarized phases.

In Section 3.2.1, we found the maximal limit of the fully-paired superfluid, $\eta_c < \mu_{\downarrow}/\mu_{\uparrow}$, and Eq. (3.8) sets a lowerbound $-0.09 \approx \eta_c \leq \eta_{\alpha} < \mu_{\downarrow}/\mu_{\uparrow}$. The natural next step is to establish an upper bound on η_{β} . To do so, we make an approximation that the PP region contains only the partially-polarized normal Fermi liquid, see Fig. 3.2 b). The actual phase diagram can contain a larger PP region. In this approximation, the FP-PP transition, η'_{β} , must satisfy $\eta_{\beta} \leq \eta'_{\beta}$. This transition point corresponds to the addition of a single spin-down atom to a fully-polarized spin-up Fermi sea, which is referred to as the $N+1$ body problem. If one can show $\eta'_{\beta} < \eta_c$, then the inequality $\eta_{\beta} \leq \eta'_{\beta} < \eta_c \leq \eta_{\alpha}$ requires the existence of one or more partially-polarized phases. On the other hand, if $\eta'_{\beta} > \eta_c$, then one cannot make any conclusion.

In the next section, we will outline Chevy's variational solution to the

$N + 1$ body problem.

3.3 $N + 1$ Body Problem in the Uniform System

In this section, we discuss the problem a single spin-down atom interacting resonantly with a spin-up Fermi sea in the uniform system. This is referred to as the $N + 1$ body problem. This is the $x \rightarrow 0$ limit of the partially-polarized normal state, and the corresponding chemical potential ratio, $\eta'_\beta = \eta \equiv (\mu_\downarrow/\mu_\uparrow)_{N+1}$, denotes the transition point between a partially-polarized normal Fermi liquid and the fully-polarized normal state. As discussed previously, due to competitions with other phases, the actual extent of the fully-polarized region may be shorter, $\mu_\downarrow/\mu_\uparrow < \eta_\beta \leq \eta$. Therefore, the knowledge of the $N + 1$ body energy may establish whether one or more partially-polarized phases are found in unitary asymmetric Fermi gases. In this section, we describe Chevy's variational calculation of the $N + 1$ body energy in the uniform system.

3.3.1 Variational Calculation of the $N + 1$ Body Energy

In the unitary regime $1/k_F a = 0$, the energy of adding a single impurity to the majority Fermi sea is universal, $E = \mu_\downarrow = \eta\mu_\uparrow$, where $\mu_\uparrow = E_F$. Here we outline the variational calculation of the $N + 1$ body problem in the uniform system, an approach introduced by Chevy⁶ [17, 18, 22]. We consider the addition of a single spin-down fermion carrying a momentum \mathbf{p} to a Fermi sea of the spin-up fermions.

For S -wave interactions, the Hamiltonian H is given by

$$H = \sum_{\mathbf{k}, \sigma} \epsilon_{\mathbf{k}} a_{\mathbf{k}, \sigma}^\dagger a_{\mathbf{k}, \sigma} + \frac{g(\Lambda)}{V} \sum_{\mathbf{k}, \mathbf{k}', \Delta \mathbf{k}} a_{\mathbf{k} + \Delta \mathbf{k}, \uparrow}^\dagger a_{\mathbf{k}' - \Delta \mathbf{k}, \downarrow}^\dagger a_{\mathbf{k}', \downarrow} a_{\mathbf{k}, \uparrow}, \quad (3.9)$$

where $\epsilon_{\mathbf{k}} = k^2/2m$, $a_{\mathbf{k}, \sigma}$ annihilates a particle of spin σ and momentum \mathbf{k} , and $g(\Lambda)$ is the S -wave coupling constant. As discussed in Section. 2.3, the contact interaction of Eq. (3.9) requires a renormalization of the coupling constant. Therefore, in the subsequent calculation, we introduce an ultraviolet cutoff Λ in momentum space. Then, according to Eq. (2.35), the

⁶ The first calculation was performed for the addition of a single impurity at zero momentum $\mathbf{p} = \mathbf{0}$ [17, 18]. The calculation can be generalized to $\mathbf{p} \neq \mathbf{0}$ [22], and provides additional insight. We will consider general \mathbf{p} .

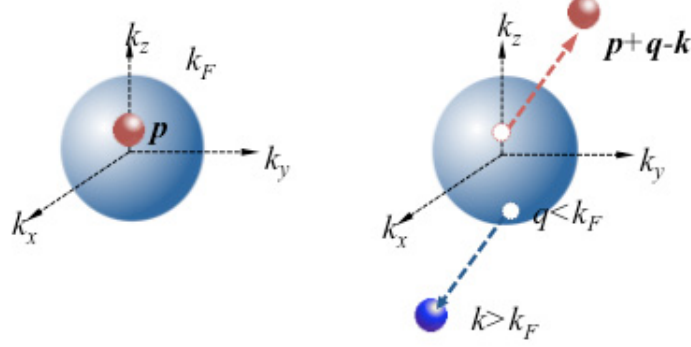


Figure 3.3: Graphical representation of the components of the trial wavefunction Eq. (3.11). On the left is the state $|\Omega\rangle$, which is a spin-up Fermi sea with a spin-down impurity at momentum \mathbf{p} . On the right is the state $|\mathbf{k}, \mathbf{q}\rangle$, in which a spin-up atom with momentum \mathbf{q} below the Fermi surface ($q < k_F$) is excited to a momentum \mathbf{k} above the Fermi surface ($k > k_F$). The impurity now has a momentum $\mathbf{p} + \mathbf{q} - \mathbf{k}$ to satisfy momentum conservation.

renormalized coupling constant can be written as

$$\frac{1}{g(\Lambda)} = \frac{m}{4\pi a} - \frac{1}{V} \sum_{\mathbf{k}} \frac{1}{2\epsilon_{\mathbf{k}}}. \quad (3.10)$$

Keeping up to one-particle-one-hole excitations, the trial state has the following form

$$|\psi\rangle = \phi_0 |\Omega\rangle + \sum_{\mathbf{k}, \mathbf{q}} \phi_{\mathbf{k}, \mathbf{q}} |\mathbf{k}, \mathbf{q}\rangle. \quad (3.11)$$

where $|\Omega\rangle$ is a spin-up Fermi sea with a spin-down impurity at momentum \mathbf{p} , and $|\mathbf{k}, \mathbf{q}\rangle$ is the perturbed Fermi sea where a spin-up atom with momentum \mathbf{q} below the Fermi surface ($q < k_F$) is excited to a momentum \mathbf{k} above the Fermi surface ($k > k_F$). The impurity then has a momentum $\mathbf{p} + \mathbf{q} - \mathbf{k}$ to satisfy momentum conservation. The components of the trial state wavefunction are represented graphically in Fig. 3.3.

We write Eq. (3.9) as $H = H_0 + V$, where H_0 is the non-interacting Hamiltonian, and V is the interacting part. We proceed to calculate the energy of the trial state $\langle H \rangle = \langle H_0 \rangle + \langle V \rangle$, with

$$\langle H_0 \rangle = |\phi_0|^2 \epsilon_{\mathbf{p}} + \sum_{\mathbf{k}, \mathbf{q}} |\phi_{\mathbf{k}, \mathbf{q}}|^2 (\epsilon_{\mathbf{k}} + \epsilon_{\mathbf{p} + \mathbf{q} - \mathbf{k}} - \epsilon_{\mathbf{q}}), \quad (3.12)$$

3.3. $N + 1$ Body Problem in the Uniform System

where we have subtracted the energy of the non-interacting ground state $\sum_{q < k_F} \epsilon_{\mathbf{q}}$, and

$$\begin{aligned} \langle V \rangle &= \frac{g(\Lambda)}{V} \left(\sum_{\mathbf{q}} |\phi_0|^2 + \sum_{\mathbf{q}, \mathbf{k}} (\phi_0 \phi_{\mathbf{k}, \mathbf{q}}^* + \phi_0^* \phi_{\mathbf{k}, \mathbf{q}}) + \sum_{\mathbf{q}, \mathbf{k}, \mathbf{k}'} \phi_{\mathbf{k}, \mathbf{q}} \phi_{\mathbf{k}', \mathbf{q}}^* \right) \\ &\quad + \frac{g(\Lambda)}{V} \sum_{\mathbf{q}, \mathbf{q}', \mathbf{k}} \phi_{\mathbf{k}, \mathbf{q}}^* \phi_{\mathbf{k}, \mathbf{q}'}. \end{aligned} \quad (3.13)$$

The sums over \mathbf{q} and \mathbf{k} are implicitly restricted to $q < k_F$ and $k_F < k$. As we will check later, $\phi_{\mathbf{k}, \mathbf{q}} \sim 1/k^2$ for large k . Most of the unrestricted sums over \mathbf{k} diverge as $\Lambda \rightarrow \infty$. This divergent behavior is regularized by the renormalization of the coupling constant $g(\Lambda) \sim -1/\Lambda$ for $1/a = 0$. However, the last sum of $\langle V \rangle$ converges, and gives zero contribution when multiplied by $g(\Lambda)$. Therefore, this term does not contribute to the energy, and we can omit it from the rest of the calculation.

Minimizing $\langle H \rangle$ with respect to ϕ_0 and $\phi_{\mathbf{k}, \mathbf{q}}$ yields the following set of equations:

$$E\phi_0 = \frac{g(\Lambda)}{V} \sum_{q < k_F} \left(\phi_0 + \sum_{k > k_F} \phi_{\mathbf{k}, \mathbf{q}} \right) + \epsilon_{\mathbf{p}} \phi_0, \quad (3.14)$$

$$E\phi_{\mathbf{k}, \mathbf{q}} = \phi_{\mathbf{k}, \mathbf{q}} (\epsilon_{\mathbf{k}} + \epsilon_{\mathbf{p} + \mathbf{q} - \mathbf{k}} - \epsilon_{\mathbf{q}}) + \frac{g(\Lambda)}{V} \left(\phi_0 + \sum_{k' > k_F} \phi_{\mathbf{k}', \mathbf{q}} \right), \quad (3.15)$$

where E is the $N + 1$ body energy, and also the Lagrange multiplier associated with the variational calculation. To solve these equations, we define $\chi(\mathbf{q}) \equiv \phi_0 + \sum_{k > k_F} \phi_{\mathbf{k}, \mathbf{q}}$, and solve for $\phi_{\mathbf{k}, \mathbf{q}}$ in Eq. (3.15):

$$\phi_{\mathbf{k}, \mathbf{q}} = \frac{g(\Lambda)}{V} \frac{\chi(\mathbf{q})}{E - (\epsilon_{\mathbf{k}} + \epsilon_{\mathbf{p} + \mathbf{q} - \mathbf{k}} - \epsilon_{\mathbf{q}})}. \quad (3.16)$$

This verifies the large k behavior for $\phi_{\mathbf{k}, \mathbf{q}} \sim 1/k^2$. Inserting Eq. (3.16) in the definition of $\chi(\mathbf{q})$ allows us to eliminate $\phi_{\mathbf{k}, \mathbf{q}}$. Finally, we can use Eq. (3.14) to obtain the self-consistent equation for E :

$$E = \epsilon_{\mathbf{p}} + \frac{1}{V} \sum_{q < k_F} \frac{1}{\frac{1}{g(\Lambda)} + \frac{1}{V} \sum_{k > k_F} \frac{1}{\epsilon_{\mathbf{k}} + \epsilon_{\mathbf{p} + \mathbf{q} - \mathbf{k}} - \epsilon_{\mathbf{q}} - E}}. \quad (3.17)$$

3.3. $N + 1$ Body Problem in the Uniform System

Using Eq. (3.10) for the expression of $g(\Lambda)$ leads to

$$E = \epsilon_{\mathbf{p}} + \frac{1}{V} \sum_{q < k_F} \frac{1}{\frac{m}{4\pi a} + \frac{1}{V} \sum_{\mathbf{k}} \left(\frac{\Theta(k^2/k_F^2 - 1)}{\epsilon_{\mathbf{k} + \epsilon_{\mathbf{p} + \mathbf{q} - \mathbf{k}} - \epsilon_{\mathbf{q}} - E} - \frac{1}{2\epsilon_{\mathbf{k}}} \right)}. \quad (3.18)$$

Alternatively, we can write the above equation in the following form,

$$E = \epsilon_{\mathbf{p}} + \Sigma \left(\frac{1}{k_F a}, \epsilon_{\mathbf{p}}, E \right), \quad (3.19)$$

where the self-energy $\Sigma(1/k_F a, \epsilon_{\mathbf{p}}, E)$ is the second term in the right-hand side of Eq. (3.18) [22]. The self-energy has the following form

$$\Sigma \left(\frac{1}{k_F a}, \epsilon_{\mathbf{p}}, E \right) = \left(\frac{2\pi^2}{mk_F} \right) \frac{1}{V} \sum_{q < k_F} \frac{1}{\frac{\pi}{2k_F a} + I_0 \left(\frac{|\mathbf{p} + \mathbf{q}|}{k_F}, \frac{\epsilon_{\mathbf{q}} + E}{E_F} \right)}, \quad (3.20)$$

where we have defined $I_0(|\mathbf{v}|, \omega) \equiv \frac{1}{2\pi} \int d^3k \left(\frac{\Theta(k^2 - 1)}{k^2 + |\mathbf{v} - \mathbf{k}|^2 - \omega} - \frac{1}{2k^2} \right)$. For $\mathbf{p} = \mathbf{0}$, we have $v < 1$, and the dimensionless function $I_0(v, \omega)$ has the following analytic expression⁷:

$$\begin{aligned} I_0(v < 1, \omega) &= -\frac{1}{2} - \frac{\sqrt{v^2 - 2\omega}}{2} \text{ArcCot} \left(\frac{2 + v}{\sqrt{v^2 - 2\omega}} \right) \\ &+ \frac{\sqrt{v^2 - 2\omega}}{4} \left[\text{ArcTan} \left(\frac{2 - v}{\sqrt{v^2 - 2\omega}} \right) - \text{ArcTan} \left(\frac{2 + v}{\sqrt{v^2 - 2\omega}} \right) \right] \\ &+ \frac{2 - \omega}{8v} \log \left(\frac{2 - 2v + v^2 - \omega}{2 + 2v + v^2 - \omega} \right). \end{aligned} \quad (3.21)$$

3.3.2 BEC and BCS Limit of the Chevy Equation

In the case of $\mathbf{p} = \mathbf{0}$, we can check that the trial state recovers the correct result in the limits $a \rightarrow 0^-$ and $a \rightarrow 0^+$. First, consider the weakly-interacting BCS limit, $a \rightarrow 0^-$. For $a < 0$, the self-energy Σ of Eq. (3.20) has no poles. Therefore, the energy of the impurity in the limit $1/k_F a \rightarrow -\infty$ is

$$E = \frac{4\pi a N}{m} \frac{1}{V} + O(a^2), \quad (3.22)$$

⁷A generalized form of this integral, $I(\gamma, |\mathbf{v}|, \omega)$, is discussed in Section 5.1.2, and $I_0(|\mathbf{v}|, \omega) = I(0, |\mathbf{v}|, \omega)$ for $v < 1$. For the derivation of the analytic form of $I(\gamma, |\mathbf{v}|, \omega)$, we refer to Section 5.1.2.

3.3. $N + 1$ Body Problem in the Uniform System

where $N = \sum_{q < k_F} 1$ is the number of the majority atoms. Therefore, we recover the mean-field correction to the energy, $\frac{4\pi a}{m} \frac{N}{V}$, in the limit of weak interactions. For $1/k_F a \gg 1$, the self-energy Σ develops poles at $-E/E_F \gg 1$, which correspond to the emergence of molecular bound states. For $|E|/E_F \gg 1$,

$$I_o \left(\frac{|\mathbf{p} + \mathbf{q}|}{k_F}, \frac{\epsilon_{\mathbf{q}} - |E|}{E_F} \right) = -\frac{\pi}{2\sqrt{2}} \sqrt{\frac{|E|}{E_F}} + O \left(\left(\frac{|E|}{E_F} \right)^{-1/2} \right). \quad (3.23)$$

Therefore, the poles occur at

$$E = -E_B = -\frac{1}{ma^2}, \quad (3.24)$$

and we recover the molecular binding energy in the BEC limit.

3.3.3 $N + 1$ Body Energy at $\mathbf{p} = \mathbf{0}$

Due to resonant interactions, the spin-down particle dressed in a spin-up Fermi sea acts as a quasiparticle with a polaron energy and effective mass that differs from those of a bare particle. This quasiparticle is referred to as a Fermi polaron [45, 46, 51]. In the case of $\mathbf{p} = \mathbf{0}$, Eq. (3.17) gives the ground state energy of the polaron, and has the following diagrammatic representation:

$$E = \text{[diagram 1]} + \text{[diagram 2]} + \text{[diagram 3]} + \dots \quad (3.25)$$

The self-consistent equation, Eq. (3.17), at $\mathbf{p} = \mathbf{0}$ can be solved easily with the aid of Eqs. (3.19)-(3.21), and yields $\eta = -0.607$, confirming the value found in Chevy's calculation [17].

The variational $1p1h$ η value agrees very well with the fixed-node diffusion Monte Carlo result $\eta \approx -0.59$ [13, 38, 43] and the diagrammatic Monte Carlo result $\eta \approx -0.615$ [45, 46]. In addition, Combescot and Giraud showed that $2p2h$ and higher-order contributions are small due to nearly perfect destructive interference in the higher order contributions [21]. In their full many-body treatment, they found the second-order contribution brings typically a 10^{-2} correction to the first order one, and estimated the third order correction to be at most of the order 10^{-4} . Based on these findings, one can conclude that the variational wavefunction gives a very good estimate to the ground-state energy of the $N + 1$ body system.

3.3. $N + 1$ Body Problem in the Uniform System

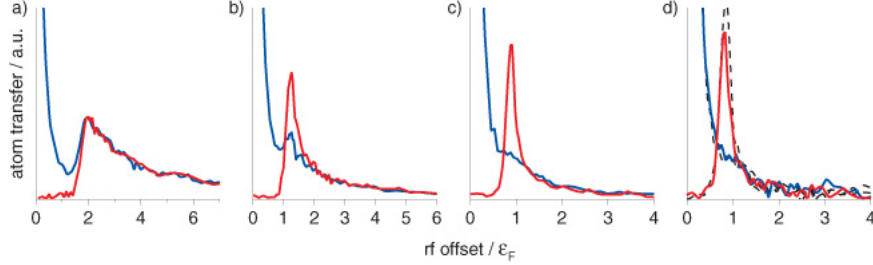


Figure 3.4: RF spectroscopy on polarons. The figure is taken from Ref. [51]. The spectra are spatially resolved and 3D reconstructed. The majority ($|1\rangle$) spectrum is shown in blue, and the minority ($|3\rangle$) spectrum is shown in red. The local concentration was $x = 0.05(2)$ for all spectra. (a) Spectra for $1/k_F a = 0.76(2)$ in the molecular regime. The overlap of both spectra signals molecule pairing. (b) Spectra for $1/k_F a = 0.43(1)$ and (c) $1/k_F a = 0.20(1)$ show the emergence of the polaron, signaled by a distinctive peak in the minority spectrum. (d) Spectra for $1/k_F a = 0$ at unitarity. The peak location gives the polaron energy. The dashed lines in (d) give the spectra when $|1\rangle$ and $|3\rangle$ are switched.

In addition to the theoretical results, the polaron energy has also been measured experimentally via RF spectroscopy [51]. In this experiment, the lowest hyperfine state $|1\rangle$ of ${}^6\text{Li}$ atoms is used as the majority atoms, and the hyperfine state $|3\rangle$ is used as the impurity. About 5×10^6 atoms were prepared at $T = 0.14(3)T_F$. At resonance, RF spectroscopy was performed by transferring the impurity atoms and the majority atoms into an empty state $|2\rangle$, accessible to both species. RF transitions for a local concentration $x = n_{\downarrow}/n_{\uparrow} = 0.05(2)$ are measured for both species, and shown in Fig. 3.4. In all cases, the bulk of the majority spectrum is found at zero offset. Attractions between the two species leads to a shift in the spectra: the RF photon must supply additional energy to transfer a particle into the final state. At unitarity, a narrow peak in the minority spectrum, which is not matched by the majority spectrum, see Fig. 3.4 (d), reveals the formation of the Fermi polaron. The location of the peak gives the polaron energy, $E = -0.64(7)E_F$. In the case where $|1\rangle$ serves as the impurity, the polaron energy is $E = -0.72(9)E_F$. The experimental values agree well with $\eta = -0.607$, and gives further support to the validity of the variational wavefunction.

3.4. *Towards General Asymmetry: The $N + M$ Body System as a Landau Fermi Liquid*

3.3.4 On the Existence of Partially-Polarized Phases

Following the discussion of Section 3.2.2, we now have the following inequality:

$$\eta_\beta \leq \eta'_\beta = \eta = -0.607 < -0.09(3) \leq \eta_\alpha. \quad (3.26)$$

The strict inequality $\eta_\beta < \eta_\alpha$ requires the existence of one or more partially-polarized phases in the uniform system.

3.3.5 Effective Mass of the Fermi Polaron

The ground state energy of the quasiparticle is $\eta E_F < 0$, differing from $E = 0$ of the bare particle. The small p behavior in the dispersion relation of the spin-down impurity is modified by the effective mass m^* . The dispersion relation for the polaron has the form

$$E(p) \approx \eta E_F + \frac{p^2}{2m^*}. \quad (3.27)$$

To find the effective mass, one can expand the left hand side of Eq. (3.19) in small p , $E(p) \sim \eta E_F + p^2/2m^*$, and take derivatives of both sides. This gives the following equation for the effective mass [22]:

$$\frac{m^*}{m} = \frac{1 - \frac{\partial \Sigma}{\partial E}}{1 + \frac{\partial \Sigma}{\partial \epsilon_{\mathbf{p}}}}, \quad (3.28)$$

where the derivatives are taken for $p = 0$ and $E = \eta E_F$. In the unitary limit $1/k_F a \rightarrow 0$, the effective mass is found to be $m^*/m = 1.17$ [22].

3.4 Towards General Asymmetry: The $N + M$ Body System as a Landau Fermi Liquid

The discussion of the Fermi polaron in an $N+1$ body system gives us insight into the nature of the partially-polarized normal state. As one continues to add minority atoms into the system, these particles become quasiparticles dressed by resonant interactions with the surrounding majority Fermi sea. This is in contrast with the BEC and BCS limit. In the BCS regime, each spin-down impurity feels only a weak mean-field attraction from the spin-up Fermi sea, while in the BEC regime, the attraction is strong enough that each spin-down atom picks a spin-up partner to form a molecule.

The quasiparticles retain their Fermi statistics, but have a modified energy and effective mass. The addition of spin-down atoms build up a Fermi

3.4. Towards General Asymmetry: The $N + M$ Body System as a Landau Fermi Liquid

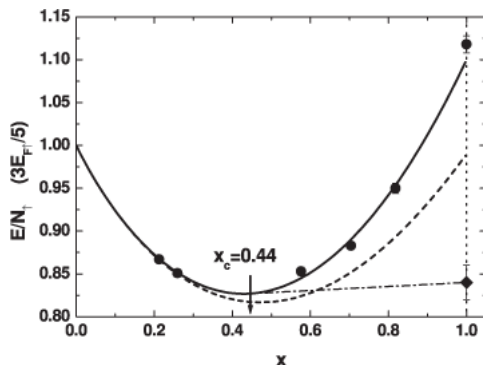


Figure 3.5: Equation of state of the asymmetric Fermi gas based on the MC results of Ref. [38]. This figure is taken from Ref. [38]. The circles are the MC results. The solid line is a polynomial best fit. The dashed line corresponds to the expansion, Eq. (3.29), with $\eta = -0.58(1)$ and $m^*/m = 1.04(3)$ obtained from the single-impurity MC calculations at $N_\uparrow = 33$. The dot-dashed line is the coexistence line between the normal and fully-paired superfluid states, and the arrow indicates the critical concentration x_c at the transition point. For $x = 1$, the energies of both the normal and superfluid (diamond) states are shown.

sea of these quasiparticles. Therefore, for $x \ll 1$, the energy of the normal state can be approximated by the form [38]

$$E_N(x, n_\uparrow) = \frac{3}{5} N_\uparrow E_F \left(1 + \frac{5}{3} \eta x + \frac{m}{m^*} x^{5/3} + \dots \right), \quad (3.29)$$

where $E_F = (6\pi^2 n_\uparrow)^{2/3} / 2m$ is the Fermi energy of the spin-up particles. The first term of the energy expansion corresponds to the energy of the non-interacting spin-up Fermi gas. The second term is the energy of adding the spin-down impurities, and the third term corresponds to the Fermi pressure of the quasiparticles with effective mass m^* . The next terms in this expansion are terms that account for the interactions between quasiparticles.

The solution to the $N + M$ body problem using a variational approach will be considered in Chapter V. Here, we will review the Monte Carlo (MC) calculations of $N + M$ body system [38, 43]. In Ref. [38], the energy of the Hamiltonian, Eq. (3.9), is obtained using MC methods for closed-shell configurations $M = N_\downarrow = 7, 19, 27, 33$ and $N = N_\uparrow = 27, 33$. The equation of state obtained from the calculations is shown in Fig. 3.5. The

3.4. Towards General Asymmetry: The $N + M$ Body System as a Landau Fermi Liquid

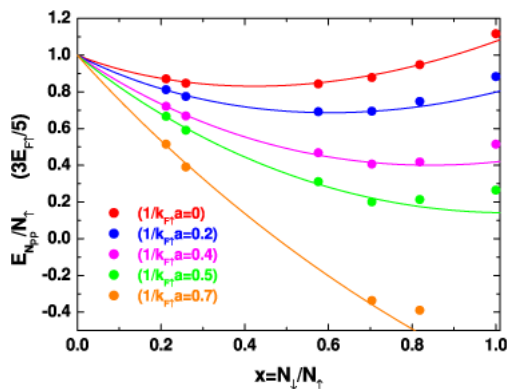


Figure 3.6: Equation of state of the asymmetric Fermi gas based on the MC results of Ref. [43]. This figure is taken from Ref. [43]. The solid lines correspond to best fits to the energy expansion, Eq. (3.30), with the values of η and m^* obtained from the single-impurity calculations. The energy is shown for several values of $1/k_F a$.

result is compared with the expansion, Eq. (3.29), with $\eta = -0.58(1)$ and $m^*/m = 1.04(3)$ obtained from the $N + 1$ body calculations at $N = 33$. We see that the expansion agrees well with the MC results up to values of x where the transition to the fully-paired superfluid phase takes place (see Section 3.5.2).

Ref. [43] performed very similar MC calculations, show in Fig. 3.6. The values $\eta = -0.59(1)$ and $m^*/m = 1.09(2)$ were extracted from single-impurity calculations, in agreement with Ref. [38], and the MC results of the equation of state are fitted to the form

$$E = \frac{3}{5} N_{\uparrow} E_F \left(1 + \frac{5}{3} \eta x + \frac{m}{m^*} x^{5/3} + Bx^2 \right), \quad (3.30)$$

with a higher-order term $B = 0.14$ that accounts for interactions between quasiparticles. From Fig. 3.6, we see this expansion agrees with the MC results up to large x . The MC results for the normal state indicate that the Landau Fermi-liquid seems to be an accurate description of the partially-polarized normal state.

3.5 Application to Trapped Fermi Gases

The discussion so far focuses on Fermi gases in the uniform system. Experimental studies employ harmonic traps to confine atomic gases, which introduce spatial variations of the densities and therefore separate phases in traps. In this section, we discuss the theory of trapped Fermi gases based on the Local Density Approximation (LDA). Next, we will apply the results obtained in the uniform system to traps in the limit of large particle numbers.

3.5.1 Local Density Approximation

In a trap containing a large number of particles, the density changes slowly on the length scale of the confining potential. Therefore, gradient terms may be neglected from the energy density functional. One can then approximate the energy density at each point by the one corresponding to a uniform gas at the local value of the density. The Local Density Approximation (LDA) introduces an effective local chemical potential

$$\mu_\sigma(\mathbf{r}) = \mu_\sigma^0 - V(\mathbf{r}), \quad (3.31)$$

where $\sigma = \uparrow, \downarrow$, and μ_σ^0 fix the total numbers of spin-up and spin-down particles.

Near phase boundaries where the densities can change rapidly, the LDA may cease to be accurate. Gradient terms will spread out these transition regions and result in surface tension near the boundaries [24]. The LDA also ceases to be accurate at small particle numbers. As we will discuss later, the breakdown of the LDA was observed experimentally in Refs. [40, 41].

3.5.2 Phase Separation and Density Profile in Trapped Fermi Gases

The effective chemical potentials of the LDA imply that a confining potential separates phases. The most general scenario contains a fully-paired superfluid core, and shells of polarized phases, where the inner shell is partially-polarized, and the outermost region is fully-polarized. This picture is consistent with the phase diagram discussed in Section 3.2.2, and agrees well with the experimental findings, see Fig. 3.7, which we will discuss in Section 3.6.

Before we move on to derive the density profile, we first discuss the qualitative picture as a trapped gas moves from being fully-polarized, $P = 1$,

3.5. Application to Trapped Fermi Gases

to being symmetric, $P = 0$. For small concentrations of spin-down particles, $N_\downarrow \ll N_\uparrow$, the superfluid phase does not exist. When the local concentration of spin-down particles at the center reaches a critical value, $x(\mathbf{r} = \mathbf{0}) = x_c$, a superfluid core emerges. The critical polarization, P_c , sets the maximum asymmetry for the superfluid core to exist. The superfluid needs to be in equilibrium with the surrounding phase, which therefore has to have the same concentration $x = x_c$ at the phase boundary. As $P \rightarrow 0$, the entire system becomes superfluid at $T = 0$.

The density profile of a trapped Fermi gas can be derived in the LDA, provided that one knows the equation of states of the phases. We follow Ref. [47] to construct the density profiles. Recall the unitary superfluid has the following energy density,

$$\epsilon_S(n_S) \equiv \frac{E_S}{N_S} = \xi \frac{3}{5} \frac{1}{2m} (6\pi^2 n_S)^{2/3}, \quad (3.32)$$

where $\xi = 0.42(1)$, and $n_S = n_\uparrow = n_\downarrow$ for the superfluid phase. We assume a generic form for the equation of state of the normal phase,

$$\frac{E_N}{N_\uparrow} \equiv \frac{3}{5} E_F \epsilon(x), \quad (3.33)$$

where $E_F = (6\pi^2 n_\uparrow)^{2/3}/2m$ is the local Fermi energy of the majority gas. We will assume an isotropic trap, $V(\mathbf{r}) = m\omega^2 r^2/2$. In this trap, the superfluid core extends for $0 < r < R_S$. The normal shell is partially-polarized for $R_S < r < R_\downarrow$, and fully polarized for $R_\downarrow < r < R_\uparrow$. In the case of an anisotropic trap, $V(\mathbf{r}) = 1/2m\omega^2 \sum_{i=x,y,z} \alpha_i^2 x_i^2$, a simple rescaling $\tilde{x}_i = \alpha_i x_i$ permits us to apply the same results in the coordinates $\tilde{\mathbf{x}}$.

In the LDA, the free energy is given by [47],

$$\begin{aligned} E &= 2 \int_{r < R_S} d^3r (\epsilon_S(n_S(\mathbf{r})) - \mu_S + V(\mathbf{r})) n_S(\mathbf{r}) \\ &\quad + \int_{R_S < r < R_\uparrow} d^3r \left(\frac{3}{5} E_F \epsilon(x(\mathbf{r})) n_\uparrow(\mathbf{r}) - \mu_\uparrow(\mathbf{r}) n_\uparrow(\mathbf{r}) - \mu_\downarrow(\mathbf{r}) n_\downarrow(\mathbf{r}) \right), \end{aligned} \quad (3.34)$$

where $\mu_\sigma(\mathbf{r}) = \mu_\sigma^0 - V(\mathbf{r})$, and $\mu_S = (\mu_\uparrow^0 + \mu_\downarrow^0)/2$.

The ground state of the system is determined by requiring that the energy functional, Eq. (3.34), is stationary with respect to variations of the densities and the phase boundary R_S . By varying the densities, Eq. (3.34)

3.5. Application to Trapped Fermi Gases

yields the following equations,

$$\mu_S = \xi \frac{1}{2m} (6\pi^2 n_S)^{2/3} + V(\mathbf{r}), \quad (3.35)$$

$$\mu_{\uparrow}^0 = E_F \left(\epsilon(x) - \frac{3}{5} x \epsilon'(x) \right) + V(\mathbf{r}), \quad (3.36)$$

$$\mu_{\downarrow}^0 = \frac{3}{5} E_F \epsilon'(x) + V(\mathbf{r}). \quad (3.37)$$

Requiring the energy functional, Eq. (3.34), to be stationary with respect to variation of R_S gives the following,

$$\left(n_S^2 \frac{\partial \epsilon_S}{\partial n_S} \right)_{R_S} = \frac{1}{2} \left(n_{\uparrow}^2 \frac{\partial \epsilon_N}{\partial n_{\uparrow}} + n_{\uparrow} n_{\downarrow} \frac{\partial \epsilon_N}{\partial n_{\downarrow}} \right)_{R_S}, \quad (3.38)$$

where $\epsilon_N \equiv \frac{E_N}{N_{\uparrow}} = \frac{3}{5} E_F \epsilon(x)$. This condition indicates that the pressure of the two phases must be equal at the boundary. With Eqs. (3.35)-(3.37), and $\mu_S = \frac{1}{2}(\mu_{\uparrow} + \mu_{\downarrow})$, Eq. (3.38) yields the following,

$$\epsilon(x_c) + \frac{3}{5}(1 - x_c)\epsilon'(x_c) - (2\xi)^{3/5} (\epsilon(x_c))^{2/5} = 0, \quad (3.39)$$

where x_c is the critical concentration of the normal phase at the phase boundary.

The conditions of chemical equilibrium, Eqs. (3.35)-(3.37), determine the densities. The superfluid density, $n_{\uparrow} = n_{\downarrow} = n_S$ for $r < R_S$, can be determined from Eq. (3.35). Eqs. (3.36)-(3.37) determine the concentration x in the partially-polarized region, $R_S < r < R_{\downarrow}$. In the fully-polarized region that extends to $R_{\downarrow} < r < R_{\uparrow}$, $x = 0$. Given x , Eq. (3.36) determines $n_{\uparrow}(\mathbf{r})$ and $n_{\downarrow}(\mathbf{r})$.

Next, we summarize the results. The spatially-independent quantities are ξ , x_c , μ_{\downarrow}^0 , μ_{\uparrow}^0 , R_S , R_{\downarrow} , and R_{\uparrow} . They are related by

$$0 = \epsilon(x_c) + \frac{3}{5}(1 - x_c)\epsilon'(x_c) - (2\xi)^{3/5} (\epsilon(x_c))^{2/5}, \quad (3.40)$$

$$R_S = \left(\frac{2}{m\omega^2} \right)^{1/2} \sqrt{\frac{\mu_{\uparrow}^0 \epsilon'(x_c) - \frac{5}{3} \mu_{\downarrow}^0 \delta \epsilon(x_c)}{\epsilon'(x_c) - \frac{5}{3} \delta \epsilon(x_c)}}, \quad (3.41)$$

$$R_{\downarrow} = \left(\frac{2}{m\omega^2} \right)^{1/2} \sqrt{\frac{\mu_{\uparrow}^0 \epsilon'(0) - \frac{5}{3} \mu_{\downarrow}^0}{\epsilon'(0) - \frac{5}{3}}}, \quad (3.42)$$

$$R_{\uparrow} = \left(\frac{2\mu_{\uparrow}}{m\omega^2} \right)^{1/2}, \quad (3.43)$$

3.6. Experiments with Spin-Polarized Fermi Gases

where we have defined $\delta\epsilon(x) \equiv \epsilon(x) - \frac{3}{5}x\epsilon'(x)$.

The density profile is then given by

$$0 = \left(\mu_{\uparrow}^0 \epsilon'(x) - \frac{5}{3} \mu_{\downarrow}^0 \delta\epsilon(x) \right) - \left(\epsilon'(x) - \frac{5}{3} \delta\epsilon(x) \right) V(\mathbf{r}), \quad (3.44)$$

$$n_{\uparrow}(\mathbf{r}) = \begin{cases} n_S(\mathbf{r}) \equiv \frac{1}{6\pi^2} \left(\frac{m(\mu_{\uparrow}^0 + \mu_{\downarrow}^0 - 2V(\mathbf{r}))}{\xi} \right)^{3/2} & 0 < r < R_S, \\ \frac{1}{6\pi^2} \left(\frac{2m(\mu_{\uparrow}^0 - V(\mathbf{r}))}{\delta\epsilon(x(\mathbf{r}))} \right)^{3/2} & R_S < r < R_{\downarrow}, \\ \frac{1}{6\pi^2} \left(2m(\mu_{\uparrow}^0 - V(\mathbf{r})) \right)^{3/2} & R_{\downarrow} < r < R_{\uparrow}, \end{cases} \quad (3.45)$$

$$n_{\downarrow}(\mathbf{r}) = \begin{cases} n_S(\mathbf{r}) & 0 < r < R_S, \\ x(\mathbf{r})n_{\uparrow}(\mathbf{r}) & R_S < r < R_{\downarrow}, \\ 0 & R_{\downarrow} < r < R_{\uparrow}. \end{cases} \quad (3.46)$$

3.5.3 Trapped Fermi Gases Containing Large Particle Numbers

In Section 3.4, we have constructed the equation of state for the normal Fermi liquid, $\epsilon(x) = 1 + 5/3\eta x + m/m^* x^{5/3} + Bx^2$. The polaron energy η constrains the equation of state for large asymmetries, and thus the phase structure in traps with large particle numbers. In the uniform system, $\eta = -0.607$, and in conjunction with $m^*/m = 1.09$ and $B = 0.14$ from Ref. [43], it leads⁸ to a critical concentration $x_c = 0.47$, and a critical polarization $P_c = (N_{\uparrow} - N_{\downarrow})/N_{tot} = 0.74$. These results are valid in traps containing large particle numbers.

3.6 Experiments with Spin-Polarized Fermi Gases

Experimental studies have been performed with spin-polarized Fermi gases by the MIT [54, 58, 59] and the Rice University [40, 41] groups. The two groups found differences in the observed phase structure and the critical polarization. The MIT experiment [54, 58, 59] observed phase separation in the trap, which contains a core with equal densities, surrounded by a

⁸Lobo *et al.* performed the first calculations of critical concentration and critical polarization. They obtained $\eta = -0.58(1)$ and $m^*/m = 1.04(3)$ (and set $B = 0$) from MC calculations of the $N + 1$ body problem (see Section 3.4), and with these values, $x_c = 0.44$ and $P_c = 0.77$ [38]. Ref. [47] obtained the same values using slightly different parameters, $\eta = -0.59(1)$, $m^*/m = 1.09(2)$, and $B = 0.14$ from Ref. [43].

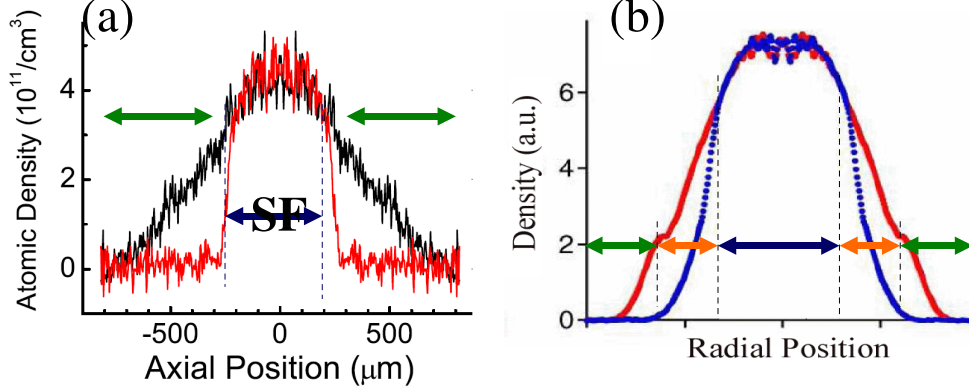


Figure 3.7: Density profiles of spin-polarized Fermi gases. (a) Center-line axial density $n(r = 0, z)$ in the Rice experiment [41]. The density of the majority atoms is given by the upper curve and the lower curve is for the minority atoms. The trap frequencies are $f_r = 325$ Hz and $f_z = 7.2$ Hz. The system contains $N \approx 10^5$ ${}^6\text{Li}$ atoms at a polarization $P = (N_\uparrow - N_\downarrow)/N = 0.35$. The system is found to contain a fully-paired core with equal densities, surrounded by a normal shell containing only the majority atoms. (b) Radial density profile $n(r, z = 0)$ measured at MIT [58]. The density of the majority atoms is given by the upper curve and the lower curve is for the minority atoms. The trap frequencies are $f_r = 110$ Hz and $f_z = 23$ Hz. The system contains $N \approx 10^7$ ${}^6\text{Li}$ atoms at a polarization $P = 0.46$. In this case, there exists a superfluid core of equal densities and an outer normal shell with only the majority atoms, as well as an intermediate partially-polarized phase containing both species. The figures are taken from Ref. [41, 58].

partially-polarized shell and an outer region of normal majority fermions. The equal-density core is confirmed to be superfluid by the presence of vortices [58]. Fig. 3.7 (b) shows a density profile from the MIT experiment. The study of vortices [58], *in situ* density distributions [59], and the condensate fraction [54, 58] established a critical polarization $P_c = 0.70(3)$. In addition, a tomography measurement found $x_c \approx 0.47$ [55].

The Rice experiment [40, 41] also observed phase separation, with a fully-paired core surrounded by normal majority fermions, but with a sharp phase boundary and extremely thin partially-polarized shell for low temperatures. Fig. 3.7 (a) shows a sample of the density profile from the Rice experiment.

3.6. Experiments with Spin-Polarized Fermi Gases

The unpolarized core was found to exist to high polarization $P_c \gtrsim 0.9$.

These experiments were performed in harmonic traps with cylindrical symmetry ($\omega_x = \omega_y = \alpha\omega$; $\omega_z = \omega$). The MIT experiment had aspect ratio $\alpha \sim 5$ and total particle numbers $N_{tot} = N_\uparrow + N_\downarrow \sim 10^6 - 10^7$. The Rice experiments are in a highly elongated trap, with aspect ratio $\alpha \sim 35 - 45$, and for lower $N_{tot} \sim 10^5$. For these conditions, the core deformation and the double-peak structure in the axial density imply a breakdown of the LDA in Refs. [40, 41].

The critical polarization is influenced by the energy of the competing normal polarized phase. For large asymmetries, this is governed by the polaron energy $E = \eta E_F$. In the uniform system, $\eta = -0.607$, and it requires the existence of at least one partially-polarized phase, and in LDA, leads to $P_c = 0.74$ and $x_c = 0.47$ in traps with large particle numbers. These results are in good agreement with the MIT experiment. In comparison, the Rice experiment uses smaller particle numbers and more elongated trap, so the effects of particle number and anisotropic confinement may have significant influence on the phase structure. In traps, the polaron energy is a universal function of α and N . In the next chapter, we study the polaron energy in anisotropic traps for different particle numbers and show that the experimental differences can be understood partially based on our microscopic results.

Chapter 4

$N + 1$ Body Problem in Trapped Fermi Gases

The critical polarization of trapped Fermi gases is influenced by the energies of the fully-paired superfluid and the polarized normal gas. For large asymmetries, the latter is governed by the energy of a spin-down fermion interacting resonantly with a spin-up Fermi sea. In this chapter, we study the energy of this Fermi polaron in anisotropic traps for different particle numbers, and show that the MIT-Rice differences can be understood partially based on our microscopic results. We will begin by deriving the self-consistent equation for the $N + 1$ body energy in traps. Next, we will present the results for the polaron energy. Lastly, we will apply the LDA to explore the impact of the polaron energy to the phase structure. The work described in this chapter is published in Ref. [34].

4.1 Evaluation of $N + 1$ Body Energy in Harmonic-Oscillator Traps

The formalism of our problem is as follow. We assume a trap with cylindrical symmetry, $\omega_x = \omega_y = \alpha\omega = \alpha\omega_z$. The strongly-interacting Fermi gas in a harmonic-oscillator trap is given by the Hamiltonian

$$H = \sum_{\mathbf{n}, \sigma} \varepsilon_{\mathbf{n}} a_{\mathbf{n}, \sigma}^{\dagger} a_{\mathbf{n}, \sigma} + \sum_{\mathbf{n}_{\uparrow}, \mathbf{n}_{\downarrow}, \mathbf{n}'_{\uparrow}, \mathbf{n}'_{\downarrow}} \langle \mathbf{n}'_{\uparrow}, \mathbf{n}'_{\downarrow} | V | \mathbf{n}_{\uparrow}, \mathbf{n}_{\downarrow} \rangle a_{\mathbf{n}'_{\uparrow}, \uparrow}^{\dagger} a_{\mathbf{n}'_{\downarrow}, \downarrow}^{\dagger} a_{\mathbf{n}_{\downarrow}, \downarrow} a_{\mathbf{n}_{\uparrow}, \uparrow}, \quad (4.1)$$

where $\varepsilon_{\mathbf{n}} = \alpha\omega(n_x + n_y + 1) + \omega(n_z + 1/2)$ are the harmonic oscillator energies. The operator $a_{\mathbf{n}, \sigma}$ annihilates a particle with spin $\sigma = \uparrow, \downarrow$ in a state with quantum numbers $\mathbf{n} = (n_x, n_y, n_z)$. We use a contact interaction regulated by smooth cutoff in momentum space (see Section 2.3),

$$\langle \mathbf{p}, \mathbf{P} | V | \mathbf{p}', \mathbf{P}' \rangle = C(\Lambda) (2\pi)^3 \delta^3(\mathbf{P} - \mathbf{P}') e^{-\frac{p^2 + p'^2}{\Lambda^2}} \quad \text{with } C(\Lambda) = \frac{4\pi/m}{\frac{1}{a} - \frac{\Lambda}{\sqrt{2\pi}}}, \quad (4.2)$$

where \mathbf{p}, \mathbf{P} (\mathbf{p}', \mathbf{P}') are the incoming (outgoing) relative and center-of-mass momenta, m is the fermion mass and Λ a momentum cutoff. In this section, we adopt Chevy's variational method to study the $N + 1$ body problem in harmonic-oscillator traps.

4.1.1 Interaction Matrix Elements in a Harmonic-Oscillator Basis

The first step is to evaluate the interaction matrix $\langle \mathbf{n}_1, \mathbf{n}_2 | V | \mathbf{n}_3, \mathbf{n}_4 \rangle$. We will divide this problem into two steps. First, we will study the basis transformation between a harmonic-oscillator two-body eigenstate, $|\mathbf{n}_1, \mathbf{n}_2\rangle$, and a center-of-mass and relative eigenstate, $|\mathbf{S}, \mathbf{n}\rangle$. We will then apply the result to evaluate the interaction matrix elements.

Harmonic-Oscillator Basis Transformation

We first study the basis transformation bracket $\langle \mathbf{n}_1, \mathbf{n}_2 | \mathbf{S}, \mathbf{n} \rangle$, where $|\mathbf{n}_1, \mathbf{n}_2\rangle$ is a harmonic-oscillator two-body eigenstate, and $|\mathbf{S}, \mathbf{n}\rangle$ is a center-of-mass and relative eigenstate.

The Hamiltonian for two particles of mass m in a harmonic oscillator with $\omega_x, \omega_y, \omega_z$ is given by

$$\begin{aligned} H &= \sum_{i=x,y,z} \left(\frac{p_{1i}^2}{2m} + \frac{1}{2}m\omega_i^2 x_{1i}^2 + \frac{p_{2i}^2}{2m} + \frac{1}{2}m\omega_i^2 x_{2i}^2 \right) \\ &= \sum_{i=x,y,z} \omega_i \left(a_{1i}^\dagger a_{1i} + a_{2i}^\dagger a_{2i} + 1 \right), \end{aligned} \quad (4.3)$$

where p_{σ_i} and x_{σ_i} are the $i = x, y, z$ component of momentum and coordinate of the $\sigma = 1, 2$ particle. The lowering operators are $a_{\sigma_i} = \sqrt{m\omega_i/2}(x_{\sigma_i} + ip_{\sigma_i}/(m\omega_i))$. The two-body eigenstates are given by

$$|\mathbf{n}_1, \mathbf{n}_2\rangle = \prod_{i=x,y,z} \frac{1}{\sqrt{n_{1i}!}} (a_{1i}^\dagger)^{n_{1i}} \frac{1}{\sqrt{n_{2i}!}} (a_{2i}^\dagger)^{n_{2i}} |0\rangle, \quad (4.4)$$

and have energies $\varepsilon_{\mathbf{n}_1} + \varepsilon_{\mathbf{n}_2}$.

The Hamiltonian can be decomposed into the center-of-mass and the relative components,

$$\begin{aligned} H &= \sum_{i=x,y,z} \left(\frac{P_i^2}{2M} + \frac{1}{2}M\omega_i^2 X_i^2 + \frac{p^2}{2m_r} + \frac{1}{2}m_r\omega_i^2 r_i^2 \right) \\ &= \sum_{i=x,y,z} \omega_i \left(a_i^\dagger a_i + A_i^\dagger A_i + 1 \right), \end{aligned} \quad (4.5)$$

4.1. Evaluation of $N + 1$ Body Energy in Harmonic-Oscillator Traps

where $\mathbf{X} = \frac{1}{2}(\mathbf{x}_1 + \mathbf{x}_2)$, $\mathbf{P} = \mathbf{p}_1 + \mathbf{p}_2$ are the center-of-mass coordinate and momentum, $\mathbf{r} = \mathbf{x}_1 - \mathbf{x}_2$, $\mathbf{p} = \frac{1}{2}(\mathbf{p}_1 - \mathbf{p}_2)$ are the relative coordinate and momentum, $M = 2m$ is the total mass, and $m_r = m/2$ is the reduced mass. The corresponding lowering operators are $A_i = \sqrt{M\omega_i/2}(X_i + iP_i/(M\omega_i))$ for the center-of-mass component, and $a_i = \sqrt{m_r\omega_i/2}(r_i + ip_i/(m_r\omega_i))$ for the relative component. Equation (4.5) allows us to construct the center-of-mass and relative eigenstates

$$|\mathbf{S}, \mathbf{n}\rangle = \prod_{i=x,y,z} \frac{1}{\sqrt{S_i!}} (A_i^\dagger)^{S_i} \frac{1}{\sqrt{n_i!}} (a_i^\dagger)^{n_i} |0\rangle, \quad (4.6)$$

with energies $\varepsilon_{\mathbf{S}} + \varepsilon_{\mathbf{n}}$, where \mathbf{S} and \mathbf{n} are the center-of-mass and relative quantum numbers.

We are ready to evaluate the basis transformation $\langle \mathbf{n}_1, \mathbf{n}_2 | \mathbf{S}, \mathbf{n} \rangle$. First, we note that the center-of-mass and relative lowering operators can be written as

$$\begin{aligned} A_i &= \frac{1}{\sqrt{2}}(a_{1i} + a_{2i}), \\ a_i &= \frac{1}{\sqrt{2}}(a_{1i} - a_{2i}). \end{aligned} \quad (4.7)$$

Equations (4.4) and (4.7) allow us to express Eq. (4.6) in terms of the two-body eigenstates,

$$\begin{aligned} |\mathbf{S}, \mathbf{n}\rangle &= \prod_{i=x,y,z} \sum_{j_i=0}^{S_i} \sum_{k_i=0}^{n_i} (-1)^{k_i} \sqrt{\binom{S_i + n_i}{j_i + k_i}^{-1} \frac{(S_i + n_i)!}{2^{S_i + n_i} S_i! n_i!}} \\ &\quad \times \binom{S_i}{j_i} \binom{n_i}{k_i} |(\mathbf{S} + \mathbf{n}) - (\mathbf{j} + \mathbf{k}), \mathbf{j} + \mathbf{k}\rangle. \end{aligned} \quad (4.8)$$

In the evaluation of $\langle \mathbf{n}_1, \mathbf{n}_2 | \mathbf{S}, \mathbf{n} \rangle$, only the terms with $\mathbf{n}_1 + \mathbf{n}_2 = \mathbf{S} + \mathbf{n}$ and $\mathbf{k} = \mathbf{n}_2 - \mathbf{j}$ give non-trivial contributions. We can therefore eliminate \mathbf{k} , and \mathbf{j} are summed over the range

$$\max\{n_{2i} - n_i, 0\} \leq j_i \leq \min\{n_{2i}, S_i\}. \quad (4.9)$$

The basis transformation is then given by

$$\langle \mathbf{n}_1, \mathbf{n}_2 | \mathbf{S}, \mathbf{n} \rangle = \prod_{i=x,y,z} (-1)^{n_{2i}} \sqrt{\frac{n_{1i}! n_{2i}!}{2^{n_{1i} + n_{2i}} S_i! n_i!}} f(n_i, S_i, n_{2i}) \delta_{n_{1i} + n_{2i}, S_i + n_i}, \quad (4.10)$$

4.1. Evaluation of $N + 1$ Body Energy in Harmonic-Oscillator Traps

where we have defined

$$\frac{1}{n_i!} f(n_i, N_i, n_{2_i}) = \sum_{j_i=\max\{n_{2_i}-n_i, 0\}}^{\min\{n_{2_i}, S_i\}} \frac{(-1)^{j_i} S_i!}{j_i!(S_i - j_i)!(n_{2_i} - j_i)!(n_i - n_{2_i} + j_i)!}. \quad (4.11)$$

Evaluation of the Interaction Matrix Elements

Now, we are ready to evaluate $\langle \mathbf{n}_1, \mathbf{n}_2 | V | \mathbf{n}_3, \mathbf{n}_4 \rangle$. Inserting the identities $1 = \int \frac{d^3 P}{(2\pi)^3} \frac{d^3 p}{(2\pi)^3} |\mathbf{p}, \mathbf{P}\rangle \langle \mathbf{p}, \mathbf{P}|$ and $1 = \sum_{\mathbf{S}, \mathbf{n}} |\mathbf{S}, \mathbf{n}\rangle \langle \mathbf{n}, \mathbf{S}|$, we find

$$\langle \mathbf{n}_1, \mathbf{n}_2, | V | \mathbf{n}_3, \mathbf{n}_4 \rangle = C(\Lambda) \sum_{\mathbf{S}} F(\mathbf{n}_1, \mathbf{n}_2, \mathbf{S}) F(\mathbf{n}_3, \mathbf{n}_4, \mathbf{S}), \quad (4.12)$$

where we have defined

$$F(\mathbf{n}_1, \mathbf{n}_2, \mathbf{S}) = \sum_{\mathbf{n}} \langle \mathbf{n}_1, \mathbf{n}_2 | \mathbf{S}, \mathbf{n} \rangle \int \frac{d^3 p}{(2\pi)^3} \langle \mathbf{p} | \mathbf{n} \rangle e^{-\frac{p^2}{\Lambda^2}}. \quad (4.13)$$

The momentum-space harmonic-oscillator wavefunction for the relative component⁹ is

$$\langle \mathbf{p} | \mathbf{n} \rangle = \prod_{i=x,y,z} \frac{1}{\sqrt{2^{n_i} n_i!}} \left(\frac{4\pi}{m_r \omega_i} \right)^{1/4} H_{n_i} \left(\frac{p_i}{\sqrt{m_r \omega_i}} \right) e^{-\frac{p_i^2}{2m_r \omega_i}}, \quad (4.14)$$

where $m_r = m/2$, and $H_n(u)$ are the Hermite polynomials. Eq. (4.13) requires the integral $\int_{-\infty}^{\infty} H_n(u) e^{-u^2(1/2+\lambda^2)} du / 2\pi$, which is given by [31]

$$\int_{-\infty}^{\infty} \frac{du}{2\pi} H_n(u) e^{-u^2(1/2+\lambda^2)} = \begin{cases} (n-1)!! \sqrt{\frac{2^n(1-2\lambda^2)^n}{2\pi(1+2\lambda^2)^{n+1}}} & \text{n even,} \\ 0 & \text{n odd.} \end{cases} \quad (4.15)$$

Together with Eqs. (4.10), (4.14), and (4.15), Eq. (4.13) yields

$$F(\mathbf{n}_1, \mathbf{n}_2, \mathbf{S}) = \prod_{i=x,y,z} (m\omega_i)^{1/4} \tilde{F}(n_{1_i}, n_{2_i}, S_i, \lambda_i = \sqrt{m\omega_i/2}/\Lambda), \quad (4.16)$$

⁹The commutation relation $[x, p] = i$ implies $x = i \frac{d}{dp}$. Therefore, the harmonic-oscillator wavefunction in momentum-space is identical to the real-space wavefunction, with $\sqrt{m\omega}x \rightarrow p/\sqrt{m\omega}$ and $\int d^3 x |\psi(\mathbf{x})|^2 = 1 \rightarrow \int \frac{d^3 p}{(2\pi)^3} |\psi(\mathbf{p})|^2 = 1$.

4.1. Evaluation of $N + 1$ Body Energy in Harmonic-Oscillator Traps

and the dimensionless function \tilde{F} is given by

$$\begin{aligned} \tilde{F}(n_{1_i}, n_{2_i}, S_i, \lambda_i) &= (-1)^{n_{2_i}} \left(\frac{1}{2\pi} \right)^{1/4} \sqrt{\frac{n_{1_i}! n_{2_i}! (1 - 2\lambda_i^2)^{n_{1_i} + n_{2_i} - S_i}}{2^{n_{1_i} + n_{2_i}} S_i! (1 + 2\lambda_i^2)^{n_{1_i} + n_{2_i} - S_i + 1}}} \\ &\quad \times f(n_{1_i} + n_{2_i} - S_i, S_i, n_{2_i}) \frac{(n_{1_i} + n_{2_i} - S_i - 1)!!}{(n_{1_i} + n_{2_i} - S_i)!}, \end{aligned} \quad (4.17)$$

where the relative quantum numbers $n_i = n_{1_i} + n_{2_i} - S_i$ have to be even and positive.

At this point, it is useful to discuss the form of the function f . A direct evaluation of Eq. (4.11) gives

$$f(n_i, S_i, n_{2_i}) = \binom{n_i}{n_{2_i}} {}_2F_1(-n_{2_i}, -S_i, 1 - n_{2_i} + n_i, -1) \quad (4.18)$$

for $n_{2_i} \leq n_i$, with hypergeometric function ${}_2F_1$, and

$$f(n_i, S_i, n_{2_i}) = (-1)^{n_{2_i} + n_i} \binom{S_i}{n_{2_i} - n_i} {}_2F_1(-n_i, n_{2_i} - n_i - S_i, 1 + n_{2_i} - n_i, -1) \quad (4.19)$$

for $n_{2_i} > n_i$.

The above form is useful for numerical evaluations. We will derive another form of \tilde{F} , which will be useful in Section 4.1.3. The expression of Eq. (4.11) can be simplified with the identity $\frac{1}{(-n)!} = 0$ for any positive integer n . One can check that Eq. (4.11) remains the same for all n_i , N_i , and n_{2_i} , if the upper limit of the summation is extended to $j_i \leq S_i$, and the lower limit to $0 \leq j_i$. To meet the requirement that n_i has to be even, we insert the factor $(1 + (-1)^{n_i})/2$. Then, we obtain

$$\frac{1}{n_i!} f(n_i, S_i, n_{2_i}) = \frac{1 + (-1)^{n_i}}{2} \sum_{j_i=0}^{S_i} \frac{(-1)^{j_i} S_i!}{j_i! (S_i - j_i)! (n_{2_i} - j_i)! (n_i - n_{2_i} + j_i)!}. \quad (4.20)$$

Since $n_i = n_{1_i} + n_{2_i} - S_i$ is even, we can use the identity $\Gamma(n_i + \frac{1}{2}) = \sqrt{\pi} \frac{(2n_i - 1)!!}{2^{n_i}}$. We will define $u_i \equiv \frac{1 - 2\lambda_i^2}{1 + 2\lambda_i^2}$ to simplify the expression. This

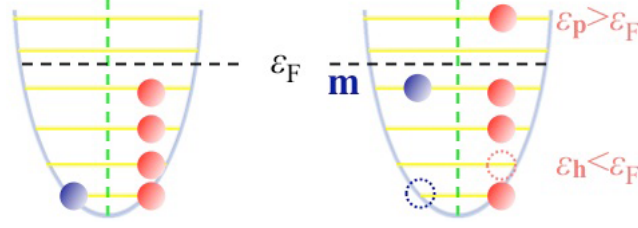


Figure 4.1: Graphical representation of the components of the trial wavefunction Eq. (4.22) in traps. *Left*: the unperturbed majority Fermi sea with the spin-down particle in the $\mathbf{n} = \mathbf{0}$ level. This is the state $|\Omega\rangle$. *Right*: the state $|\mathbf{m}, \mathbf{h}, \mathbf{p}\rangle$ consist of a spin-up fermion in \mathbf{h} excited to a level \mathbf{p} above the Fermi energy ε_F , and the spin-down particle occupies the level \mathbf{m} .

gives an alternative form for the function \tilde{F} ,

$$\begin{aligned} & \tilde{F}(n_{1_i}, n_{2_i}, S_i, \lambda_i) \\ &= (-1)^{n_{2_i}} \left(\frac{1 + (-1)^{n_{1_i} + n_{2_i} - S_i}}{2} \right) \left(\frac{1}{2\pi} \right)^{1/4} \sqrt{\frac{n_{1_i}! n_{2_i}! S_i! u_i^{(n_{1_i} + n_{2_i} - S_i)/2}}{2^{S_i} \pi}} \frac{1}{\sqrt{1 + 2\lambda_i^2}} \\ & \times \Gamma \left(\frac{n_{1_i} + n_{2_i} - S_i + 1}{2} \right) \sum_{j_i=0}^{S_i} \frac{(-1)^{j_i}}{j_i! (S_i - j_i)! (n_{2_i} - j_i)! (n_{1_i} - S_i + j_i)!}. \end{aligned} \quad (4.21)$$

4.1.2 Variational Solution to the $N + 1$ Body Ground State Energy in Harmonic-Oscillator Traps

In this part, we derive the self-consistent equation for the $N + 1$ body energy in harmonic-oscillator traps. Following the variational wavefunction of Refs. [17, 18], we calculate the energy E of an impurity in a majority Fermi sea, including $1p1h$ in the wave function (see Fig. 4.1),

$$|\psi\rangle = \phi_0 |\Omega\rangle + \sum_{\mathbf{m}, \mathbf{h}, \mathbf{p}} \phi_{\mathbf{m}, \mathbf{h}, \mathbf{p}} |\mathbf{m}, \mathbf{h}, \mathbf{p}\rangle, \quad (4.22)$$

where $|\Omega\rangle$ denotes the Fermi sea with the spin-down particle in the $\mathbf{n} = \mathbf{0}$ level¹⁰, and $|\mathbf{m}, \mathbf{h}, \mathbf{p}\rangle$ consist of a spin-up fermion in \mathbf{h} excited to a level \mathbf{p}

¹⁰The restriction to $\mathbf{n} = \mathbf{0}$ (justified for large N) enables our still involved numerical solution.

4.1. Evaluation of $N + 1$ Body Energy in Harmonic-Oscillator Traps

above the Fermi energy ε_F , and the spin-down particle occupies the level \mathbf{m} . Therefore, the sum over \mathbf{h} is restricted to occupied states, whereas \mathbf{p} is over unoccupied states above ε_F .

We write the Hamiltonian Eq. (4.1) as $H = H_0 + V$, where H_0 is the non-interacting harmonic-oscillator Hamiltonian, and V gives the interacting part. We proceed by calculating $\langle \psi | H_0 | \psi \rangle$:

$$\begin{aligned} H_0 | \psi \rangle &= \phi_0 \left(\sum_{\mathbf{n}} \varepsilon_{\mathbf{n}} a_{\mathbf{n},\uparrow}^\dagger a_{\mathbf{n},\uparrow} | \Omega \rangle + \sum_{\mathbf{n}} \varepsilon_{\mathbf{n}} a_{\mathbf{n},\downarrow}^\dagger a_{\mathbf{n},\downarrow} | \Omega \rangle \right) \\ &+ \sum_{\mathbf{m}, \mathbf{h}, \mathbf{p}} \phi_{\mathbf{m}, \mathbf{h}, \mathbf{p}} \left(\sum_{\mathbf{n}} \varepsilon_{\mathbf{n}} a_{\mathbf{n},\uparrow}^\dagger a_{\mathbf{n},\uparrow} | \mathbf{m}, \mathbf{h}, \mathbf{p} \rangle + \sum_{\mathbf{n}} \varepsilon_{\mathbf{n}} a_{\mathbf{n},\downarrow}^\dagger a_{\mathbf{n},\downarrow} | \mathbf{m}, \mathbf{h}, \mathbf{p} \rangle \right). \end{aligned} \quad (4.23)$$

The operators act on the states to yield

$$a_{\mathbf{n},\uparrow}^\dagger a_{\mathbf{n},\uparrow} | \Omega \rangle = \begin{cases} 0 & \varepsilon_{\mathbf{n}} > \varepsilon_F, \\ | \Omega \rangle & \varepsilon_{\mathbf{n}} \leq \varepsilon_F, \end{cases} \quad (4.24)$$

$$a_{\mathbf{n},\downarrow}^\dagger a_{\mathbf{n},\downarrow} | \Omega \rangle = \begin{cases} 0 & \mathbf{n} \neq \mathbf{0}, \\ | \Omega \rangle & \mathbf{n} = \mathbf{0}, \end{cases} \quad (4.25)$$

$$a_{\mathbf{n},\uparrow}^\dagger a_{\mathbf{n},\uparrow} | \mathbf{m}, \mathbf{h}, \mathbf{p} \rangle = \begin{cases} | \mathbf{m}, \mathbf{h}, \mathbf{p} \rangle & \mathbf{n} = \mathbf{p}, \\ | \mathbf{m}, \mathbf{h}, \mathbf{p} \rangle & \varepsilon_{\mathbf{n}} \leq \varepsilon_F \text{ and } \mathbf{n} \neq \mathbf{h}, \\ 0 & \text{else,} \end{cases} \quad (4.26)$$

$$a_{\mathbf{n},\downarrow}^\dagger a_{\mathbf{n},\downarrow} | \mathbf{m}, \mathbf{h}, \mathbf{p} \rangle = \begin{cases} 0 & \mathbf{n} \neq \mathbf{m}, \\ | \mathbf{m}, \mathbf{h}, \mathbf{p} \rangle & \mathbf{n} = \mathbf{m}. \end{cases} \quad (4.27)$$

Therefore, we find

$$\langle \psi | H_0 | \psi \rangle = \varepsilon_{\mathbf{0}} |\phi_{\mathbf{0}}|^2 + \sum_{\mathbf{m}, \mathbf{h}, \mathbf{p}} |\phi_{\mathbf{m}, \mathbf{h}, \mathbf{p}}|^2 (\varepsilon_{\mathbf{p}} + \varepsilon_{\mathbf{m}} - \varepsilon_{\mathbf{h}}) + \sum_{\varepsilon_{\mathbf{n}} \leq \varepsilon_F} \varepsilon_{\mathbf{n}}. \quad (4.28)$$

The last term gives the energy of the non-interacting spin-up fermions and is subtracted when we study the energy gain.

Next, we calculate $\langle \psi | V | \psi \rangle$, making use of the result $\langle \mathbf{n}_1, \mathbf{n}_2 | V | \mathbf{n}_3, \mathbf{n}_4 \rangle =$

4.1. Evaluation of $N + 1$ Body Energy in Harmonic-Oscillator Traps

$C(\Lambda) \sum_{\mathbf{S}} F(\mathbf{n}_1, \mathbf{n}_2, \mathbf{S}) F(\mathbf{n}_3, \mathbf{n}_4, \mathbf{S})$ from Section 4.1.1:

$$\begin{aligned}
V|\psi\rangle &= C(\Lambda)\phi_0 \sum_{\mathbf{S}} \sum_{\mathbf{n}_{\uparrow}, \mathbf{n}_{\downarrow}, \mathbf{n}'_{\uparrow}, \mathbf{n}'_{\downarrow}} F(\mathbf{n}_{\downarrow}, \mathbf{n}_{\uparrow}, \mathbf{S}) F(\mathbf{n}'_{\downarrow}, \mathbf{n}'_{\uparrow}, \mathbf{S}) \\
&\quad \times a_{\mathbf{n}'_{\uparrow}, \uparrow}^{\dagger} a_{\mathbf{n}'_{\downarrow}, \downarrow}^{\dagger} a_{\mathbf{n}_{\downarrow}, \downarrow} a_{\mathbf{n}_{\uparrow}, \uparrow} |\Omega\rangle \\
&\quad + C(\Lambda) \sum_{\mathbf{S}} \sum_{\mathbf{n}_{\uparrow}, \mathbf{n}_{\downarrow}, \mathbf{n}'_{\uparrow}, \mathbf{n}'_{\downarrow}} F(\mathbf{n}_{\downarrow}, \mathbf{n}_{\uparrow}, \mathbf{S}) F(\mathbf{n}'_{\downarrow}, \mathbf{n}'_{\uparrow}, \mathbf{S}) \\
&\quad \times \sum_{\mathbf{m}, \mathbf{h}, \mathbf{p}} \phi_{\mathbf{m}, \mathbf{h}, \mathbf{p}} a_{\mathbf{n}'_{\uparrow}, \uparrow}^{\dagger} a_{\mathbf{n}'_{\downarrow}, \downarrow}^{\dagger} a_{\mathbf{n}_{\downarrow}, \downarrow} a_{\mathbf{n}_{\uparrow}, \uparrow} |\mathbf{m}, \mathbf{h}, \mathbf{p}\rangle.
\end{aligned} \tag{4.29}$$

Keeping up to one-particle-one-hole excitations, the relevant terms are

$$a_{\mathbf{n}'_{\uparrow}, \uparrow}^{\dagger} a_{\mathbf{n}'_{\downarrow}, \downarrow}^{\dagger} a_{\mathbf{n}_{\downarrow}, \downarrow} a_{\mathbf{n}_{\uparrow}, \uparrow} |\Omega\rangle = \begin{cases} |\Omega\rangle & \mathbf{n}_{\downarrow} = \mathbf{0}, \quad \varepsilon_{\mathbf{n}_{\uparrow}} \leq \varepsilon_F, \\ & \mathbf{n}'_{\uparrow} = \mathbf{n}_{\uparrow}, \quad \mathbf{n}'_{\downarrow} = \mathbf{0}, \\ |\mathbf{n}'_{\downarrow}, \mathbf{n}_{\uparrow}, \mathbf{n}'_{\uparrow}\rangle & \mathbf{n}_{\downarrow} = \mathbf{0}, \quad \varepsilon_{\mathbf{n}_{\uparrow}} \leq \varepsilon_F, \\ & \varepsilon_{\mathbf{n}'_{\uparrow}} > \varepsilon_F, \end{cases} \tag{4.30}$$

$$a_{\mathbf{n}'_{\uparrow}, \uparrow}^{\dagger} a_{\mathbf{n}'_{\downarrow}, \downarrow}^{\dagger} a_{\mathbf{n}_{\downarrow}, \downarrow} a_{\mathbf{n}_{\uparrow}, \uparrow} |\mathbf{m}, \mathbf{h}, \mathbf{p}\rangle = \begin{cases} |\mathbf{n}'_{\downarrow}, \mathbf{h}, \mathbf{n}'_{\uparrow}\rangle & \mathbf{n}_{\downarrow} = \mathbf{m}, \quad \mathbf{n}_{\uparrow} = \mathbf{p}, \\ & \varepsilon_{\mathbf{n}'_{\uparrow}} > \varepsilon_F, \\ |\Omega\rangle & \mathbf{n}_{\downarrow} = \mathbf{m}, \quad \mathbf{n}_{\uparrow} = \mathbf{p}, \\ & \mathbf{n}'_{\uparrow} = \mathbf{h}, \quad \mathbf{n}'_{\downarrow} = \mathbf{0}, \\ |\mathbf{n}'_{\downarrow}, \mathbf{n}_{\uparrow}, \mathbf{p}\rangle & \mathbf{n}_{\downarrow} = \mathbf{m}, \quad \varepsilon_{\mathbf{n}_{\uparrow}} \leq \varepsilon_F, \\ & \mathbf{n}_{\uparrow} \neq \mathbf{h}, \quad \mathbf{n}'_{\uparrow} = \mathbf{h}, \\ |\mathbf{n}'_{\downarrow}, \mathbf{h}, \mathbf{p}\rangle & \mathbf{n}_{\downarrow} = \mathbf{m}, \quad \varepsilon_{\mathbf{n}_{\uparrow}} \leq \varepsilon_F, \\ & \mathbf{n}_{\uparrow} \neq \mathbf{h}, \quad \mathbf{n}'_{\uparrow} = \mathbf{n}_{\uparrow}. \end{cases} \tag{4.31}$$

Making the following change of indices $\mathbf{n}_{\uparrow} \rightarrow \mathbf{h}'$, $\mathbf{n}'_{\uparrow} \rightarrow \mathbf{p}'$, $\mathbf{n}'_{\downarrow} \rightarrow \mathbf{m}'$, we

obtain

$$\begin{aligned}
 V|\psi\rangle &= C(\Lambda)\phi_0 \sum_{\mathbf{S}} \sum_{\mathbf{h}'} F^2(\mathbf{0}, \mathbf{h}', \mathbf{S})|\Omega\rangle \\
 &+ C(\Lambda)\phi_0 \sum_{\mathbf{m}', \mathbf{h}', \mathbf{p}'} F(\mathbf{0}, \mathbf{h}', \mathbf{S})F(\mathbf{m}', \mathbf{p}', \mathbf{S})|\mathbf{m}', \mathbf{h}', \mathbf{p}'\rangle \\
 &+ C(\Lambda) \sum_{\mathbf{S}} \sum_{\mathbf{m}, \mathbf{h}, \mathbf{p}} \phi_{\mathbf{m}, \mathbf{h}, \mathbf{p}} F(\mathbf{m}, \mathbf{p}, \mathbf{S})F(\mathbf{0}, \mathbf{h}, \mathbf{S})|\Omega\rangle \\
 &+ C(\Lambda) \sum_{\mathbf{S}} \sum_{\mathbf{m}, \mathbf{h}, \mathbf{p}} \phi_{\mathbf{m}, \mathbf{h}, \mathbf{p}} \sum_{\mathbf{m}', \mathbf{p}'} F(\mathbf{m}, \mathbf{p}, \mathbf{S})F(\mathbf{m}', \mathbf{p}', \mathbf{S})|\mathbf{m}', \mathbf{h}, \mathbf{p}'\rangle \\
 &+ C(\Lambda) \sum_{\mathbf{S}} \sum_{\mathbf{m}, \mathbf{h}, \mathbf{p}} \phi_{\mathbf{m}, \mathbf{h}, \mathbf{p}} \sum_{\mathbf{m}', \mathbf{h}' \neq \mathbf{h}} F(\mathbf{m}, \mathbf{h}', \mathbf{S})F(\mathbf{m}', \mathbf{h}, \mathbf{S})|\mathbf{m}', \mathbf{h}', \mathbf{p}\rangle \\
 &+ C(\Lambda) \sum_{\mathbf{S}} \sum_{\mathbf{m}, \mathbf{h}, \mathbf{p}} \phi_{\mathbf{m}, \mathbf{h}, \mathbf{p}} \sum_{\mathbf{m}', \mathbf{h}' \neq \mathbf{h}} F(\mathbf{m}, \mathbf{h}', \mathbf{S})F(\mathbf{m}', \mathbf{h}', \mathbf{S})|\mathbf{m}', \mathbf{h}, \mathbf{p}\rangle.
 \end{aligned} \tag{4.32}$$

Each of the sums over \mathbf{m}' , \mathbf{h}' , and \mathbf{p} follow the same convention as those over \mathbf{m} , \mathbf{h} , and \mathbf{p} , respectively. We then have

$$\begin{aligned}
 \langle \psi|V|\psi\rangle &= C(\Lambda) \sum_{\mathbf{S}} \sum_{\mathbf{h}} F^2(\mathbf{0}, \mathbf{h}, \mathbf{S})|\phi_0|^2 \\
 &+ C(\Lambda) \sum_{\mathbf{S}} \sum_{\mathbf{m}, \mathbf{h}, \mathbf{p}} \phi_0^* \phi_{\mathbf{m}, \mathbf{h}, \mathbf{p}} F(\mathbf{m}, \mathbf{p}, \mathbf{S})F(\mathbf{0}, \mathbf{h}, \mathbf{S}) \\
 &+ C(\Lambda) \sum_{\mathbf{S}} \sum_{\mathbf{m}, \mathbf{h}, \mathbf{p}} F(\mathbf{0}, \mathbf{h}, \mathbf{S})F(\mathbf{m}, \mathbf{p}, \mathbf{S})\phi_{\mathbf{m}, \mathbf{h}, \mathbf{p}}^* \phi_0 \\
 &+ C(\Lambda) \sum_{\mathbf{S}} \sum_{\mathbf{m}, \mathbf{h}, \mathbf{p}, \mathbf{m}', \mathbf{p}'} F(\mathbf{m}, \mathbf{p}, \mathbf{S})F(\mathbf{m}', \mathbf{p}', \mathbf{S})\phi_{\mathbf{m}', \mathbf{h}, \mathbf{p}'}^* \phi_{\mathbf{m}, \mathbf{h}, \mathbf{p}} \\
 &+ C(\Lambda) \sum_{\mathbf{S}} \sum_{\mathbf{m}, \mathbf{h}, \mathbf{p}, \mathbf{m}', \mathbf{h}' \neq \mathbf{h}} F(\mathbf{m}, \mathbf{h}', \mathbf{S})F(\mathbf{m}', \mathbf{h}, \mathbf{S})\phi_{\mathbf{m}', \mathbf{h}', \mathbf{p}}^* \phi_{\mathbf{m}, \mathbf{h}, \mathbf{p}} \\
 &+ C(\Lambda) \sum_{\mathbf{S}} \sum_{\mathbf{m}, \mathbf{h}, \mathbf{p}, \mathbf{m}', \mathbf{h}' \neq \mathbf{h}} F(\mathbf{m}, \mathbf{h}', \mathbf{S})F(\mathbf{m}', \mathbf{h}', \mathbf{S})\phi_{\mathbf{m}', \mathbf{h}, \mathbf{p}}^* \phi_{\mathbf{m}, \mathbf{h}, \mathbf{p}}.
 \end{aligned} \tag{4.33}$$

The cutoff dependence of the sum is cancelled by the coupling constant $C(\Lambda)$. In the limit of large cutoffs, the last two sums are convergent and when multiplied by $C(\Lambda)$, will give a zero contribution. Therefore, they do not contribute to the energy gain, and will be omitted in the rest of the calculation.

4.1. Evaluation of $N + 1$ Body Energy in Harmonic-Oscillator Traps

Combining Eqs. (4.28) and (4.33), the energy to be minimized is

$$\begin{aligned}
\langle \psi | H | \psi \rangle &= \varepsilon_0 |\phi_0|^2 + \sum_{\mathbf{m}, \mathbf{h}, \mathbf{p}} |\phi_{\mathbf{m}, \mathbf{h}, \mathbf{p}}|^2 (\varepsilon_{\mathbf{p}} + \varepsilon_{\mathbf{m}} - \varepsilon_{\mathbf{h}}) \\
&+ C(\Lambda) \sum_{\mathbf{S}} \sum_{\mathbf{h}} F^2(\mathbf{0}, \mathbf{h}, \mathbf{S}) |\phi_0|^2 \\
&+ C(\Lambda) \sum_{\mathbf{S}} \sum_{\mathbf{m}, \mathbf{h}, \mathbf{p}} F(\mathbf{m}, \mathbf{p}, \mathbf{S}) F(\mathbf{0}, \mathbf{h}, \mathbf{S}) (\phi_0^* \phi_{\mathbf{m}, \mathbf{h}, \mathbf{p}} + \phi_0 \phi_{\mathbf{m}, \mathbf{h}, \mathbf{p}}^*) \\
&+ C(\Lambda) \sum_{\mathbf{S}} \sum_{\mathbf{m}, \mathbf{h}, \mathbf{p}} \sum_{\mathbf{m}', \mathbf{p}'} F(\mathbf{m}, \mathbf{p}, \mathbf{S}) F(\mathbf{m}', \mathbf{p}', \mathbf{S}) \phi_{\mathbf{m}, \mathbf{h}, \mathbf{p}} \phi_{\mathbf{m}', \mathbf{h}, \mathbf{p}'}^* .
\end{aligned} \tag{4.34}$$

Minimizing $\langle \psi | H | \psi \rangle$ with respect to ϕ_0 and $\phi_{\mathbf{m}, \mathbf{h}, \mathbf{p}}$ yields the following set of equations:

$$\begin{aligned}
E\phi_0 &= \varepsilon_0 \phi_0 \\
&+ C(\Lambda) \sum_{\mathbf{S}} \sum_{\mathbf{h}} F(\mathbf{0}, \mathbf{h}, \mathbf{S}) \left[F(\mathbf{0}, \mathbf{h}, \mathbf{S}) \phi_0 + \sum_{\mathbf{m}, \mathbf{p}} F(\mathbf{m}, \mathbf{p}, \mathbf{S}) \phi_{\mathbf{m}, \mathbf{h}, \mathbf{p}} \right] ,
\end{aligned} \tag{4.35}$$

$$\begin{aligned}
E\phi_{\mathbf{m}, \mathbf{h}, \mathbf{p}} &= (\varepsilon_{\mathbf{p}} + \varepsilon_{\mathbf{m}} - \varepsilon_{\mathbf{h}}) \phi_{\mathbf{m}, \mathbf{h}, \mathbf{p}} \\
&+ C(\Lambda) \sum_{\mathbf{S}} F(\mathbf{m}, \mathbf{p}, \mathbf{S}) \left[F(\mathbf{0}, \mathbf{h}, \mathbf{S}) \phi_0 + \sum_{\mathbf{m}', \mathbf{p}'} F(\mathbf{m}', \mathbf{p}', \mathbf{S}) \phi_{\mathbf{m}', \mathbf{h}, \mathbf{p}'} \right] .
\end{aligned} \tag{4.36}$$

To simplify these equations, we define

$$\chi(\mathbf{h}, \mathbf{S}) = F(\mathbf{0}, \mathbf{h}, \mathbf{S}) \phi_0 + \sum_{\mathbf{m}, \mathbf{p}} F(\mathbf{m}, \mathbf{p}, \mathbf{S}) \phi_{\mathbf{m}, \mathbf{h}, \mathbf{p}} . \tag{4.37}$$

Then Eqs. (4.35) and (4.36) can be written as

$$\phi_0 = \frac{C(\Lambda)}{E - \varepsilon_0} \sum_{\mathbf{h}} \sum_{\mathbf{S}} F(\mathbf{0}, \mathbf{h}, \mathbf{S}) \chi(\mathbf{h}, \mathbf{S}) , \tag{4.38}$$

$$\phi_{\mathbf{m}, \mathbf{h}, \mathbf{p}} = \frac{C(\Lambda)}{E - (\varepsilon_{\mathbf{p}} + \varepsilon_{\mathbf{m}} - \varepsilon_{\mathbf{h}})} \sum_{\mathbf{S}} F(\mathbf{m}, \mathbf{p}, \mathbf{S}) \chi(\mathbf{h}, \mathbf{S}) . \tag{4.39}$$

4.1. Evaluation of $N + 1$ Body Energy in Harmonic-Oscillator Traps

Substituting Eq. (4.39) into the definition for $\chi(\mathbf{h}, \mathbf{S})$ yields

$$\begin{aligned} \chi(\mathbf{h}, \mathbf{S}) &= F(\mathbf{0}, \mathbf{h}, \mathbf{S})\phi_0 \\ &+ \sum_{\mathbf{L}} \sum_{\mathbf{m}, \mathbf{p}} \frac{F(\mathbf{m}, \mathbf{p}, \mathbf{S})}{E - (\varepsilon_{\mathbf{p}} + \varepsilon_{\mathbf{m}} - \varepsilon_{\mathbf{h}})} C(\Lambda) F(\mathbf{m}, \mathbf{p}, \mathbf{L}) \chi(\mathbf{h}, \mathbf{L}), \end{aligned} \quad (4.40)$$

which can be written in the form of a matrix equation

$$\chi(\mathbf{h}, \mathbf{S}) = F(\mathbf{0}, \mathbf{h}, \mathbf{S})\phi_0 + \sum_{\mathbf{L}} A_{\mathbf{S}, \mathbf{L}} \chi(\mathbf{h}, \mathbf{L}), \quad (4.41)$$

where the matrix $A_{\mathbf{S}, \mathbf{L}}$ is given by

$$A_{\mathbf{S}, \mathbf{L}} = \sum_{\mathbf{m}, \mathbf{p}} \frac{C(\Lambda)}{E + \varepsilon_{\mathbf{h}} - (\varepsilon_{\mathbf{p}} + \varepsilon_{\mathbf{m}})} F(\mathbf{m}, \mathbf{p}, \mathbf{S}) F(\mathbf{m}, \mathbf{p}, \mathbf{L}). \quad (4.42)$$

Then, the solution to $\chi(\mathbf{h}, \mathbf{S})$ is straightforward:

$$\chi(\mathbf{h}, \mathbf{S}) = \sum_{\mathbf{L}} [(1 - A)^{-1}]_{\mathbf{S}, \mathbf{L}} F(\mathbf{0}, \mathbf{h}, \mathbf{L})\phi_0. \quad (4.43)$$

Substituting this into Eq. (4.38) yields the self-consistent equation for E in anisotropic traps,

$$E - \varepsilon_0 = \sum_{\varepsilon_{\mathbf{h}} \leq \varepsilon_F} \sum_{\mathbf{S}, \mathbf{L}} F(\mathbf{0}, \mathbf{h}, \mathbf{S}) [M^{-1}(\varepsilon_F, E + \varepsilon_{\mathbf{h}})]_{\mathbf{S}, \mathbf{L}} F(\mathbf{0}, \mathbf{h}, \mathbf{L}), \quad (4.44)$$

where E is measured from the energy of the Fermi sea, in weak coupling $E \approx \varepsilon_0$, and the matrix M is given by

$$\begin{aligned} &M(\varepsilon_F, E + \varepsilon_{\mathbf{h}})_{\mathbf{S}, \mathbf{L}} \\ &= \frac{\delta_{\mathbf{S}, \mathbf{L}}}{C(\Lambda)} - M_u(\alpha, E + \varepsilon_{\mathbf{h}})_{\mathbf{S}, \mathbf{L}} + \sum_{\varepsilon_{\mathbf{p}} \leq \varepsilon_F} \sum_{\mathbf{m}} \frac{F(\mathbf{m}, \mathbf{p}, \mathbf{S}) F(\mathbf{m}, \mathbf{p}, \mathbf{L})}{E + \varepsilon_{\mathbf{h}} - (\varepsilon_{\mathbf{p}} + \varepsilon_{\mathbf{m}})}, \end{aligned} \quad (4.45)$$

where $M_u(\alpha, E + \varepsilon_{\mathbf{h}})_{\mathbf{S}, \mathbf{L}}$ is identical to the last term of Eq. (4.45) with unrestricted sum over \mathbf{p} . The unrestricted sum of $M_u(\alpha, E + \varepsilon_{\mathbf{h}})_{\mathbf{S}, \mathbf{L}}$ is divergent for large Λ . As we will see shortly, the divergent behavior of $M_u(\alpha, E + \varepsilon_{\mathbf{h}})_{\mathbf{S}, \mathbf{L}}$ for large Λ cancels with the cutoff in the $1/C(\Lambda)$ term in Eq. (4.45). Therefore, E is cutoff independent for large Λ .

4.1.3 Evaluation of the Unrestricted Sum $M_u(\alpha, E + \varepsilon_{\mathbf{h}})_{\mathbf{S}, \mathbf{L}}$

In this part, we study $M_u(\alpha, \mathcal{E} = E + \varepsilon_{\mathbf{h}})_{\mathbf{S}, \mathbf{L}}$ in detail. We will demonstrate that $M_u(\alpha, \mathcal{E})_{\mathbf{S}, \mathbf{L}}$ is diagonal, and $\delta_{\mathbf{S}, \mathbf{L}}/C(\Lambda) - M_u(\alpha, \mathcal{E})_{\mathbf{S}, \mathbf{L}}$ is cutoff independent for large Λ . We will also produce expressions for $M_u(\alpha, \mathcal{E})_{\mathbf{S}, \mathbf{L}}$ that are useful for numerical evaluation.

The form for $F(\mathbf{m}, \mathbf{p}, \mathbf{S})$ given by Eq. (4.16) allows us to write

$$\begin{aligned} & M_u(\alpha, \mathcal{E})_{\mathbf{S}, \mathbf{L}} \\ &= \frac{\alpha(m\omega)^{3/2}}{\omega} \sum_{\mathbf{m}, \mathbf{p}} \frac{1}{\tilde{\mathcal{E}} - (\tilde{\varepsilon}_{\mathbf{m}} + \tilde{\varepsilon}_{\mathbf{p}})} \prod_{i=x,y,z} \tilde{F}(m_i, p_i, S_i, \lambda_i) \tilde{F}(m_i, p_i, L_i, \lambda_i), \end{aligned} \quad (4.46)$$

where $\tilde{\varepsilon}_{\mathbf{n}} = \alpha(n_x + n_y + 1) + n_z + 1/2$ and $\tilde{\mathcal{E}} = \mathcal{E}/\omega$. We have also previously defined $\lambda_i = \sqrt{m\omega_i/2}/\Lambda$. A Laplace transform on Eq. (4.46) with analytic continuation for all \mathcal{E} yields

$$M_u(\alpha, \mathcal{E})_{\mathbf{S}, \mathbf{L}} = -\frac{\alpha(m\omega)^{3/2}}{\omega} \int_0^\infty e^{(\tilde{\mathcal{E}} - (2\alpha+1)s)} \prod_{i=x,y,z} F_s(S_i, L_i, \lambda_i, \alpha_i s) ds, \quad (4.47)$$

where $\alpha_x = \alpha_y = \alpha$, $\alpha_z = 1$, and we have defined

$$F_s(S_i, L_i, \lambda_i, t) = \sum_{m_i=0}^\infty \sum_{p_i=0}^\infty e^{-(m_i+p_i)t} \tilde{F}(m_i, p_i, S_i, \lambda_i) \tilde{F}(m_i, p_i, L_i, \lambda_i). \quad (4.48)$$

We want to derive an analytic expression for $F_s(S_i, L_i, \lambda_i, t)$. Using the form of $\tilde{F}(m_i, p_i, S_i, \lambda_i)$ given by Eq. (4.21) and the identity for the gamma function $\Gamma(t) = 2 \int_0^\infty dx e^{-x^2} x^{2t-1}$, we find

$$\begin{aligned} F_s(S_i, L_i, \lambda_i, t) &= \frac{2(2\pi)^{-3/2}}{1 + 2\lambda_i^2} \sqrt{\frac{S_i! L_i!}{(2u_i)^{S_i+L_i}}} \int_0^\infty \int_0^\infty dx dy e^{-x^2-y^2} x^{-S_i} y^{-L_i} \\ &\times \left[(1 + (-1)^{S_i+L_i}) g(S_i, L_i, xyu_i e^{-t}) \right. \\ &\quad \left. + ((-1)^{S_i} + (-1)^{L_i}) g(S_i, L_i, -xyu_i e^{-t}) \right], \end{aligned} \quad (4.49)$$

4.1. Evaluation of $N + 1$ Body Energy in Harmonic-Oscillator Traps

where $u_i = (1 - 2\lambda_i^2)/(1 + 2\lambda_i^2)$, and we have defined

$$g(S_i, L_i, t) = \sum_{j=0}^{S_i} \sum_{k=0}^{L_i} \frac{(-1)^j}{j!(S_i - j)!} \frac{(-1)^k}{k!(L_i - k)!} P_F(S_i - j, L_i - k, t) P_F(j, k, t), \quad (4.50)$$

with $P_F(j, k, t) = \sum_{p=0}^{\infty} \frac{p! t^p}{(p-j)!(p-k)!}$. The function P_F is symmetric in j, k , and for $j \geq k$ has a closed form

$$P_F(j, k, t) = \frac{t^j j!}{(j-k)!} {}_1F_1(1+j, 1+j-k, t), \quad (4.51)$$

where ${}_1F_1$ is the confluent hypergeometric function of the first kind (also known as Kummer's function of the first kind).

With the help of Eqs. (4.49)-(4.51), we evaluate the function F_s and find

$$F_s(S_i, L_i, \lambda_i, t) = \delta_{S_i, L_i} \frac{e^{-S_i t}}{(1 + 2\lambda_i^2) \sqrt{2\pi} \sqrt{1 - u_i^2} e^{-2t}}. \quad (4.52)$$

After a change of variable $z = e^{-s}$, Eq. (4.47) becomes

$$M_u(\alpha, \mathcal{E})_{\mathbf{S}, \mathbf{L}} = D(\alpha, \Delta \tilde{E}) \delta_{\mathbf{S}, \mathbf{L}}, \quad (4.53)$$

with

$$\begin{aligned} D(\alpha, \Delta \tilde{E}) &= - \frac{\alpha(m\omega)^{3/2}}{\omega(2\pi)^{3/2}(1 + 2\alpha\lambda^2)^2(1 + 2\lambda^2)} \int_0^1 dz \frac{z^{\Delta \tilde{E} - 1}}{(1 - u_r^2 z^{2\alpha})(1 - u^2 z^2)^{1/2}}, \end{aligned} \quad (4.54)$$

where $\Delta \tilde{E} = \alpha(S_x + S_y + 2) + S_z + 1 - \tilde{\mathcal{E}}$, $u = u_z = (1 - 2\lambda^2)/(1 + 2\lambda^2)$ and $u_r = u_x = u_y = (1 - 2\alpha\lambda^2)/(1 + 2\alpha\lambda^2)$.

At this point, we make two observations. First, the unrestricted matrix $M_u(\alpha, \mathcal{E})_{\mathbf{S}, \mathbf{L}}$ is diagonal in \mathbf{S} and \mathbf{L} . Second, it does not depend on the components of center-of-mass quantum numbers \mathbf{S} , but only the center-of-mass excitation $\tilde{\mathcal{E}}_{\mathbf{S}} = \alpha(S_x + S_y + 1) + S_z + 1/2$.

For $\Delta \tilde{E} > 0$, this integral is well-defined. It is divergent for large Λ , and is regularized by the subtraction of the cutoff $-(2\pi)^{-3/2} m\Lambda/2$ in the $1/C(\Lambda)$. The cutoff can be written as

$$- \frac{m\Lambda}{2(2\pi)^{3/2}} = - \frac{1}{\omega} \left(\frac{m\omega}{2\pi} \right)^{3/2} \frac{1}{1 + 2\lambda^2} \int_0^1 \frac{dz}{(1 - u^2 z^2)^{3/2}}. \quad (4.55)$$

We can then write Eq. (4.54) in the following form,

$$D(\alpha, \Delta\tilde{E}) = -\frac{m\Lambda}{2(2\pi)^{3/2}} - \frac{1}{\omega} \left(\frac{m\omega}{2\pi}\right)^{3/2} \int_0^1 dz \left(\frac{\alpha z^{\Delta E-1}}{(1-z^{2\alpha})(1-z^2)^{1/2}} - \frac{1}{(1-z^2)^{3/2}} \right), \quad (4.56)$$

where we have taken the limit $\Lambda \rightarrow \infty$ in the integral. The subtraction of the second term in the integral regulates the singular behavior near $x = 1$. To see it explicitly, we note $1/(1-z^{2\alpha}) \simeq -(z-1)^{-1}/2\alpha + O(z-1)$ for $x \approx 1$. The subtraction removes the part of the integrand that behaves as $-(z-1)^{-1}(1-z^2)^{-1/2}/2$, leaving only finite contributions.

For $\Delta\tilde{E} \leq 0$, the integral in Eq. (4.54) cannot be used directly. Instead, we expand $1/(1-u_r^2 z^{2\alpha})$ using a geometric series, and find

$$D(\alpha, \Delta\tilde{E}) = -\frac{\alpha}{\omega} \left(\frac{m\omega}{2\pi}\right)^{3/2} \frac{1}{(1+2\alpha\lambda^2)^2(1+2\lambda^2)} \times \sum_{n=0}^{\infty} \frac{1}{2} u^{-2n\alpha-\Delta\tilde{E}} u_r^{2n} \beta\left(u^2, n\alpha + \frac{\Delta\tilde{E}}{2}, \frac{1}{2}\right), \quad (4.57)$$

where $\beta(x, a, b)$ is the incomplete Beta function. This form is valid for all $\Delta\tilde{E}$. However, Eq. (4.56) allows a much faster numerical computation of $D(\alpha, \Delta\tilde{E})$ in the case $\Delta\tilde{E} > 0$. The cancellation of Eq. (4.57) with the cutoff of $1/C(\Lambda)$ for large Λ is not explicit. However, we have verified that this is the case for all studied α and use $\Lambda > 10^4 \sqrt{m\omega/2}$.

For an isotropic trap $\alpha = 1$, Eq. (4.56) gives a simple analytic form

$$D(1, \Delta\tilde{E}) = -\frac{m\Lambda}{2(2\pi)^{3/2}} + \frac{1}{\omega} \left(\frac{m\omega}{2\pi}\right)^{3/2} \frac{\sqrt{\pi}\Gamma(\Delta\tilde{E}/2)}{\Gamma((\Delta\tilde{E}-1)/2)}, \quad (4.58)$$

which can be analytically extended for all $(\Delta\tilde{E}-1)/2 \neq -1, -2, \dots$

4.2 Polaron Energy in Traps

In this section, we present the numerical results of the $N+1$ body energy Eq. (4.44). We consider only closed shells, which allows us to define the Fermi level $n_F = 0, 1, 2, \dots$ and the Fermi energy $\varepsilon_F = \omega(\alpha n_F + (2\alpha+1)/2)$.

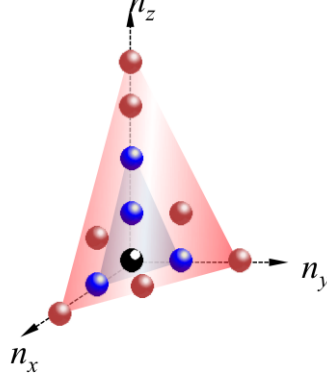


Figure 4.2: Examples of closed-shell configurations, shown for $\alpha = 2$. Only one spin-up particle exists for $n_F = 0$. The particles colored in blue fill the Fermi sea to the next Fermi level $n_F = 1$. The particles colored in red fill the Fermi sea to the level $n_F = 2$.

Fig. 4.2 shows examples of closed-shell configurations. Closed shells are convenient because any sum over the occupied states can be written as

$$\sum_{\varepsilon_{\mathbf{n}} \leq \varepsilon_F} \equiv \sum_{\alpha(n_x+n_y)+n_z \leq \alpha n_F} = \sum_{n_x=0}^{n_F} \sum_{n_y=0}^{n_F-n_x} \sum_{n_z=0}^{\alpha(n_F-n_x-n_y)}. \quad (4.59)$$

The majority particle number is then given by

$$N = \sum_{\varepsilon_{\mathbf{n}} \leq \varepsilon_F} 1 = \frac{1}{6}(1+n_F)(2+n_F)(3+\alpha n_F). \quad (4.60)$$

4.2.1 Generalized Energy Scaling in Traps

For large scattering lengths, $1/a = 0$, the energy E is a universal function of the aspect ratio and the spin-up particle number $N = N_{\uparrow}$. We look for a generalized scaling relation in traps which, in the large- N limit, reproduces the scaling relation in the uniform system, $E = \mu_{\downarrow} = \eta \mu_{\uparrow}$ where $\mu_{\uparrow} = E_F$. The natural way to proceed is to use the Local Density Approximation (LDA) discussed in Section 3.5.1. In a trapped non-interacting system, the spin-up chemical potential μ_{\uparrow}^0 that determines N is equal to the local Fermi energy at the center of the trap, $\mu_{\uparrow}^0 = k_F^2(\mathbf{0})/2m$. Therefore, we generalize

4.2. Polaron Energy in Traps

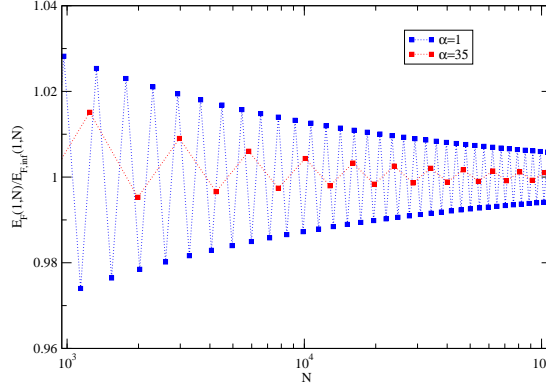


Figure 4.3: Local Fermi energy $E_F(\alpha, N)$ at the center of the trap divided by the large- N expression $E_{F,\infty}(\alpha, N)$ as a function of spin-up particle number N .

the scaling for the uniform system to anisotropic traps,

$$E = \eta(\alpha, N)E_F(\alpha, N), \quad (4.61)$$

where $E_F(\alpha, N) = (6\pi^2 n_\uparrow(\mathbf{r} = \mathbf{0}))^{2/3}/2m$ is the local Fermi energy of the spin-up particles at the center of the trap. The local density $n_\uparrow(\mathbf{0})$ at the center of the trap is given by

$$n_\uparrow(\mathbf{0}) = \alpha \left(\frac{m\omega}{\pi} \right)^{3/2} \sum_{\varepsilon_{\mathbf{n}} \leq \varepsilon_F} \prod_{i=x,y,z} \frac{H_{n_i}^2(0)}{2^{n_i} n_i!}, \quad (4.62)$$

where $H_n(x)$ are the Hermite polynomials.

In Fig. 4.3, we show $E_F(\alpha, N)$ divided by the large- N expression $E_{F,\infty}(\alpha, N) = \omega (6\alpha^2 N)^{1/3}$ [42] for $\alpha = 1$ and 35. The points are for alternating odd-even values of the Fermi level n_F . For both α , the local Fermi energy approaches $E_{F,\infty}(\alpha, N)$ from above (below) for odd (even) n_F . With increasing α , this effect decreases and the envelopes approach the large- N result faster.

4.2.2 Results for the Polaron Energy

Direct evaluation of Eq. (4.44) is extremely involved. This is due to the multiple nested sums, and also the need to find the inverse matrix $M^{-1}(\varepsilon_F, E + \varepsilon_{\mathbf{h}})$. To enable numerical solution, we take the matrix $M(\varepsilon_F, E + \varepsilon_{\mathbf{h}})$ to

4.2. Polaron Energy in Traps

n_F	N	η : MC [5]	η : Variational
0	1		0.246
1	4	-2.89×10^{-2}	1.09×10^{-3}
2	10	-0.135	-0.137
3	20	-0.274	-0.273
4	35	-0.278	-0.282

Table 4.1: Polaron energy $\eta(1, N)$ in isotropic traps for the five lowest closed-shell configurations. The MC results are taken from Ref. [5].

be diagonal, which is correct in the large- N limit. We have also checked numerically that the off-diagonal elements are considerably smaller than the diagonal ones for all studied values of N . Furthermore, we have found numerically that the diagonal elements depend only on the center-of-mass excitation $\varepsilon_{\mathbf{S}}$.

Using Eq. (4.61), we solve Eq. (4.44) iteratively for $\eta(\alpha, N)$, with a numerical precision better than 1%. We first consider isotropic traps with $\alpha = 1$. For one spin-up fermion, we find $\eta = 0.246$. The exact ground-state energy in a trap¹¹ [12] is $E(1, 1) = \omega/2 > 0$, thus $\eta(1, 1) = (36\pi)^{-1/3} = 0.207$. In Table 4.1, we show $\eta(1, N)$ for the five lowest closed-shell configurations, $N = 1, 4, 10, 20, 35$, in comparison with the Monte-Carlo (MC) results¹² of Ref. [5]. We see that the variational wavefunction and approximation scheme produce excellent agreement with the MC results even for small N .

In Fig. 4.4, we show $\eta(1, N)$ for an isotropic trap as a function of N . The effects due to particle numbers and trapping confinement are clearly present: The odd-even systematics seen in the local Fermi energy $E_F(1, N)$ is small compared to the decrease of $\eta(1, N)$ with particle number. Therefore, the decrease is not due to the change in the local Fermi energy. With increasing N , $\eta(1, N)$ decreases and saturates. Using the Ansatz, $\eta(\alpha, N) = a(\alpha)(1 + b(\alpha)N^{-c(\alpha)})$, we fit our numerical results for odd (even) n_F separately and find $a(1) \approx -0.61$ and $c(1) \approx 0.34$ (0.32). This is in very good agreement with $\eta = -0.607$ for the uniform system [17]

¹¹The exact two-body ground-state energy [12] is reproduced, if we generalize the first term in Eq. (4.22) to include a sum over the spin-down particle in level \mathbf{n} , $\sum_{\mathbf{n}} \phi_{\mathbf{n}}|\mathbf{n}\rangle$. This calculation is found in Appendix A.

¹²In Ref. [5], the results are given as total energies. We have converted the results to $\eta(1, N)$ using Eq. (4.61).

4.2. Polaron Energy in Traps

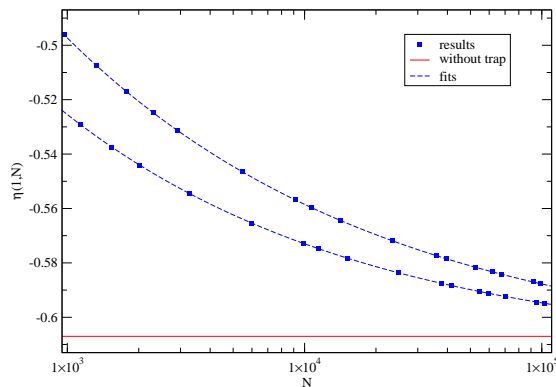


Figure 4.4: Polaron energy $\eta(1, N)$ for an isotropic trap, with fits to our numerical results (see text). The horizontal line represents $\eta = -0.607$ for the uniform system [17].

and large- N scaling $1/E_{F,\infty}(1, N) \sim N^{-1/3}$. Therefore, $\sim 10\%$ changes of η are natural for $N \sim 10^4$.

In Fig. 4.5, we show $\eta(\alpha, N)$ as a function of the spin-up particle number for various aspect ratios from $\alpha = 1$ to $\alpha = 35$. The polaron energy depends significantly on the aspect ratio, as well as the particle number. The odd-even Fermi level effect decreases with increasing N, α and is negligible for $\alpha \gtrsim 10$. For fixed N , $\eta(\alpha, N)$ increases with increasing α . For each α , $\eta(\alpha, N)$ decreases for increasing N and saturates, and the dependence on N is stronger for larger aspect ratio. For each α , we fit our combined results (including odd and even n_F) with the power-law Ansatz and show the fits in Fig. 4.5. We find $a(\alpha) \approx -0.61(1)$, consistent with the uniform result for all studied aspect ratios, and $c(\alpha)$ ranges from $c(1) \approx 0.36$ to $c(35) \approx 0.31$. The results of the fits are shown in Table 4.2.

To summarize, the polaron energy increases for lower particle numbers or higher elongation. In the uniform system, the spin-down fermion has the maximum phase space available for interactions, which lowers the energy. Therefore, reducing particle numbers or increasing elongation, which effectively lowers dimensions, moves the system away from the uniform limit and increases the polaron energy. This is expected to increase the critical polarization and decrease the critical concentration, because the polarized normal gas becomes less favored. We find that finite-size effects are stronger in highly elongated systems, while trap geometry becomes less important at higher particle numbers.

4.3. Phase Structure in Trapped Fermi Gases

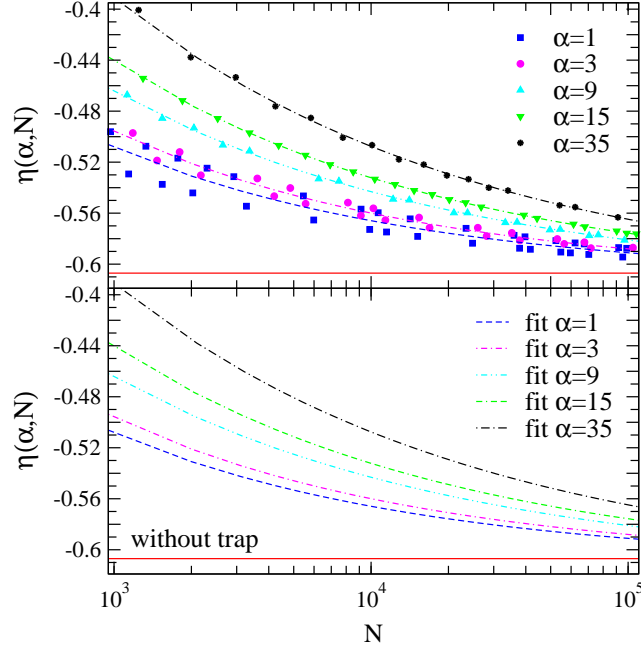


Figure 4.5: Energy $\eta(\alpha, N)$ as a function of N for various aspect ratios α , compared to $\eta = -0.607$ for the uniform system [17] (horizontal lines). The fits are discussed in the text and shown separately in the lower panel.

α	Fit
1	$-0.61(1 - 2.00N^{-0.36})$
3	$-0.61(1 - 2.21N^{-0.36})$
9	$-0.62(1 - 2.22N^{-0.32})$
15	$-0.61(1 - 2.67N^{-0.32})$
35	$-0.62(1 - 3.12N^{-0.31})$

Table 4.2: Fit results to the combined (odd and even n_F) results for $\eta(\alpha, N)$ using the Ansatz $a(\alpha)(1 + b(\alpha)N^{-c(\alpha)})$.

4.3 Phase Structure in Trapped Fermi Gases

We now apply the Local Density Approximation (LDA) to explore the impact of the calculated finite-size and confinement effects on the phase struc-

ture. In Section 3.5, we discussed the validity of the LDA, and constructed the density profile, given by Eqs. (3.40)-(3.46). As discussed in Section 3.6, the LDA breaks down for the Rice experiment [40, 41]. Here, we only use the LDA to explore the impact of $\eta(\alpha, N)$ on the critical polarization. In a full density-functional calculation, this can also be combined with surface tension [24] or gradient terms.

Eqs. (3.40)-(3.46) require the knowledge of the energy densities for both the superfluid and the normal phase. For the uniform system at unitarity, the energy density of the superfluid ϵ_s is given by (following the discussion of Section 2.4.2)

$$\epsilon_S(n_S) = \xi \frac{3}{5} \frac{(6\pi^2 n_S)^{2/3}}{2m}, \quad (4.63)$$

with superfluid density n_S and universal energy $\xi = 0.42$ of the symmetric system [13, 43]. In principle, $\xi = \xi(\alpha, N)$ in traps. In this work, we assume the uniform value because we are interested in the impact of the change in polaron energy due to particle number and trap geometry effects. In addition, the use of the uniform value is consistent with $\xi = 0.46 \pm 0.05$ in the Rice experiment [40].

The energy density of the partially-polarized normal Fermi liquid ϵ_N is given by [47]

$$\epsilon_N(x) = \frac{3}{5} \frac{(6\pi^2 n_\uparrow)^{2/3}}{2m} \epsilon(x). \quad (4.64)$$

We construct the equation of state following the discussion of Section 3.4. Assuming $x \ll 1$, the energy of adding spin-down fermions to the normal phase is determined by $\eta(\alpha, N)$, with corrections due to a spin-down quasiparticle effective mass m^* and due to quasiparticle interactions B [47]:

$$\epsilon(x) = \left[1 + \frac{5}{3} \eta(\alpha, N) x + \frac{m}{m^*} x^{5/3} + B x^2 \right]. \quad (4.65)$$

We take $\eta(\alpha, N)$ from Fig. 4.5, but for simplicity consider two cases for the quasiparticle spectrum: the non-interacting values $m^*/m = 1$, $B = 0$, as well as the MC values $m^*/m = 1.09$, $B = 0.14$ [43], which show these are corrections to the leading effects from η . This however does not include the effects of Fermi statistics of the minority particles on η .

In Fig. 4.6, we show the dependence of the critical polarization $P_c(\alpha, N_{\text{tot}})$ and the critical concentration $x_c(\alpha, N_{\text{tot}})$ as a function of aspect ratio, for total particle numbers $N_{\text{tot}} = 10^4$ and $N_{\text{tot}} = 10^5$, where the experimental differences from the uniform system exists. They are also displayed in Table 4.3, which includes an additional set of data for $N_{\text{tot}} = 10^3$. For

4.3. Phase Structure in Trapped Fermi Gases

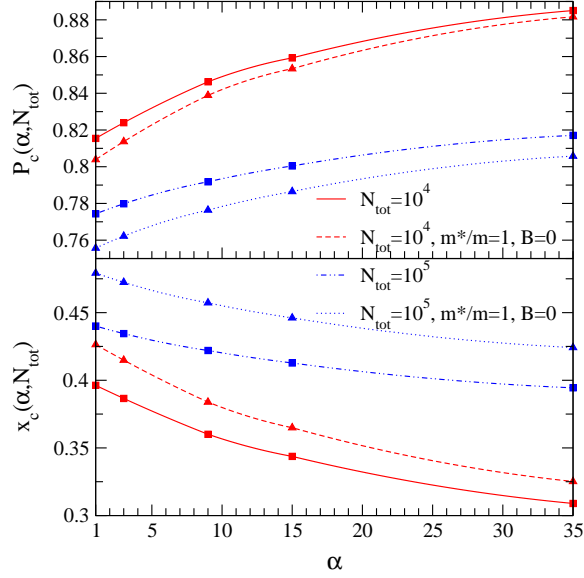


Figure 4.6: Upper panel: Critical polarization $P_c(\alpha, N_{\text{tot}})$ as a function of aspect ratio α for $N_{\text{tot}} = 10^4$ (upper) and $N_{\text{tot}} = 10^5$ (lower set of curves). Lower panel: Critical density ratio $x_c(\alpha, N_{\text{tot}})$ for $N_{\text{tot}} = 10^4$ (lower) and $N_{\text{tot}} = 10^5$ (upper set of curves). Results are shown for two approximations to the quasiparticle spectrum and interaction.

$\alpha = 1$, $N_{\text{tot}} = 10^7$ and the MC m^* , B values, we reach the uniform system $P_c = 0.74$ and $x_c = 0.47$. For fixed $N_{\text{tot}} = 10^4$ and MC parameters, P_c changes by $\sim 9\%$ and x_c by $\sim 23\%$ as α increases from 1 to 35. For fixed $\alpha = 35$ and MC parameters, P_c increases by $\sim 8 - 9\%$ for every factor 10 decrease of N_{tot} , and x_c decreases by $\sim 21 - 42\%$. In addition, we show in Fig. 4.6 the dependence on the quasiparticle parameters. For given α and N_{tot} , P_c is larger and x_c smaller for the MC m^* , B values, compared to the non-interacting values $m^*/m = 1$, $B = 0$, but as expected, the uncertainty due to m^* , B is smaller than the variation of P_c and x_c with α , N_{tot} . This dependence also becomes weaker with increasing α and decreasing N_{tot} .

In summary, for lower particle numbers and more elongated traps, the energy of the normal polarized phase increases and the superfluid extends to larger population imbalances. Finite-size effects are stronger in highly-elongated systems as the dimensionality of the problem is continuously reduced with increasing aspect ratio. This provides a microscopic understand-

4.4. Outlook: Towards the $N + M$ Body System

N_{tot}	α	P_c	P_c	x_c	x_c
		(MC m^* , B)	($m^*/m=1$, $B=0$)	(MC m^* , B)	($m^*/m=1$, $B=0$)
10^3	1	0.88	0.88	0.31	0.33
	3	0.90	0.89	0.29	0.31
	9	0.92	0.92	0.25	0.26
	15	0.94	0.94	0.23	0.23
	35	0.96	0.96	0.18	0.18
10^4	1	0.82	0.80	0.40	0.43
	3	0.82	0.81	0.39	0.41
	9	0.85	0.84	0.36	0.38
	15	0.86	0.85	0.34	0.36
	35	0.89	0.88	0.31	0.33
10^5	1	0.77	0.76	0.44	0.48
	3	0.78	0.76	0.43	0.47
	9	0.79	0.78	0.42	0.46
	15	0.80	0.79	0.41	0.45
	35	0.82	0.81	0.39	0.42

Table 4.3: Critical polarization P_c and critical concentration x_c as a function of aspect ratio α and total particle numbers N_{tot} . Results are shown for the MC values $m^*/m = 1.09$ and $B = 0.14$ in the uniform system, and for the non-interacting values $m^*/m = 1$ and $B = 0$.

ing of the MIT-Rice differences due to the dependence of the polaron energy on the particle number and the trap geometry.

4.4 Outlook: Towards the $N + M$ Body System

The $N + 1$ body problem is a natural first step towards general asymmetries and towards contributions to the total energy beyond $\eta(\alpha, N)$. The study of a general $N + M$ body system will allow for a better quantitative understanding of the critical polarization and the MIT-Rice differences. The next chapter will outline the work on $N + M$ body problem in both the uniform system and trapped Fermi gases.

Chapter 5

$N + M$ Body Problem

In Chapter 4, we saw that finite-size and confinement effects due to the variations of the polaron energy lead to significant changes in the phase structure: for lower particle numbers or higher elongation, the polaron energy decreases, lowering the energy of the normal state, which leads to a decrease in the critical concentration and an increase in the critical polarization. This trend is in agreement with the experimental results. The natural next step is to microscopically study finite-size and confinement effects for general asymmetry. This will allow for a better understanding of the trapped system and of the experimental differences.

In this chapter, I will present results for the $N + M$ body problem. To study general asymmetry, one can consider the formation of a partially-polarized normal gas by building a Fermi sea of spin-down quasiparticles. We will generalize the variational Ansatz beyond a single minority particle to calculate the energy gain $E = \mu_{\downarrow}(N_{\uparrow}, N_{\downarrow})$ of adding the N_{\downarrow}^{th} spin-down fermion. In the following sections, I will present our work on the $N + M$ body problem in the uniform and the trapped systems, and provide an outlook.

5.1 $N + M$ Body Problem in the Uniform System

In this section, I will present our work on the $N + M$ body problem in the uniform system. First, we investigate $N + M$ body problem in the uniform system. We will derive the self-consistent equation for the energy gain, construct the equation of state of the partially-polarized normal Fermi liquid, and apply the result to compute the critical concentration and critical polarization for traps containing large particle numbers.

5.1.1 Derivation of the $N + M$ Body Energy

The formalism of the $N + M$ body problem in the uniform system is as follow. We consider a two-component Fermi gas with Fermi energies $E_{F,\sigma} = k_{F,\sigma}^2/2m$, where $k_{F,\sigma} = (6\pi^2 n_{\sigma})^{1/3}$ and $\sigma = \uparrow, \downarrow$. We assume the asymmetric configuration $k_{F,\downarrow} < k_{F,\uparrow}$, and define $\gamma = k_{F,\downarrow}/k_{F,\uparrow} = x^{1/3}$, which measures

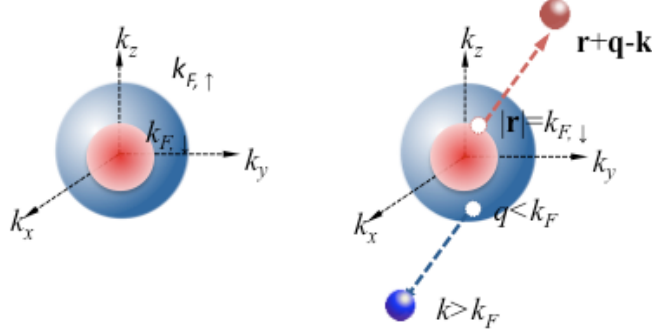


Figure 5.1: Graphical representation of the components of the trial wavefunction Eq. (5.1). On the left is the state $|\Omega\rangle$, which consists of a spin-up Fermi sea with the majority Fermi momentum $k_{F,\uparrow}$ and a spin-down Fermi sea with the minority Fermi momentum $k_{F,\downarrow}$. On the right is the state $|\mathbf{k}, \mathbf{q}, \mathbf{r}\rangle$, in which a spin-up fermion with momentum \mathbf{q} below the majority Fermi surface ($q < k_{F,\uparrow}$) is excited to a momentum \mathbf{k} above the Fermi surface ($k > k_{F,\uparrow}$), and a spin-down fermion with momentum $\mathbf{r} = \hat{\mathbf{r}}k_{F,\downarrow}$ on the spin-down Fermi surface now has momentum $\mathbf{r} + \mathbf{q} - \mathbf{k}$ to satisfy momentum conservation. The state $|\mathbf{k}, \mathbf{q}, \mathbf{r}\rangle$ has to satisfy $|\mathbf{r} + \mathbf{q} - \mathbf{k}| > k_{F,\downarrow}$ due to Pauli exclusion.

the asymmetry of the system. The Hamiltonian is given by Eq. (3.9), with the coupling constant Eq. (3.10). In the unitary regime $1/k_{F,\uparrow}a = 0$, we study the energy $E = \mu_\downarrow(N_\uparrow, N_\downarrow)$ of adding a single impurity. In the unitary regime, this energy is a universal function of $x = \gamma^3$, $E = \mu_\downarrow = \eta(x)\mu_\uparrow$, where $\mu_\uparrow = E_{F,\uparrow}$ and $x = n_\downarrow/n_\uparrow$.

We generalize the Chevy Ansatz [17, 18, 22] to include general asymmetry γ . Keeping up to one-particle–one-hole excitations, the trial state has the following form

$$|\psi\rangle = \phi_0|\Omega\rangle + \sum_{\mathbf{k}, \mathbf{q}, \mathbf{r}} \phi_{\mathbf{k}, \mathbf{q}, \mathbf{r}} \Theta_{\mathbf{k}, \mathbf{q}, \mathbf{r}} |\mathbf{k}, \mathbf{q}, \mathbf{r}\rangle. \quad (5.1)$$

Here, $|\Omega\rangle$ is the non-interacting ground state with the spin-up fermions filled up to $k < k_{F,\uparrow}$ level, and spin-down fermions filled up to $k < k_{F,\downarrow}$ level. In the state $|\mathbf{k}, \mathbf{q}, \mathbf{r}\rangle$, a spin-up fermion with momentum \mathbf{q} below the majority Fermi surface ($q < k_{F,\uparrow}$) is excited to a momentum \mathbf{k} above the majority Fermi surface ($k > k_{F,\uparrow}$), and a spin-down fermion with momentum

5.1. $N + M$ Body Problem in the Uniform System

$\mathbf{r} = \hat{\mathbf{r}}k_{F,\downarrow}$ on the spin-down Fermi surface now has momentum $\mathbf{r} + \mathbf{q} - \mathbf{k}$ to satisfy momentum conservation. The sums over \mathbf{k} , \mathbf{q} , and \mathbf{r} are implicitly restricted to $q < k_{F,\uparrow}$, $k_{F,\uparrow} < k$, and $|\mathbf{r}| = k_{F,\downarrow}$. A prefactor $\Theta_{\mathbf{k},\mathbf{q},\mathbf{r}} = \Theta(|\mathbf{r} + \mathbf{q} - \mathbf{k}|^2 - k_{F,\downarrow}^2)$ in the second sum ensures the restriction $|\mathbf{r} + \mathbf{q} - \mathbf{k}| > k_{F,\downarrow}$ to satisfy Pauli exclusion.

We write Eq. (3.9) as $H = H_0 + V$, where H_0 is the non-interacting Hamiltonian, and V is the interacting part. We first evaluate $\langle \psi | H_0 | \psi \rangle$:

$$\begin{aligned} H_0 | \psi \rangle &= \phi_0 \left(\sum_{\mathbf{k}'} \epsilon_{\mathbf{k}'} a_{\mathbf{k}',\uparrow}^\dagger a_{\mathbf{k}',\uparrow} | \Omega \rangle + \sum_{\mathbf{k}'} \epsilon_{\mathbf{k}'} a_{\mathbf{k}',\downarrow}^\dagger a_{\mathbf{k}',\downarrow} | \Omega \rangle \right) \\ &+ \sum_{\mathbf{k},\mathbf{q},\mathbf{r}} \phi_{\mathbf{k},\mathbf{q},\mathbf{r}} \Theta_{\mathbf{k},\mathbf{q},\mathbf{r}} \sum_{\mathbf{k}'} \epsilon_{\mathbf{k}'} \left(a_{\mathbf{k}',\uparrow}^\dagger a_{\mathbf{k}',\uparrow} | \mathbf{k}, \mathbf{q}, \mathbf{r} \rangle + a_{\mathbf{k}',\downarrow}^\dagger a_{\mathbf{k}',\downarrow} | \mathbf{k}, \mathbf{q}, \mathbf{r} \rangle \right). \end{aligned} \quad (5.2)$$

Here, the sums over \mathbf{k}' run over all levels. The operators act on the states to yield:

$$a_{\mathbf{k}',\uparrow}^\dagger a_{\mathbf{k}',\uparrow} | \Omega \rangle = \begin{cases} | \Omega \rangle & \epsilon_{\mathbf{k}'} \leq E_{F,\uparrow}, \\ 0 & \text{else,} \end{cases} \quad (5.3)$$

$$a_{\mathbf{k}',\downarrow}^\dagger a_{\mathbf{k}',\downarrow} | \Omega \rangle = \begin{cases} | \Omega \rangle & \epsilon_{\mathbf{k}'} \leq E_{F,\downarrow}, \\ 0 & \text{else,} \end{cases} \quad (5.4)$$

$$a_{\mathbf{k}',\uparrow}^\dagger a_{\mathbf{k}',\uparrow} | \mathbf{k}, \mathbf{q}, \mathbf{r} \rangle = \begin{cases} | \mathbf{k}, \mathbf{q}, \mathbf{r} \rangle & \epsilon_{\mathbf{k}'} \leq E_{F,\uparrow} \text{ and } \mathbf{k}' \neq \mathbf{q}, \\ | \mathbf{k}, \mathbf{q}, \mathbf{r} \rangle & \mathbf{k}' = \mathbf{k}, \\ 0 & \text{else,} \end{cases} \quad (5.5)$$

$$a_{\mathbf{k}',\downarrow}^\dagger a_{\mathbf{k}',\downarrow} | \mathbf{k}, \mathbf{q}, \mathbf{r} \rangle = \begin{cases} | \mathbf{k}, \mathbf{q}, \mathbf{r} \rangle & \epsilon_{\mathbf{k}} \leq E_{F,\downarrow} \text{ and } \mathbf{k}' \neq \mathbf{r}, \\ | \mathbf{k}, \mathbf{q}, \mathbf{r} \rangle & \mathbf{k}' = \mathbf{r} + \mathbf{q} - \mathbf{k}, \\ 0 & \text{else.} \end{cases} \quad (5.6)$$

Therefore, we find

$$\begin{aligned} \langle \psi | H_0 | \psi \rangle &= \sum_{\mathbf{k},\mathbf{q},\mathbf{r}} \Theta_{\mathbf{k},\mathbf{q},\mathbf{r}} |\phi_{\mathbf{k},\mathbf{q},\mathbf{r}}|^2 (\epsilon_{\mathbf{k}} + \epsilon_{\mathbf{r} + \mathbf{q} - \mathbf{k}} - \epsilon_{\mathbf{q}} - E_{F,\downarrow}) \\ &+ \left(\sum_{\epsilon_{\mathbf{k}} \leq E_{F,\uparrow}} \epsilon_{\mathbf{k}} + \sum_{\epsilon_{\mathbf{k}} \leq E_{F,\downarrow}} \epsilon_{\mathbf{k}} \right). \end{aligned} \quad (5.7)$$

The last term gives the energy of the non-interacting system, and is subtracted when we study the energy gain.

5.1. $N + M$ Body Problem in the Uniform System

Next, we proceed to calculate $\langle \psi | V | \psi \rangle$:

$$\begin{aligned}
 V|\psi\rangle &= \frac{g(\Lambda)}{V} \sum_{\mathbf{k}', \mathbf{k}'', \Delta \mathbf{k}} a_{\mathbf{k}'+\Delta \mathbf{k}, \uparrow}^\dagger a_{\mathbf{k}''-\Delta \mathbf{k}, \downarrow}^\dagger a_{\mathbf{k}'', \downarrow} a_{\mathbf{k}', \uparrow} |\Omega\rangle \\
 &+ \frac{g(\Lambda)}{V} \sum_{\mathbf{k}, \mathbf{q}, \mathbf{r}} \phi_{\mathbf{k}, \mathbf{q}, \mathbf{r}} \Theta_{\mathbf{k}, \mathbf{q}, \mathbf{r}} \sum_{\mathbf{k}', \mathbf{k}'', \Delta \mathbf{k}} a_{\mathbf{k}'+\Delta \mathbf{k}, \uparrow}^\dagger a_{\mathbf{k}''-\Delta \mathbf{k}, \downarrow}^\dagger a_{\mathbf{k}'', \downarrow} a_{\mathbf{k}', \uparrow} |\mathbf{k}, \mathbf{q}, \mathbf{r}\rangle.
 \end{aligned} \tag{5.8}$$

Here, the sums over \mathbf{k} , \mathbf{k}'' are over all levels. Keeping up to one-particle-one-hole excitations, the relevant terms are

$$\begin{aligned}
 &a_{\mathbf{k}'+\Delta \mathbf{k}, \uparrow}^\dagger a_{\mathbf{k}''-\Delta \mathbf{k}, \downarrow}^\dagger a_{\mathbf{k}'', \downarrow} a_{\mathbf{k}', \uparrow} |\Omega\rangle \\
 = &\begin{cases} |\Omega\rangle & \begin{array}{l} \epsilon_{\mathbf{k}'} \leq E_{F, \uparrow}, \quad \epsilon_{\mathbf{k}''} \leq E_{F, \downarrow}, \\ \Delta \mathbf{k} = \mathbf{0}, \end{array} \\ \Theta_{\mathbf{k}, \mathbf{q}, \mathbf{r}} |\mathbf{k} = \mathbf{k}' + \Delta \mathbf{k}, \mathbf{q} = \mathbf{k}', \mathbf{r}\rangle & \begin{array}{l} \epsilon_{\mathbf{k}'} \leq E_{F, \uparrow}, \quad |\mathbf{k}''| = k_{F, \downarrow}, \\ \epsilon_{\mathbf{k}'+\Delta \mathbf{k}} > E_{F, \uparrow}, \quad \epsilon_{\mathbf{k}''-\Delta \mathbf{k}} > E_{F, \downarrow}, \end{array} \\ 0 & \text{else,} \end{cases}
 \end{aligned} \tag{5.9}$$

$$\begin{aligned}
 & a_{\mathbf{k}' + \Delta\mathbf{k}, \uparrow}^\dagger a_{\mathbf{k}'' - \Delta\mathbf{k}}^\dagger a_{\mathbf{k}'', \downarrow} a_{\mathbf{k}', \uparrow} |\mathbf{k}, \mathbf{q}, \mathbf{r}\rangle \\
 = & \left\{ \begin{array}{ll}
 |\mathbf{k}, \mathbf{q}, \mathbf{r}\rangle & \begin{array}{l} \epsilon_{\mathbf{k}''} \leq \epsilon_{F, \downarrow} \text{ and } \mathbf{k}'' \neq \mathbf{r}, \\ \epsilon_{\mathbf{k}'} \leq E_{F, \uparrow} \text{ and } \mathbf{k}' \neq \mathbf{q}, \Delta\mathbf{k} = \mathbf{0}, \end{array} \\
 |\mathbf{k}, \mathbf{k}' = \mathbf{q} + \mathbf{r} - \mathbf{r}', \mathbf{r}'\rangle & \begin{array}{l} \mathbf{k}'' = \mathbf{r}' \neq \mathbf{r}, \mathbf{r}' - \Delta\mathbf{k} = \mathbf{r}, \\ \mathbf{k}' + \Delta\mathbf{k} = \mathbf{q} \text{ and } \epsilon_{\mathbf{k}'} \leq E_{F, \uparrow}, \end{array} \\
 |\mathbf{k} + \mathbf{r}' - \mathbf{r}, \mathbf{q}, \mathbf{r}'\rangle & \begin{array}{l} \mathbf{k}'' = \mathbf{r}' \neq \mathbf{r}, \mathbf{r}' - \Delta\mathbf{k} = \mathbf{r}, \\ \mathbf{k}' = \mathbf{k} \text{ and } \epsilon_{\mathbf{k}' + \Delta\mathbf{k}} > E_{F, \uparrow}, \end{array} \\
 |\Omega\rangle & \begin{array}{l} \mathbf{k}'' = \mathbf{r} + \mathbf{q} - \mathbf{k}, \mathbf{k}'' - \Delta\mathbf{k} = \mathbf{r}, \mathbf{k}' = \mathbf{k}, \end{array} \\
 \Theta_{\mathbf{p}, \mathbf{q}, \mathbf{r}} |\mathbf{p} = \mathbf{k}' + \Delta\mathbf{k}, \mathbf{q}, \mathbf{r}\rangle & \begin{array}{l} \mathbf{k}'' = \mathbf{r} + \mathbf{q} - \mathbf{k}, \epsilon_{\mathbf{k}'' - \Delta\mathbf{k}} > E_{F, \downarrow}, \\ \mathbf{k}' = \mathbf{k}, \text{ and } \epsilon_{\mathbf{k}' + \Delta\mathbf{k}} > E_{F, \uparrow}, \end{array} \\
 \Theta_{\mathbf{k}, \mathbf{q}, \mathbf{r}} |\mathbf{k}, \mathbf{q}' = \mathbf{k}', \mathbf{r}\rangle & \begin{array}{l} \mathbf{k}'' = \mathbf{r} + \mathbf{q} - \mathbf{k}, \epsilon_{\mathbf{k}'' - \Delta\mathbf{k}} > E_{F, \downarrow}, \\ \mathbf{k}' + \Delta\mathbf{k} = \mathbf{q}, \epsilon_{\mathbf{k}} \leq E_{F, \uparrow} \text{ and } \mathbf{k}' \neq \mathbf{q}, \end{array} \\
 0 & \text{else.} \end{array} \right. \tag{5.10}
 \end{aligned}$$

Making the following change of indices $\mathbf{k}'' \rightarrow \mathbf{q}_\downarrow$ and $\mathbf{p} \rightarrow \mathbf{k}$, we obtain

$$\begin{aligned}
 V|\psi\rangle &= \frac{g(\Lambda)}{V} \phi_0 \left(\sum_{\mathbf{q}, \mathbf{q}_\downarrow} |\Omega\rangle + \sum_{\mathbf{k}, \mathbf{q}, \mathbf{r}} \Theta_{\mathbf{k}, \mathbf{q}, \mathbf{r}} |\mathbf{k}, \mathbf{q}, \mathbf{r}\rangle \right) + \frac{g(\Lambda)}{V} \sum_{\mathbf{k}, \mathbf{q}, \mathbf{r}} \Theta_{\mathbf{k}, \mathbf{q}, \mathbf{r}} \phi_{\mathbf{k}, \mathbf{q}, \mathbf{r}} \\
 &\times \left(\sum_{\mathbf{q}' \neq \mathbf{q}, \mathbf{q}_\downarrow \neq \mathbf{r}} |\mathbf{k}, \mathbf{q}, \mathbf{r}\rangle + \sum_{\mathbf{q}' \neq \mathbf{q}} \Theta_{\mathbf{k}, \mathbf{q}', \mathbf{r}} |\mathbf{k}, \mathbf{q}', \mathbf{r}\rangle + \sum_{\mathbf{q}', \mathbf{r}' \neq \mathbf{r}} |\mathbf{k}, \mathbf{q}', \mathbf{r}'\rangle \right. \\
 &\left. + \sum_{\mathbf{r}' \neq \mathbf{r}} |\mathbf{k} + \mathbf{r}' - \mathbf{r}, \mathbf{q}, \mathbf{r}'\rangle + |\Omega\rangle + \sum_{\mathbf{k}'} \Theta_{\mathbf{k}', \mathbf{q}, \mathbf{r}} |\mathbf{k}', \mathbf{q}, \mathbf{r}\rangle \right), \tag{5.11}
 \end{aligned}$$

where the sums over \mathbf{q}' , \mathbf{k}' , and \mathbf{r}' follow the same convention as those over \mathbf{q} , \mathbf{k} , and \mathbf{r} respectively, and the sum over \mathbf{q}_\downarrow is restricted to $q_\downarrow < k_{F, \downarrow}$.

5.1. $N + M$ Body Problem in the Uniform System

Finally, we obtain

$$\begin{aligned}
\langle \psi | V | \psi \rangle &= \frac{g(\Lambda)}{V} |\phi_0|^2 \sum_{\mathbf{q}, \mathbf{q}_\perp} 1 + \frac{g(\Lambda)}{V} \sum_{\mathbf{k}, \mathbf{q}, \mathbf{r}} \Theta_{\mathbf{k}, \mathbf{q}, \mathbf{r}} (\phi_0 \phi_{\mathbf{k}, \mathbf{q}, \mathbf{r}}^* + \phi_{\mathbf{k}, \mathbf{q}, \mathbf{r}} \phi_0^*) \\
&+ \frac{g(\Lambda)}{V} \sum_{\mathbf{k}, \mathbf{q}, \mathbf{r}, \mathbf{k}'} \Theta_{\mathbf{k}, \mathbf{q}, \mathbf{r}} \Theta_{\mathbf{k}', \mathbf{q}, \mathbf{r}} \phi_{\mathbf{k}, \mathbf{q}, \mathbf{r}} \phi_{\mathbf{k}', \mathbf{q}, \mathbf{r}}^* \\
&+ \frac{g(\Lambda)}{V} \sum_{\mathbf{k}, \mathbf{q}, \mathbf{r}, \mathbf{q}' \neq \mathbf{q}} \Theta_{\mathbf{k}, \mathbf{q}, \mathbf{r}} \left(\sum_{\mathbf{q}_\perp \neq \mathbf{r}} |\phi_{\mathbf{k}, \mathbf{q}, \mathbf{r}}|^2 + \Theta_{\mathbf{k}, \mathbf{q}', \mathbf{r}} \phi_{\mathbf{k}, \mathbf{q}, \mathbf{r}} \phi_{\mathbf{k}, \mathbf{q}', \mathbf{r}}^* \right) \\
&+ \frac{g(\Lambda)}{V} \sum_{\mathbf{k}, \mathbf{q}, \mathbf{r}, \mathbf{r}' \neq \mathbf{r}} \Theta_{\mathbf{k}, \mathbf{q}, \mathbf{r}} (\phi_{\mathbf{k}, \mathbf{q}, \mathbf{r}} \phi_{\mathbf{k}, \mathbf{q} + \mathbf{r} - \mathbf{r}', \mathbf{r}'}^* + \phi_{\mathbf{k}, \mathbf{q}, \mathbf{r}} \phi_{\mathbf{k} + \mathbf{r}' - \mathbf{r}, \mathbf{q}, \mathbf{r}'}^*).
\end{aligned} \tag{5.12}$$

As we will check later, $\phi_{\mathbf{k}, \mathbf{q}, \mathbf{r}} \sim 1/k^2$, for large k . Therefore, all but the sums in the last two lines diverge as $\Lambda \rightarrow \infty$. The divergent sums are regularized by the renormliaztion of the coupling constant $g(\Lambda)$. However, the sums in the last two lines converge, and give zero contribution when multiplied by $g(\Lambda)$. Therefore, we can omit them from the rest of the calculation.

Combining Eq. (5.7) and Eq. (5.12), the energy to be minimized is

$$\begin{aligned}
\langle \psi | H | \psi \rangle &= \sum_{\mathbf{k}, \mathbf{q}, \mathbf{r}} \Theta_{\mathbf{k}, \mathbf{q}, \mathbf{r}} |\phi_{\mathbf{k}, \mathbf{q}, \mathbf{r}}|^2 (\epsilon_{\mathbf{k}} + \epsilon_{\mathbf{r} + \mathbf{q} - \mathbf{k}} - \epsilon_{\mathbf{q}} - E_{F, \downarrow}) + \frac{g(\Lambda)}{V} |\phi_0|^2 \sum_{\mathbf{q}_\perp, \mathbf{q}} 1 \\
&+ \frac{g(\Lambda)}{V} \sum_{\mathbf{k}, \mathbf{q}, \mathbf{r}} \Theta_{\mathbf{k}, \mathbf{q}, \mathbf{r}} \left(\phi_0 \phi_{\mathbf{k}, \mathbf{q}, \mathbf{r}}^* + \phi_{\mathbf{k}, \mathbf{q}, \mathbf{r}} \phi_0^* + \sum_{\mathbf{k}'} \Theta_{\mathbf{k}, \mathbf{q}, \mathbf{r}} \phi_{\mathbf{k}, \mathbf{q}, \mathbf{r}} \phi_{\mathbf{k}', \mathbf{q}, \mathbf{r}}^* \right).
\end{aligned} \tag{5.13}$$

Minimizing $\langle \psi | H | \psi \rangle$ with respect to ϕ_0 and $\phi_{\mathbf{k}, \mathbf{q}, \mathbf{r}}$ yields the following sets of equations:

$$E \phi_0 = \frac{g(\Lambda)}{V} \sum_{\mathbf{q}, \mathbf{q}_\perp} \phi_0 + \frac{g(\Lambda)}{V} \sum_{\mathbf{q}, \mathbf{r}} \left(\phi_0 + \sum_{\mathbf{k}} \Theta_{\mathbf{k}, \mathbf{q}, \mathbf{r}} \phi_{\mathbf{k}, \mathbf{q}, \mathbf{r}} \right), \tag{5.14}$$

$$E \phi_{\mathbf{k}, \mathbf{q}, \mathbf{r}} = (\epsilon_{\mathbf{k}} + \epsilon_{\mathbf{r} + \mathbf{q} - \mathbf{k}} - \epsilon_{\mathbf{q}} - E_{F, \downarrow}) \phi_{\mathbf{k}, \mathbf{q}, \mathbf{r}} + \frac{g(\Lambda)}{V} \left(\phi_0 + \sum_{\mathbf{k}'} \Theta_{\mathbf{k}', \mathbf{q}, \mathbf{r}} \phi_{\mathbf{k}', \mathbf{q}, \mathbf{r}} \right). \tag{5.15}$$

To simplify these equations, we define

$$\chi(\mathbf{q}, \mathbf{r}) = \phi_0 + \sum_{\mathbf{k}'} \Theta_{\mathbf{k}', \mathbf{q}, \mathbf{r}} \phi_{\mathbf{k}', \mathbf{q}, \mathbf{r}}, \tag{5.16}$$

5.1. $N + M$ Body Problem in the Uniform System

and solve for $\phi_{\mathbf{k},\mathbf{q},\mathbf{r}}$ in Eq. (5.15):

$$\phi_{\mathbf{k},\mathbf{q},\mathbf{r}} = \frac{1}{E + \epsilon_{\mathbf{q}} + E_{F,\downarrow} - \epsilon_{\mathbf{k}} - \epsilon_{\mathbf{r}+\mathbf{q}-\mathbf{k}}} \frac{g(\Lambda)}{V} \chi(\mathbf{q}, \mathbf{r}). \quad (5.17)$$

This verifies the large k behavior for $\phi_{\mathbf{k},\mathbf{q},\mathbf{r}} \sim 1/k^2$. Inserting Eq. (5.17) back into Eq. (5.16) allows us to eliminate $\phi_{\mathbf{k},\mathbf{q},\mathbf{r}}$, and we find

$$\chi(\mathbf{q}, \mathbf{r}) = \frac{\phi_0}{1 - \frac{g(\Lambda)}{V} \sum_{\mathbf{k}} \frac{\Theta_{\mathbf{k},\mathbf{q},\mathbf{r}}}{E + \epsilon_{\mathbf{q}} + E_{F,\downarrow} - \epsilon_{\mathbf{k}} - \epsilon_{\mathbf{r}+\mathbf{q}-\mathbf{k}}}}. \quad (5.18)$$

Then, we can use Eq. (5.14) to obtain the following,

$$E - \frac{g(\Lambda)}{V} \sum_{\mathbf{q},\mathbf{q}_{\downarrow}} 1 = \frac{g(\Lambda)}{V} \sum_{\mathbf{q},\mathbf{r}} \frac{1}{1 - \frac{g(\Lambda)}{V} \sum_{\mathbf{k}} \frac{\Theta_{\mathbf{k},\mathbf{q},\mathbf{r}}}{E + \epsilon_{\mathbf{q}} + E_{F,\downarrow} - \epsilon_{\mathbf{k}} - \epsilon_{\mathbf{r}+\mathbf{q}-\mathbf{k}}}}. \quad (5.19)$$

The coupling constant cancels the converging sum in the left-hand side. We then write the self-consistent equation for the energy E ,

$$E = \frac{1}{V} \sum_{q < k_{F,\uparrow}} \sum_{r = k_{F,\downarrow}} \frac{1}{\frac{1}{g(\Lambda)} + \frac{1}{V} \sum_{k > k_{F,\uparrow}} \frac{\Theta_{\mathbf{k},\mathbf{q},\mathbf{r}}}{\epsilon_{\mathbf{k}} + \epsilon_{\mathbf{r}+\mathbf{q}-\mathbf{k}} - E - \epsilon_{\mathbf{q}} - E_{F,\downarrow}}}. \quad (5.20)$$

Finally, using Eq. (3.10) for the expression of $g(\Lambda)$ leads to the self-consistent equation for the energy gain:

$$E = \frac{1}{V} \sum_{q < k_{F,\uparrow}} \sum_{r = k_{F,\downarrow}} \frac{1}{\frac{m}{4\pi a} + \frac{1}{V} \sum_{\mathbf{k}} \left(\frac{\Theta(k^2 - k_{F,\uparrow}^2) \Theta(|\mathbf{r} + \mathbf{q} - \mathbf{k}|^2 - k_{F,\downarrow}^2)}{\epsilon_{\mathbf{k}} + \epsilon_{\mathbf{r}+\mathbf{q}-\mathbf{k}} - E - \epsilon_{\mathbf{q}} - E_{F,\downarrow}} - \frac{1}{2\epsilon_{\mathbf{k}}} \right)}. \quad (5.21)$$

The Chevy equation Eq. (3.18) for the $N + 1$ body energy at $\mathbf{p} = \mathbf{0}$ is reproduced for $k_{F,\downarrow} = 0$.

5.1.2 Analytic Expression of the $N + M$ Body Energy in the Uniform System

Here, we will derive a form of Eq. (5.21) that is useful for numerical evaluation. First of all, we want to transform the sums into integrals. For the surface sum, we have

$$\sum_{\mathbf{r} = \hat{\mathbf{r}} k_{F,\downarrow}} f(\mathbf{r}) = \sum_{\mathbf{r}} \delta^3(r^2 - k_{F,\downarrow}^2) f(\mathbf{r}) = \int \frac{d\Omega_r}{4\pi} f(k_{F,\downarrow} \hat{\mathbf{r}}), \quad (5.22)$$

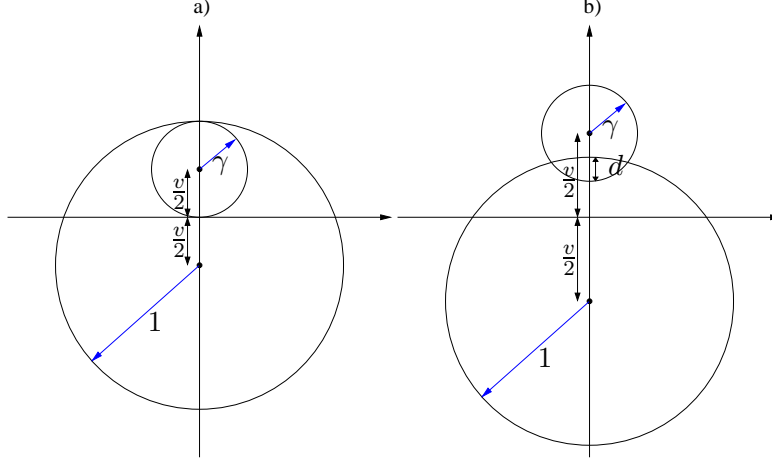


Figure 5.2: Geometries for the angular integral Eq. (5.27). a) The circle $|\mathbf{k} - \frac{\mathbf{v}}{2}|^2 = \gamma^2$ is completely inside the circle $|\mathbf{k} + \frac{\mathbf{v}}{2}|^2 = 1$. This is for the condition $0 \leq v \leq 1 - \gamma$. b) The circle centered at $|\mathbf{k} - \frac{\mathbf{v}}{2}|^2 = \gamma^2$ has partial overlap with the circle $|\mathbf{k} + \frac{\mathbf{v}}{2}|^2 = 1$, and $d = 1 + \gamma - v$ from the geometry. This is for the condition $1 - \gamma < v \leq 1 + \gamma$.

where $\int d\Omega_r = \int \sin \theta_r d\theta_r d\phi_r$ with (ϕ_r, θ_r) describing the spherical coordinates of a unit vector $\hat{\mathbf{r}}$, and we have used the identity $\delta^3(r^2 - R^2) = \delta(r - R)/(4\pi R^2)$. In order to solve Eq. (5.21), we divide both sides by $E_{F,\uparrow} = k_{F,\uparrow}^2/2m$, and replace each sum with an integral

$$\frac{1}{V} \sum_{\mathbf{k}} f(\mathbf{k}) \rightarrow \int \frac{d^3 k}{(2\pi)^3} f(\mathbf{k}). \quad (5.23)$$

After a change of variables $\mathbf{q}/k_{F,\uparrow} \rightarrow \mathbf{q}$, $\mathbf{k}/k_{F,\uparrow} \rightarrow \mathbf{k}$, $\mathbf{r}/k_{F,\uparrow} \rightarrow \mathbf{r} = \gamma \hat{\mathbf{r}}$, we obtain

$$\eta = \int_{q < 1} d^3 q \int \frac{d\Omega_r}{4\pi} \frac{1}{\frac{\pi^2}{k_{F,\uparrow}^2 a} + 2\pi I(\gamma, |\mathbf{r} + \mathbf{q}|, \eta + q^2 + \gamma^2)}, \quad (5.24)$$

where we have defined

$$I(\gamma, |\mathbf{v}|, \omega) = \frac{1}{2\pi} \int d^3 k \left(\frac{\Theta(|\mathbf{k} - \mathbf{v}|^2 - \gamma^2) \Theta(k^2 - 1)}{k^2 + |\mathbf{v} - \mathbf{k}|^2 - \omega} - \frac{1}{2k^2} \right). \quad (5.25)$$

We want to produce an analytic expression of $I(\gamma, |\mathbf{v}|, \omega)$. To do so, we symmetrize the first term of the integrand with a change of variable

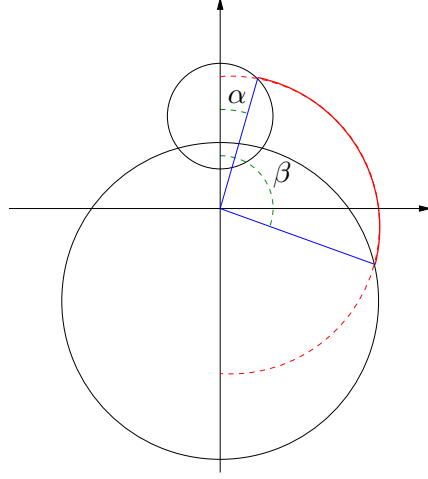


Figure 5.3: Graphical illustration of the angular integral $I_\theta(\gamma, k, v)$. For a given set of k , v , and γ , the circle of radius k centered at the origin is outside both circles $|\mathbf{k} - \frac{\mathbf{v}}{2}|^2 = \gamma^2$ and $|\mathbf{k} + \frac{\mathbf{v}}{2}|^2 = 1$ for the angular interval $0 \leq \alpha \leq \theta \leq \beta \leq \pi$. If this interval is empty, then $\alpha = \beta$.

$\mathbf{k} \rightarrow \mathbf{k} + \frac{\mathbf{v}}{2}$, and obtain

$$I(\gamma, |\mathbf{v}|, \omega) = \int_0^\infty dk \left(\frac{k^2}{2k^2 + \frac{v^2}{2} - \omega} I_\theta(\gamma, k, v) - 1 \right), \quad (5.26)$$

where we have defined the angular integral

$$I_\theta(\gamma, k, v) = \int_0^\pi \sin \theta d\theta \Theta(|\mathbf{k} - \frac{\mathbf{v}}{2}|^2 - \gamma^2) \Theta(|\mathbf{k} + \frac{\mathbf{v}}{2}|^2 - 1). \quad (5.27)$$

The angular integral $I_\theta(\gamma, k, v)$ can be understood in the following way. For given parameters k , v , γ , and integration variable θ , the integrand of $I_\theta(\gamma, k, v)$ is 1 if the circle of radius k centered at the origin lies outside of both circles $|\mathbf{k} - \frac{\mathbf{v}}{2}|^2 = \gamma^2$ and $|\mathbf{k} + \frac{\mathbf{v}}{2}|^2 = 1$ at the point θ , and 0 otherwise. The two geometries to be considered are given in Fig. 5.2. We note that since $|\mathbf{v}| = |\gamma \hat{\mathbf{r}} + \mathbf{q}|$, v must satisfy $0 \leq v \leq 1 + \gamma$ for $0 \leq q \leq 1$. Then, the conditions for each of the two cases are given by:

$$\begin{aligned} \text{a)} \quad & 0 \leq v \leq 1 - \gamma, \\ \text{b)} \quad & 1 - \gamma < v \leq 1 + \gamma. \end{aligned} \quad (5.28)$$

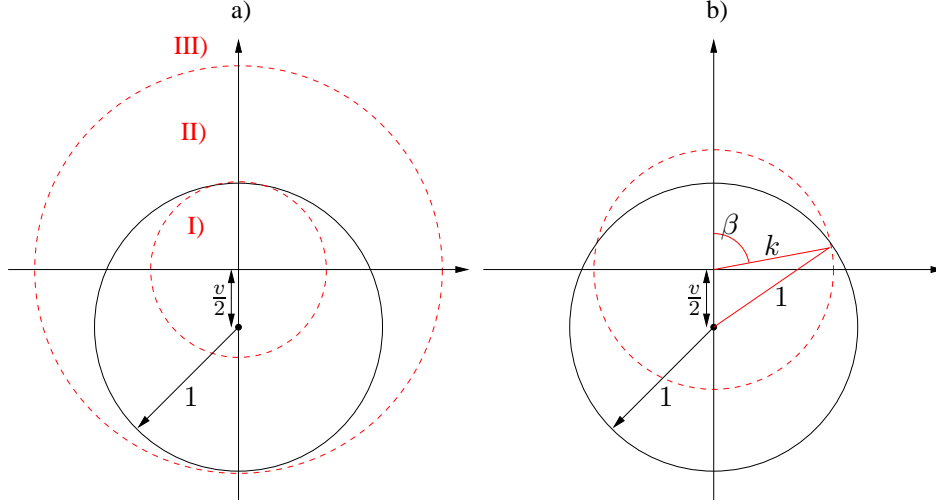


Figure 5.4: The integration region of the angular integral $I_\theta(\gamma, v, k)$ for $v < 1 - \gamma$. a) The domain for each of the three subcases I)-III). The solid circle is $|\mathbf{k} + \frac{v}{2}|^2 = 1$. The dashed circles are the boundaries that separate the subcases, and the domain of the subcases are labeled accordingly. For subcase I), it is clear that $\alpha = \beta$. For subcase III), $\alpha = 0$, and $\beta = \pi$. b) Subcase II) has $\alpha = 0$, and β can be found by with the relation $1 = k^2 + v^2/4 + kv \cos \beta$.

Suppose for a given set of k , v , and γ , the circle of radius k centered at the origin is outside both circles $|\mathbf{k} - \frac{v}{2}|^2 = \gamma^2$ and $|\mathbf{k} + \frac{v}{2}|^2 = 1$ for the angular interval $0 \leq \alpha \leq \theta \leq \beta \leq \pi$. Then, the angular integral is given by

$$I_\theta(\gamma, k, v) = \int_{\alpha(\gamma, k, v)}^{\beta(\gamma, k, v)} \sin \theta d\theta = \cos(\alpha(\gamma, k, v)) - \cos(\beta(\gamma, k, v)). \quad (5.29)$$

If this angular interval is empty, then $\alpha = \beta$, and $I_\theta(\gamma, k, v) = 0$.

We first investigate case a), with the three subcases shown in Fig. 5.4 a). Subcase I) is for the condition $k < 1 - v/2$, with $\alpha = \beta$. Subcase II), shown in Fig. 5.4 b), is for the condition $1 - v/2 < k < 1 + v/2$, with $\alpha = 0$, and $\cos \beta = (1 - k^2 - v^2/4)/kv$. Subcase III) is for $1 + v/2 < k$, with $\alpha = 0$ and $\beta = \pi$. Therefore, we have

$$I_\theta(\gamma, k, v < 1 - \gamma) = \begin{cases} 0 & k < 1 - \frac{v}{2}, \\ 1 - \frac{1 - k^2 - \frac{v^2}{4}}{kv} & 1 - \frac{v}{2} < k < 1 + \frac{v}{2}, \\ 2 & 1 + \frac{v}{2} < k. \end{cases} \quad (5.30)$$

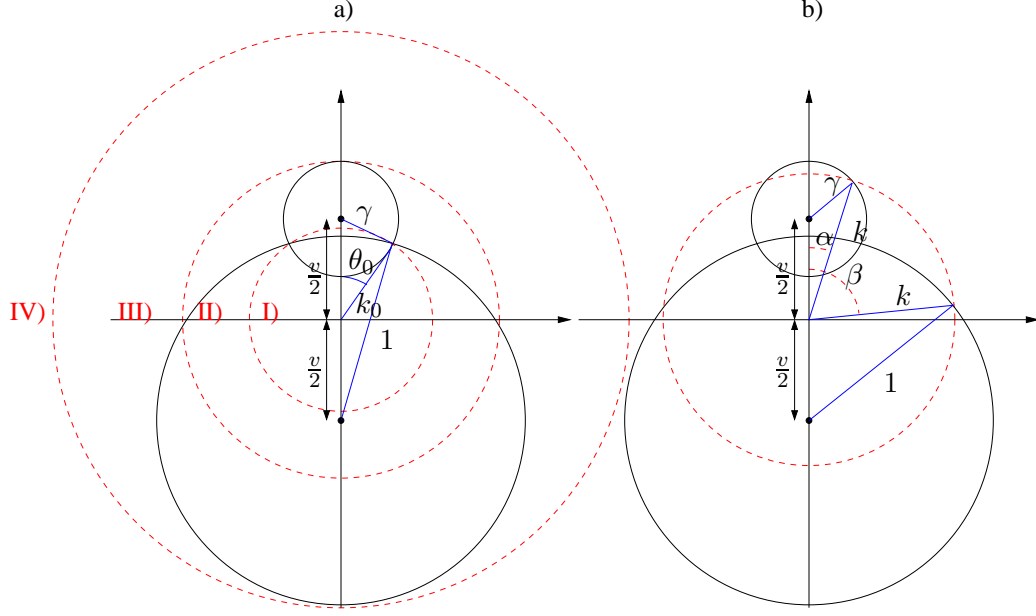


Figure 5.5: The integration region of the angular integral $I_\theta(\gamma, v, k)$ for $1 - \gamma < v < 1 + \gamma$. a) The domain for each of the three subcases I)-IV). The solid circles are $|\mathbf{k} + \frac{\mathbf{v}}{2}|^2 = 1$ and $|\mathbf{k} - \frac{\mathbf{v}}{2}|^2 = \gamma^2$. The dashed circles are the boundaries that separate the subcases, and the domain of the subcases are labeled accordingly. The boundary that separates subcase I) and II) is a circle with radius k_0 , and θ_0 is the angular position of the intersection of the two solid circles. For subcase I), it is clear that $\alpha = \beta$. For subcase IV), $\alpha = 0$, and $\beta = \pi$. b) For subcase II), α and β can be found geometrically according to the diagram shown. For subcase IV), $\alpha = 0$, and β is found in the same manner as subcase II).

Next, we investigate case b), with the four subcases shown in given by Fig. 5.5 a). We first investigate subcase I), which occurs for $k < k_0$, where k_0 is defined in Fig. 5.5 a). The geometry requires $\gamma^2 = k_0^2 + \frac{v^2}{4} - vk_0 \cos \theta_0$ and $1 = k_0^2 + \frac{v^2}{4} + vk_0 \cos \theta_0$, and together they yield

$$k_0 = \sqrt{\frac{1}{2} \left(1 + \gamma^2 - \frac{v^2}{2} \right)}. \quad (5.31)$$

For subcase I), clearly $\alpha = \beta$, and thus the integral is zero.

Subcase II), shown in Fig. 5.5 b), occurs for $k_0 < k < \gamma + \frac{v}{2}$, with $\cos \alpha =$

5.1. $N + M$ Body Problem in the Uniform System

$\frac{k^2 + \frac{v^2}{4} - \gamma^2}{kv}$ and $\cos \beta = \frac{1 - k^2 - \frac{v^2}{4}}{kv}$. Subcase III) occurs for $\gamma + \frac{v}{2} < k < 1 + \frac{v}{2}$, with $\alpha = 0$, and $\cos \beta = \frac{1 - k^2 - \frac{v^2}{4}}{kv}$ is the same as in the subcase II). Subcase IV) occurs for $1 + \frac{v}{2} < k$, with $\alpha = 0$ and $\beta = \pi$. Therefore, we have

$$I_\theta(\gamma, k, 1 - \gamma < v < 1 + \gamma) = \begin{cases} 0 & 0 < k < k_0, \\ \frac{2k^2 + \frac{v^2}{2} - \gamma^2 - 1}{kv} & k_0 < k < \gamma + \frac{v}{2}, \\ 1 - \frac{1 - k^2 - \frac{v^2}{4}}{kv} & \gamma + \frac{v}{2} < k < 1 + \frac{v}{2}, \\ 2 & 1 + \frac{v}{2} < k, \end{cases} \quad (5.32)$$

where k_0 is given by Eq. (5.31). Then, Eq. (5.24) becomes

$$\begin{aligned} \eta &= \int_0^1 dq \int_{-1}^1 dx \frac{\Theta(1 - \gamma - v(\gamma, q, x))q^2}{\frac{\pi}{2k_{F,\uparrow a}} + I_1(\gamma, v(\gamma, q, x), \eta + \gamma^2 + q^2)} \\ &+ \int_0^1 dq \int_{-1}^1 dx \frac{\Theta(\gamma + v(\gamma, q, x) - 1)\Theta(1 + \gamma - v(\gamma, q, x))q^2}{\frac{\pi}{2k_{F,\uparrow a}} + I_2(\gamma, v(\gamma, q, x), \eta + \gamma^2 + q^2)}, \end{aligned} \quad (5.33)$$

where we have defined $v(\gamma, q, x) = \sqrt{\gamma^2 + q^2 + 2q\gamma x}$, and the functions $I_1(\gamma, v, \omega) = I(\gamma, v < 1 - \gamma, \omega)$ and $I_2(\gamma, v, \omega) = I(\gamma, 1 - \gamma < v < 1 + \gamma, \omega)$. The analytic expressions for these functions are

$$\begin{aligned} I_1(\gamma, v, \omega) &= \\ &\frac{2 - \omega}{8v} \log \left(\frac{2 - 2v + v^2 - \omega}{2 + 2v + v^2 - \omega} \right) - \frac{\sqrt{v^2 - 2\omega}}{2} \text{ArcCot} \left(\frac{2 + v}{\sqrt{v^2 - 2\omega}} \right) \\ &+ \frac{\sqrt{v^2 - 2\omega}}{4} \left[\text{ArcTan} \left(\frac{2 - v}{\sqrt{v^2 - 2\omega}} \right) - \text{ArcTan} \left(\frac{2 + v}{\sqrt{v^2 - 2\omega}} \right) \right] - \frac{1}{2}, \end{aligned} \quad (5.34)$$

$$\begin{aligned} I_2(\gamma, v, \omega) &= \\ &\frac{2 - \omega}{8v} \log \left(\frac{v^2 + 2v\gamma + 2\gamma^2 - \omega}{2 + 2v + v^2 - \omega} \right) - \frac{\sqrt{v^2 - 2\omega}}{2} \text{ArcCot} \left(\frac{2 + v}{\sqrt{v^2 - 2\omega}} \right) \\ &+ \frac{\sqrt{v^2 - 2\omega}}{4} \left[\text{ArcTan} \left(\frac{2\gamma + v}{\sqrt{v^2 - 2\omega}} \right) - \text{ArcTan} \left(\frac{2 + v}{\sqrt{v^2 - 2\omega}} \right) \right] \\ &+ \frac{\omega - 1 - \gamma^2}{4v} \log \left(\frac{v^2 + 2v\gamma + 2\gamma^2 - \omega}{1 + \gamma^2 - \omega} \right) - \frac{1 + v + \gamma}{4}. \end{aligned} \quad (5.35)$$

5.1. $N + M$ Body Problem in the Uniform System

We can further simplify Eq. (5.33) by rewriting the limits of integration to remove the step functions. First consider the term in Eq. (5.33) involving $I_1(\gamma, v, \omega)$. The integrand has the domain $0 \leq q \leq 1$ and $-1 \leq x \leq 1$, with the constraint $v(\gamma, q, x) \leq 1 - \gamma$. Solving these three inequalities subject to $0 \leq \gamma \leq 1$ allows us to split the first term in Eq. (5.33) in the following way:

$$\begin{aligned}
 \gamma < 1/2 : \quad & \int_0^{1-2\gamma} dq \int_{-1}^1 dx \frac{q^2}{\frac{\pi}{2k_{F,\uparrow}a} + I_1(\gamma, v(\gamma, q, x), \eta + \gamma^2 + q^2)} \\
 & + \int_{1-2\gamma}^1 dq \int_{-1}^{\frac{1-2\gamma-q^2}{2\gamma q}} dx \frac{q^2}{\frac{\pi}{2k_{F,\uparrow}a} + I_1(\gamma, v(\gamma, q, x), \eta + \gamma^2 + q^2)}, \\
 1/2 < \gamma : \quad & \int_{2\gamma-1}^1 dq \int_{-1}^{\frac{1-2\gamma-q^2}{2\gamma q}} dx \frac{q^2}{\frac{\pi}{2k_{F,\uparrow}a} + I_1(\gamma, v(\gamma, q, x), \eta + \gamma^2 + q^2)}.
 \end{aligned} \tag{5.36}$$

Next, we consider the term in Eq. (5.33) involving $I_2(\gamma, v, \omega)$. The integrand has the domain $0 \leq q \leq 1$, $-1 \leq x \leq 1$, with the constraint $1 - \gamma \leq v(\gamma, q, x) \leq 1 + \gamma$. Solving these three inequalities subject to $0 \leq \gamma \leq 1$ allows us to split the second term in Eq. (5.33) in the following way:

$$\begin{aligned}
 \gamma < 1/2 : \quad & \int_{1-2\gamma}^1 dq \int_{\frac{1-2\gamma-q^2}{2\gamma q}}^1 dx \frac{q^2}{\frac{\pi}{2k_{F,\uparrow}a} + I_2(\gamma, v(\gamma, q, x), \eta + \gamma^2 + q^2)}, \\
 1/2 < \gamma : \quad & \int_{2\gamma-1}^1 dq \int_{\frac{1-2\gamma-q^2}{2\gamma q}}^1 dx \frac{q^2}{\frac{\pi}{2k_{F,\uparrow}a} + I_2(\gamma, v(\gamma, q, x), \eta + \gamma^2 + q^2)} \\
 & + \int_0^{2\gamma-1} dq \int_{-1}^1 dx \frac{q^2}{\frac{\pi}{2k_{F,\uparrow}a} + I_2(\gamma, v(\gamma, q, x), \eta + \gamma^2 + q^2)}.
 \end{aligned} \tag{5.37}$$

The quantity $\frac{1-2\gamma-q^2}{2\gamma q}$ has a singularity at $\gamma = 0$. Therefore, we make the following change of variables $(1 - q)/2\gamma \rightarrow q$ and $2x\gamma \rightarrow x$. Finally, we can write the self-consistent equation for the $N + M$ body energy η ,

$$\eta(x) = \Sigma(\gamma = x^{1/3}, \eta), \tag{5.38}$$

5.1. $N + M$ Body Problem in the Uniform System

where the dimensionless self-energy is given by

$$\begin{aligned}
\Sigma(\gamma, \eta) = & \int_0^{1-2\gamma} dq \int_{-1}^1 dx \frac{q^2}{\frac{\pi}{2k_{F,\uparrow}a} + I_1(\gamma, v(\gamma, q, x), \eta + \gamma^2 + q^2)} \\
& + \int_0^1 dq \int_{-2\gamma}^{x_f(\gamma, q)} dx \frac{(1-2\gamma q)^2}{\frac{\pi}{2k_{F,\uparrow}a} + I_1(\gamma, \tilde{v}(\gamma, q, x), \eta + \gamma^2 + (1-2\gamma q)^2)} \\
& + \int_0^1 dq \int_{x_f(\gamma, q)}^{2\gamma} dx \frac{(1-2\gamma q)^2}{\frac{\pi}{2k_{F,\uparrow}a} + I_2(\gamma, \tilde{v}(\gamma, q, x), \eta + \gamma^2 + (1-2\gamma q)^2)}
\end{aligned} \tag{5.39}$$

for $\gamma < 1/2$, and

$$\begin{aligned}
\Sigma(\gamma, \eta) = & \int_0^{(1-\gamma)/\gamma} dq \int_{-2\gamma}^{x_f(\gamma, q)} dx \frac{(1-2\gamma q)^2}{\frac{\pi}{2k_{F,\uparrow}a} + I_1(\gamma, \tilde{v}(\gamma, q, x), \eta + \gamma^2 + (1-2\gamma q)^2)} \\
& + \int_0^{2\gamma-1} dq \int_{-1}^1 dx \frac{q^2}{\frac{\pi}{2k_{F,\uparrow}a} + I_2(\gamma, v(\gamma, q, x), \eta + \gamma^2 + q^2)} \\
& + \int_0^{(1-\gamma)/\gamma} dq \int_{-2\gamma}^{x_f(\gamma, q)} dx \frac{(1-2\gamma q)^2}{\frac{\pi}{2k_{F,\uparrow}a} + I_2(\gamma, \tilde{v}(\gamma, q, x), \eta + \gamma^2 + (1-2\gamma q)^2)}
\end{aligned} \tag{5.40}$$

for $1/2 < \gamma$, with $v(\gamma, q, x) = (\gamma^2 + q^2 + 2\gamma qx)^{1/2}$, and we have defined $\tilde{v}(\gamma, q, x) = (\gamma^2 + (1-2\gamma q)^2 + (1-2\gamma q)x)^{1/2}$, and $x_f(\gamma, q) = 2\gamma(1-2q+2\gamma q^2)/(2\gamma q-1)$. The functions $I_1(\gamma, v, \omega)$ and $I_2(\gamma, v, \omega)$ are given by Eqs. (5.34) and (5.35).

5.1.3 Equation of State of the Normal Fermi Liquid

We are now ready to construct the equation of state for the polarized normal Fermi liquid. In a normal gas with N_\uparrow spin-up and N_\downarrow spin-down particles, the energy is given by

$$E(N_\downarrow, N_\uparrow) = E_0(N_\uparrow) + E_0(N_\downarrow) + E_{int}(N_\downarrow, N_\uparrow), \tag{5.41}$$

where $E_0(N_\sigma)$ is the non-interaction energy for the species $\sigma = \uparrow, \downarrow$, and $E_{int}(N_\downarrow, N_\uparrow)$ is the energy due to interactions. By definition, the $N + M$

5.1. $N + M$ Body Problem in the Uniform System

energy is $E = E_{F,\uparrow}\eta(N_\downarrow/N_\uparrow) = E_{int}(N_\downarrow, N_\uparrow) - E_{int}(N_\downarrow - 1, N_\uparrow)$. Therefore, the energy of the normal state is

$$E(N_\downarrow, N_\uparrow) = N_\uparrow \frac{3}{5} E_{F,\uparrow} \left(1 + \frac{E_0(N_\downarrow)}{E_0(N_\uparrow)} + \frac{5}{3} \sum_{N_i=0}^{N_\downarrow} \frac{1}{N_\uparrow} \eta \left(\frac{N_i}{N_\uparrow} \right) \right). \quad (5.42)$$

In the uniform system, $E_0(N_\sigma) = 3E_{F,\sigma}N_\sigma/5$, and we have

$$E(N_\downarrow, N_\uparrow) = N_\uparrow \frac{3}{5} E_{F,\uparrow} \epsilon(x), \quad (5.43)$$

where the equation of state $\epsilon(x)$ is given by

$$\epsilon(x) = 1 + x^{5/3} + \frac{5}{3} \int_0^x \eta(y) dy. \quad (5.44)$$

For small $\gamma = x^{1/3} \ll 1$, the minority quasiparticles have the dispersion relation $\eta(\gamma = x^{1/3}) \simeq \eta_0 + (m/m^* - 1)\gamma^2 + \dots$, and Eq. (5.44) reproduces the small- x expansion $\epsilon(x) \simeq 1 + \frac{5}{3}\eta_0 x + \frac{m}{m^*}x^{5/3} + \dots$ of Eq. (3.29).

5.1.4 Results and Comparison

We now solve the self-consistent equation Eq. (5.38) for $\eta(x)$ with general x . For $x = 0$, we reproduce the $N + 1$ body energy $\eta_0 = \eta(0) = -0.607$ and effective mass $m^*/m = 1.17$. In Fig. 5.6, we show the result for $\eta(x)$. For comparison, we also show the parametrization $\eta_0 + (m/m^* - 1)x^{2/3} + 6Bx/5$, with the polaron energy $\eta_0 = -0.607$, and m^* , B taken from different calculations. The variational $\eta(x)$ is lower than the parametrization with the MC values $m^*/m = 1.09$ and $B = 0.14$ [43]. For small x , $\eta(x)$ is well-described by a correction due to an effective mass, $m^*/m = 1.17$ [22]. For $x \gtrsim 0.1$, higher-order corrections beyond the effective mass become important. However, the form $6Bx/5$ is not adequate to describe these corrections for all x .

In Fig. 5.7, we show the equation of state Eq. (5.44) obtained from the variational $\eta(x)$, as well as based on the small- x expansion $\epsilon(x) \simeq 1 + \frac{5}{3}\eta_0 x + \frac{m}{m^*}x^{5/3} + Bx^2$ of Eq. (3.30) for several combinations of η_0 , m^* , and B . The equation of state based on variational $\eta(x)$ is lower than the small- x parametrization with MC values, $m^*/m = 1.09$ and $B = 0.14$ [43], regardless whether the MC value for the polaron energy $\eta_0 = -0.594$ [43] or the variational value $\eta_0 = -0.607$ [17] is used. For comparison, we also include two parametrizations with the diagrammatic MC value $\eta_0 = -0.615$ [45]

5.1. $N + M$ Body Problem in the Uniform System

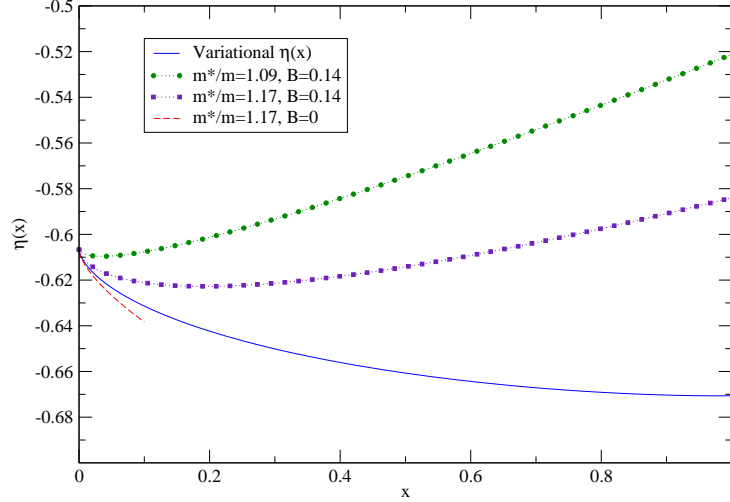


Figure 5.6: Results for $\eta(x)$ and the parametrization $\eta_0 + (m/m^* - 1)x^{2/3} + 6Bx/5$ for $\eta_0 = -0.607$ and several combinations of m^* and B . Although the plot is shown for $0 \leq x \leq 1$, one should remember that the normal-to-superfluid transition takes place at $x = x_c$. Blue curve: the variational $\eta(x)$. Green curve: MC results given by $m^*/m = 1.09$ and $B = 0.14$ [43]. Red curve: analytic result for the effective mass $m^*/m = 1.17$ [22] and $B = 0$. Purple curve: analytic result for the effective mass $m^*/m = 1.17$ and the MC result $B = 0.14$. The variational $\eta(x)$ is lower than the parametrization with the MC values $m^*/m = 1.09$ and $B = 0.14$ (green curve). For small x , $\eta(x)$ is well-described by a correction due to an effective mass, $m^*/m = 1.17$. For $x \gtrsim 0.1$, higher-order corrections beyond m^* become important, which are not well-described by $6Bx/5$.

and the analytic result $m^*/m = 1.17$, with different $B = 0$ and $B = 0.14$. In both cases, the small- x parametrizations describe the variational $\epsilon(x)$ well up to $x \lesssim 0.3$.

In summary, the equation of state $\epsilon(x)$ based on the variational $\eta(x)$ is well-described by $1 + 5/3\eta_0x + m/m^*x^{5/3}$ for small x , with $\eta_0 \approx -0.61$ and $m^*/m = 1.17$. Also, the energy for the polarized normal Fermi liquid obtained with variational $\eta(x)$ is lower than the one based on the parametrization with the MC m^* and B . Next, we will discuss the consequence of the variational energy on the phase structure of trapped Fermi gases containing large particle numbers.

5.1. $N + M$ Body Problem in the Uniform System

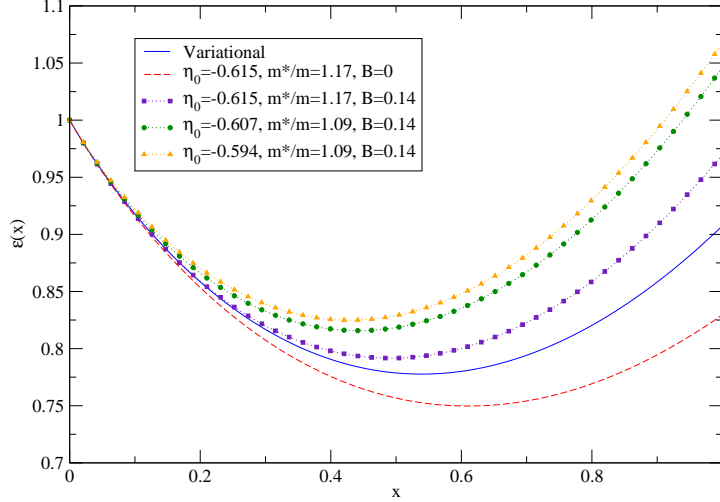


Figure 5.7: Equation of state for the polarized normal Fermi liquid in the uniform system. Blue curve: results for $\epsilon(x)$ given by Eq. (5.44), based on variational $\eta(x)$. Also shown are the small- x parametrization $\epsilon(x) \simeq 1 + \frac{5}{3}\eta_0 x + \frac{m}{m^*}x^{5/3} + Bx^2$ of Eq. (3.30) for several combinations of η_0 , m^* , and B . Orange curve uses the MC results [43] $\eta_0 = -0.594$, $m^*/m = 1.09$, and $B = 0.14$. Green curve has the variational $\eta_0 = -0.607$ with MC results for the effective mass $m^*/m = 1.09$ and $B = 0.14$. Red curve employs the diagrammatic Monte Carlo result $\eta_0 = -0.615$ [45] and analytic $m^*/m = 1.17$ [22], without higher-order corrections, $B = 0$. Purple curve is same as the red curve, but with $B = 0.14$.

5.1.5 Phase Structure of Trapped Fermi Gases with Large Particle Numbers

With Eqs. (3.40)-(3.46) and the equation of state based on variational $\eta(x)$, Eq. (5.44), we find the critical concentration x_c and critical polarization P_c for trapped Fermi gases with large particle numbers. In Fig. 5.8, we show $x_c(\xi)$ as a function of the superfluid energy parameter, ξ . The critical concentration reaches the maximum value, $x_c = 1$, for $\xi = 0.45(1)$. The critical concentration is sensitive to the superfluid energy ξ . For the MC value $\xi = 0.42(1)$ [13, 43], we have $x_c = 0.66(5)$, and for the most recent value $\xi = 0.40(1)$ [14], we obtain $x_c = 0.58(4)$. These values are higher than the experimental result $x_c \approx 0.47$ [55] of the MIT group. The uncertainties cited in our values do not take into account the uncertainty of the equation

5.1. $N + M$ Body Problem in the Uniform System

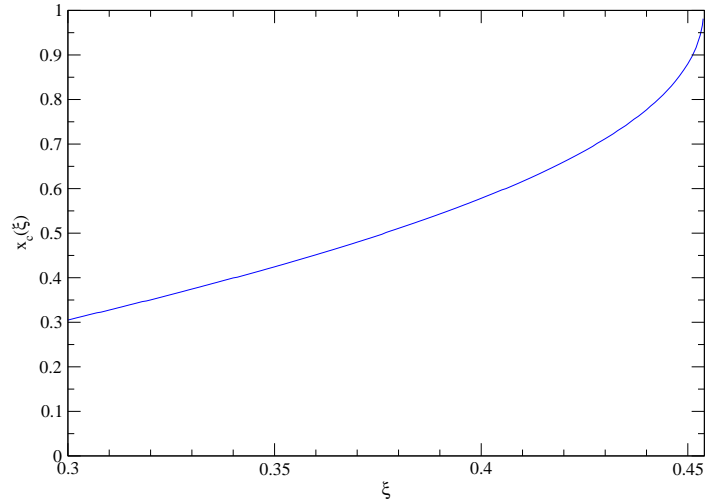


Figure 5.8: Critical concentration $x_c(\xi)$ as a function of ξ for trapped Fermi gases with large particle numbers. The result is based the equation of state obtained from variational $\eta(x)$.

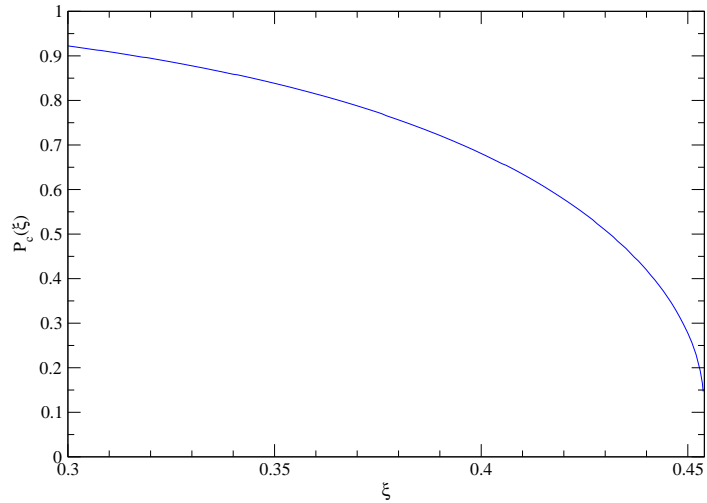


Figure 5.9: Critical poncentration $P_c(\xi)$ as a function of ξ for trapped Fermi gases with large particle numbers. The result is based the equation of state obtained from variational $\eta(x)$.

of state obtained from variational $\eta(x)$.

In Fig. 5.9, we show $P_c(\xi)$ as a function of ξ . The critical polarization is also sensitive to the value of ξ . For $\xi = 0.42(1)$, we obtain $P_c = 0.58(7)$. For the most recent value $\xi = 0.40(1)$, we have $P_c = 0.68(5)$, in agreement with the MIT result $P_c = 0.70(3)$ [54, 58, 59]. Once again, the uncertainties cited in our values do not take into account the uncertainty of the equation of state obtained from variational $\eta(x)$.

5.2 $N + M$ Body Problem in Traps

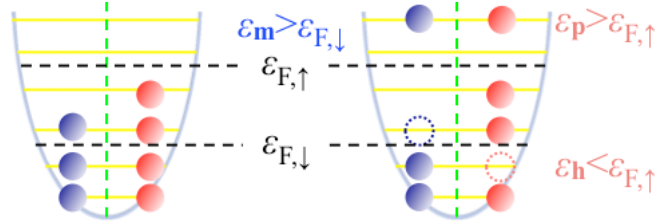


Figure 5.10: Graphical representation of the components of the trial wavefunction Eq. (5.45) in traps. *Left:* $|\Omega\rangle$ is the non-interacting ground state. It consists of a majority Fermi sea with N spin-up fermions occupying the levels $\epsilon_{\mathbf{n}} \leq \epsilon_{F,\uparrow}$, a minority Fermi sea with $M - 1$ spin-down fermions occupying the levels $\epsilon_{\mathbf{n}} \leq \epsilon_{F,\downarrow}$, and an additional impurity at the level $\mathbf{n}_{F+1,\downarrow}$ with the energy $\epsilon_{F+1,\downarrow}$. *Right:* the state $|\mathbf{m}, \mathbf{h}, \mathbf{p}\rangle$ consists of a spin-up fermion in \mathbf{h} excited to a level \mathbf{p} above the majority Fermi energy $\epsilon_{F,\uparrow}$, and the additional impurity occupies the level $\epsilon_{\mathbf{m}} > \epsilon_{F,\downarrow}$.

To allow for a better quantitative understanding of the MIT-Rice differences, it is necessary to include general asymmetry in the study of trapped Fermi gases. The $N + M$ body problem in traps enables us to study finite-size and confinement effects to the energy contributions beyond $\eta(\alpha, N)$. In this section, we present the derivation of $N + M$ body energy gain in traps. The numerical evaluation of the energy and the analysis of the phase structure are to be left for future work.

The formalism of our problem is as follow. We assume a trap with cylindrical symmetry, $\omega_x = \omega_y = \alpha\omega = \alpha\omega_z$. The Hamiltonian of a strongly-interacting Fermi gas in a harmonic oscillator-trap is given by Eq. (4.1), with the interaction Eq. (4.2). We consider a trap with N spin-up fermions and $M - 1$ spin-down fermions. In the absence of interactions, the $\sigma = \uparrow, \downarrow$

5.2. $N + M$ Body Problem in Traps

fermions occupy the levels $\varepsilon_{\mathbf{n}} = \alpha(n_x + n_y + 1) + n_z + 1/2 \leq \varepsilon_{F,\sigma}$, and we assume $\varepsilon_{F,\downarrow} < \varepsilon_{F,\uparrow}$. We calculate the energy gain E of an additional spin-down fermion, including $1p1h$ excitations in the trial wavefunction,

$$|\psi\rangle = \phi_0|\Omega\rangle + \sum_{\mathbf{m},\mathbf{h},\mathbf{p}} \phi_{\mathbf{m},\mathbf{h},\mathbf{p}}|\mathbf{m},\mathbf{h},\mathbf{p}\rangle. \quad (5.45)$$

Here, $|\Omega\rangle$ denotes the non-interacting ground state. It consists of a majority Fermi sea with N spin-up fermions occupying the levels $\varepsilon_{\mathbf{n}} \leq \varepsilon_{F,\uparrow}$, a minority Fermi sea with $M-1$ spin-down fermions occupying the levels $\varepsilon_{\mathbf{n}} \leq \varepsilon_{F,\downarrow}$, and an additional impurity occupying the level $\mathbf{n}_{F+1,\downarrow}$ with the energy $\varepsilon_{F+1,\downarrow}$. The state $|\mathbf{m},\mathbf{h},\mathbf{p}\rangle$ consists of a spin-up fermion in \mathbf{h} excited to a level \mathbf{p} above the spin-up Fermi energy $\varepsilon_{F,\uparrow}$, and the additional impurity occupying the level \mathbf{m} above the spin-down Fermi energy $\varepsilon_{F,\downarrow}$. Therefore, the sum over \mathbf{h} is restricted to occupied states $\varepsilon_{\mathbf{h}} \leq \varepsilon_{F,\uparrow}$, \mathbf{p} is over $\varepsilon_{\mathbf{p}} > \varepsilon_{F,\uparrow}$, and \mathbf{m} is over $\varepsilon_{\mathbf{m}} > \varepsilon_{F,\downarrow}$.

We write the Hamiltonian Eq. (4.1) as $H = H_0 + V$, where H_0 is the non-interacting harmonic-oscillator Hamiltonian, and V gives the interacting part. We proceed by calculating $\langle\psi|\hat{H}_0|\psi\rangle$:

$$\begin{aligned} \hat{H}_0|\psi\rangle &= \phi_0 \left(\sum_{\mathbf{n}} \varepsilon_{\mathbf{n}} a_{\mathbf{n},\uparrow}^\dagger a_{\mathbf{n},\uparrow} |\Omega\rangle + \sum_{\mathbf{n}} \varepsilon_{\mathbf{n}} a_{\mathbf{n},\downarrow}^\dagger a_{\mathbf{n},\downarrow} |\Omega\rangle \right) \\ &+ \sum_{\mathbf{m},\mathbf{h},\mathbf{p}} \phi_{\mathbf{m},\mathbf{h},\mathbf{p}} \left(\sum_{\mathbf{n}} \varepsilon_{\mathbf{n}} a_{\mathbf{n},\uparrow}^\dagger a_{\mathbf{n},\uparrow} |\mathbf{m},\mathbf{h},\mathbf{p}\rangle + \sum_{\mathbf{n}} \varepsilon_{\mathbf{n}} a_{\mathbf{n},\downarrow}^\dagger a_{\mathbf{n},\downarrow} |\mathbf{m},\mathbf{h},\mathbf{p}\rangle \right). \end{aligned} \quad (5.46)$$

The operators act on the states to yield

$$a_{\mathbf{n},\uparrow}^\dagger a_{\mathbf{n},\uparrow} |\Omega\rangle = \begin{cases} 0 & \varepsilon_{\mathbf{n}} > \varepsilon_{F,\uparrow}, \\ |\Omega\rangle & \varepsilon_{\mathbf{n}} \leq \varepsilon_{F,\uparrow}, \end{cases} \quad (5.47)$$

$$a_{\mathbf{n},\downarrow}^\dagger a_{\mathbf{n},\downarrow} |\Omega\rangle = \begin{cases} |\Omega\rangle & \mathbf{n} = \mathbf{n}_{F+1,\downarrow}, \\ |\Omega\rangle & \varepsilon_{\mathbf{n}} \leq \varepsilon_{F,\downarrow}, \\ 0 & \text{else,} \end{cases} \quad (5.48)$$

$$a_{\mathbf{n},\uparrow}^\dagger a_{\mathbf{n},\uparrow} |\mathbf{m},\mathbf{h},\mathbf{p}\rangle = \begin{cases} |\mathbf{m},\mathbf{h},\mathbf{p}\rangle & \mathbf{n} = \mathbf{p}, \\ |\mathbf{m},\mathbf{h},\mathbf{p}\rangle & \varepsilon_{\mathbf{n}} \leq \varepsilon_{F,\uparrow} \text{ and } \mathbf{n} \neq \mathbf{h}, \\ 0 & \text{else,} \end{cases} \quad (5.49)$$

$$a_{\mathbf{n},\downarrow}^\dagger a_{\mathbf{n},\downarrow} |\mathbf{m},\mathbf{h},\mathbf{p}\rangle = \begin{cases} |\mathbf{m},\mathbf{h},\mathbf{p}\rangle & \varepsilon_{\mathbf{n}} \leq \varepsilon_{F,\downarrow}, \\ |\mathbf{m},\mathbf{h},\mathbf{p}\rangle & \mathbf{n} = \mathbf{m}, \\ 0 & \text{else.} \end{cases} \quad (5.50)$$

5.2. $N + M$ Body Problem in Traps

Therefore, we find

$$\langle \psi | \hat{H}_0 | \psi \rangle = \varepsilon_{F+1,\downarrow} |\phi_0|^2 + \sum_{\mathbf{m}, \mathbf{h}, \mathbf{p}} |\phi_{\mathbf{m}, \mathbf{h}, \mathbf{p}}|^2 (\varepsilon_{\mathbf{p}} + \varepsilon_{\mathbf{m}} - \varepsilon_{\mathbf{h}}) + \sum_{\varepsilon_{\mathbf{n}} \leq \varepsilon_{F,\uparrow}} \varepsilon_{\mathbf{n}} + \sum_{\varepsilon_{\mathbf{n}} \leq \varepsilon_{F,\downarrow}} \varepsilon_{\mathbf{n}}. \quad (5.51)$$

The last two terms give the energy of the non-interacting system and are subtracted when we study the energy gain.

Next, we calculate $\langle \psi | V | \psi \rangle$, making use of the result $\langle \mathbf{n}_1, \mathbf{n}_2 | V | \mathbf{n}_3, \mathbf{n}_4 \rangle = C(\Lambda) \sum_{\mathbf{S}} F(\mathbf{n}_1, \mathbf{n}_2, \mathbf{S}) F(\mathbf{n}_3, \mathbf{n}_4, \mathbf{S})$ from Section 4.1.1:

$$\begin{aligned} V|\psi\rangle &= C(\Lambda) \phi_0 \sum_{\mathbf{S}} \sum_{\mathbf{n}_{\downarrow}, \mathbf{n}_{\uparrow}, \mathbf{n}'_{\downarrow}, \mathbf{n}'_{\uparrow}} F(\mathbf{n}_{\downarrow}, \mathbf{n}_{\uparrow}, \mathbf{S}) F(\mathbf{n}'_{\downarrow}, \mathbf{n}'_{\uparrow}, \mathbf{S}) \\ &\quad \times a_{\mathbf{n}'_{\uparrow}, \uparrow}^{\dagger} a_{\mathbf{n}'_{\downarrow}, \downarrow}^{\dagger} a_{\mathbf{n}_{\downarrow}, \downarrow} a_{\mathbf{n}_{\uparrow}, \uparrow} |\Omega\rangle \\ &+ C(\Lambda) \sum_{\mathbf{n}_{\downarrow}, \mathbf{n}_{\uparrow}, \mathbf{n}'_{\downarrow}, \mathbf{n}'_{\uparrow}} F(\mathbf{n}_{\downarrow}, \mathbf{n}_{\uparrow}, \mathbf{S}) F(\mathbf{n}'_{\downarrow}, \mathbf{n}'_{\uparrow}, \mathbf{S}) \\ &\quad \times \sum_{\mathbf{m}, \mathbf{h}, \mathbf{p}} \phi_{\mathbf{m}, \mathbf{h}, \mathbf{p}} \sum_{\mathbf{S}} a_{\mathbf{n}'_{\uparrow}, \uparrow}^{\dagger} a_{\mathbf{n}'_{\downarrow}, \downarrow}^{\dagger} a_{\mathbf{n}_{\downarrow}, \downarrow} a_{\mathbf{n}_{\uparrow}, \uparrow} |\mathbf{m}, \mathbf{h}, \mathbf{p}\rangle. \end{aligned} \quad (5.52)$$

Keeping up to one-particle–one-hole excitations, the relevant terms are

$$= \left\{ \begin{array}{l} a_{\mathbf{n}'_{\uparrow}, \uparrow}^{\dagger} a_{\mathbf{n}'_{\downarrow}, \downarrow}^{\dagger} a_{\mathbf{n}_{\downarrow}, \downarrow} a_{\mathbf{n}_{\uparrow}, \uparrow} |\Omega\rangle \\ \left. \begin{array}{l} |\Omega\rangle \\ |\Omega\rangle \\ |\mathbf{n}'_{\downarrow}, \mathbf{n}_{\uparrow}, \mathbf{n}'_{\uparrow}\rangle \\ |\mathbf{n}_{F+1,\downarrow}, \mathbf{n}_{\uparrow}, \mathbf{n}'_{\uparrow}\rangle \end{array} \right\} \begin{array}{l} \mathbf{n}_{\downarrow} = \mathbf{n}_{F+1,\downarrow}, \quad \varepsilon_{\mathbf{n}_{\uparrow}} \leq \varepsilon_{F,\uparrow}, \\ \mathbf{n}'_{\uparrow} = \mathbf{n}_{\uparrow}, \quad \mathbf{n}'_{\downarrow} = \mathbf{n}_{\downarrow}, \\ \varepsilon_{\mathbf{n}_{\downarrow}} \leq \varepsilon_{F,\downarrow}, \quad \varepsilon_{\mathbf{n}_{\uparrow}} \leq \varepsilon_{F,\uparrow}, \\ \mathbf{n}'_{\uparrow} = \mathbf{n}_{\uparrow}, \quad \mathbf{n}'_{\downarrow} = \mathbf{n}_{\downarrow}, \\ \mathbf{n}_{\downarrow} = \mathbf{n}_{F+1,\downarrow}, \quad \varepsilon_{\mathbf{n}_{\uparrow}} \leq \varepsilon_{F,\uparrow}, \\ \varepsilon_{\mathbf{n}'_{\uparrow}} > \varepsilon_{F,\uparrow}, \quad \varepsilon_{\mathbf{n}'_{\downarrow}} > \varepsilon_{F,\downarrow}, \\ \varepsilon_{\mathbf{n}_{\downarrow}} \leq \varepsilon_{F,\downarrow}, \quad \varepsilon_{\mathbf{n}_{\uparrow}} \leq \varepsilon_{F,\uparrow}, \\ \mathbf{n}'_{\downarrow} = \mathbf{n}_{\downarrow}, \quad \varepsilon_{\mathbf{n}'_{\uparrow}} > \varepsilon_{F,\uparrow}, \end{array} \end{array} \quad (5.53)$$

5.2. $N + M$ Body Problem in Traps

$$\begin{aligned}
 & a_{\mathbf{n}'_{\uparrow}, \uparrow}^{\dagger} a_{\mathbf{n}'_{\downarrow}, \downarrow}^{\dagger} a_{\mathbf{n}_{\downarrow}, \downarrow} a_{\mathbf{n}_{\uparrow}, \uparrow} | \mathbf{m}, \mathbf{h}, \mathbf{p} \rangle \\
 = & \left\{ \begin{array}{ll}
 |\Omega\rangle & \mathbf{n}_{\downarrow} = \mathbf{m}, \quad \mathbf{n}_{\uparrow} = \mathbf{p}, \\
 & \mathbf{n}'_{\uparrow} = \mathbf{h}, \quad \mathbf{n}'_{\downarrow} = \mathbf{n}_{F+1, \downarrow} \\
 |\Omega\rangle & \varepsilon_{\mathbf{n}_{\downarrow}} \leq \varepsilon_{F, \downarrow}, \quad \mathbf{n}_{\uparrow} = \mathbf{p}, \\
 & \mathbf{n}'_{\uparrow} = \mathbf{h}, \quad \mathbf{n}'_{\downarrow} = \mathbf{n}_{\downarrow}, \\
 & \text{and } \mathbf{m} = \mathbf{n}_{F+1, \downarrow}, \\
 |\mathbf{n}'_{\downarrow}, \mathbf{h}, \mathbf{n}'_{\uparrow}\rangle & \mathbf{n}_{\downarrow} = \mathbf{m}, \quad \mathbf{n}_{\uparrow} = \mathbf{p}, \\
 & \varepsilon_{\mathbf{n}'_{\uparrow}} > \varepsilon_{F, \uparrow}, \quad \varepsilon_{\mathbf{n}'_{\downarrow}} > \varepsilon_{F, \downarrow}, \\
 |\mathbf{n}'_{\downarrow}, \mathbf{n}_{\uparrow}, \mathbf{p}\rangle & \mathbf{n}_{\downarrow} = \mathbf{m}, \quad \varepsilon_{\mathbf{n}_{\uparrow}} \leq \varepsilon_{F, \uparrow} \\
 & \text{and } \mathbf{n}_{\uparrow} \neq \mathbf{h}, \\
 & \mathbf{n}'_{\uparrow} = \mathbf{h}, \quad \varepsilon_{\mathbf{n}'_{\downarrow}} > \varepsilon_{F, \downarrow} \\
 |\mathbf{n}'_{\downarrow}, \mathbf{h}, \mathbf{p}\rangle & \mathbf{n}_{\downarrow} = \mathbf{m}, \quad \varepsilon_{\mathbf{n}_{\uparrow}} \leq \varepsilon_{F, \uparrow} \\
 & \text{and } \mathbf{n}_{\uparrow} \neq \mathbf{h}, \\
 & \mathbf{n}'_{\uparrow} = \mathbf{n}_{\uparrow}, \quad \varepsilon_{\mathbf{n}'_{\downarrow}} > \varepsilon_{F, \downarrow} \\
 |\mathbf{m}, \mathbf{h}, \mathbf{n}'_{\uparrow}\rangle & \varepsilon_{\mathbf{n}_{\downarrow}} \leq \varepsilon_{F, \downarrow}, \quad \mathbf{n}_{\uparrow} = \mathbf{p}, \\
 & \varepsilon_{\mathbf{n}'_{\uparrow}} > \varepsilon_{F, \uparrow}, \quad \mathbf{n}'_{\downarrow} = \mathbf{n}_{\downarrow}, \\
 |\mathbf{m}, \mathbf{n}_{\uparrow}, \mathbf{p}\rangle & \varepsilon_{\mathbf{n}_{\downarrow}} \leq \varepsilon_{F, \downarrow}, \quad \varepsilon_{\mathbf{n}_{\uparrow}} \leq \varepsilon_{F, \uparrow} \\
 & \text{and } \mathbf{n}_{\uparrow} \neq \mathbf{h}, \\
 & \mathbf{n}'_{\uparrow} = \mathbf{h}, \quad \mathbf{n}'_{\downarrow} = \mathbf{n}_{\downarrow} \\
 |\mathbf{m}, \mathbf{h}, \mathbf{p}\rangle & \varepsilon_{\mathbf{n}_{\downarrow}} \leq \varepsilon_{F, \downarrow}, \quad \varepsilon_{\mathbf{n}_{\uparrow}} \leq \varepsilon_{F, \uparrow} \\
 & \text{and } \mathbf{n}_{\uparrow} \neq \mathbf{h}, \\
 & \mathbf{n}'_{\uparrow} = \mathbf{n}_{\uparrow}, \quad \mathbf{n}'_{\downarrow} = \mathbf{n}_{\downarrow}.
 \end{array} \right. \tag{5.54}
 \end{aligned}$$

Making the following change of indices $\mathbf{n}_{\downarrow} \rightarrow \mathbf{h}_{\downarrow}$, $\mathbf{n}_{\uparrow} \rightarrow \mathbf{h}'$, $\mathbf{n}'_{\uparrow} \rightarrow \mathbf{p}'$, and

$\mathbf{n}'_{\downarrow} \rightarrow \mathbf{m}'$, we obtain

$$\begin{aligned}
 V|\psi\rangle &= C(\Lambda)\phi_0 \sum_{\mathbf{S}} \sum_{\mathbf{h}'} \left[\sum_{\mathbf{h}_{\downarrow}} F^2(\mathbf{h}_{\downarrow}, \mathbf{h}', \mathbf{S}) + F^2(\mathbf{n}_{F+1,\downarrow}, \mathbf{h}', \mathbf{S}) \right] |\Omega\rangle \\
 &+ C(\Lambda)\phi_0 \sum_{\mathbf{S}} \sum_{\mathbf{m}, \mathbf{h}, \mathbf{p}} F(\mathbf{n}_{F+1,\downarrow}, \mathbf{h}, \mathbf{S}) F(\mathbf{m}, \mathbf{p}, \mathbf{S}) |\mathbf{m}, \mathbf{h}, \mathbf{p}\rangle \\
 &+ C(\Lambda)\phi_0 \sum_{\mathbf{S}} \sum_{\mathbf{h}, \mathbf{p}} \sum_{\mathbf{h}_{\downarrow}} F(\mathbf{h}_{\downarrow}, \mathbf{h}, \mathbf{S}) F(\mathbf{h}_{\downarrow}, \mathbf{p}, \mathbf{S}) |\mathbf{n}_{F+1,\downarrow}, \mathbf{h}, \mathbf{p}\rangle \\
 &+ C(\Lambda) \sum_{\mathbf{S}} \sum_{\mathbf{h}, \mathbf{p}} \sum_{\mathbf{h}_{\downarrow}} \phi_{\mathbf{n}_{F+1,\downarrow}, \mathbf{h}, \mathbf{p}} F(\mathbf{h}_{\downarrow}, \mathbf{p}, \mathbf{S}) F(\mathbf{h}_{\downarrow}, \mathbf{h}, \mathbf{S}) |\Omega\rangle \\
 &+ C(\Lambda) \sum_{\mathbf{S}} \sum_{\mathbf{m}, \mathbf{h}, \mathbf{p}} \phi_{\mathbf{m}, \mathbf{h}, \mathbf{p}} F(\mathbf{m}, \mathbf{p}, \mathbf{S}) F(\mathbf{n}_{F+1,\downarrow}, \mathbf{h}, \mathbf{S}) |\Omega\rangle \\
 &+ C(\Lambda) \sum_{\mathbf{S}} \sum_{\mathbf{m}, \mathbf{h}, \mathbf{p}} \phi_{\mathbf{m}, \mathbf{h}, \mathbf{p}} \sum_{\mathbf{m}', \mathbf{p}'} F(\mathbf{m}, \mathbf{p}, \mathbf{S}) F(\mathbf{m}', \mathbf{p}', \mathbf{S}) |\mathbf{m}', \mathbf{h}, \mathbf{p}'\rangle \\
 &+ C(\Lambda) \sum_{\mathbf{S}} \sum_{\mathbf{m}, \mathbf{h}, \mathbf{p}} \phi_{\mathbf{m}, \mathbf{h}, \mathbf{p}} \sum_{\mathbf{h}_{\downarrow}, \mathbf{p}'} F(\mathbf{h}_{\downarrow}, \mathbf{p}, \mathbf{S}) F(\mathbf{h}_{\downarrow}, \mathbf{p}', \mathbf{S}) |\mathbf{m}, \mathbf{h}, \mathbf{p}'\rangle \\
 &+ C(\Lambda) \sum_{\mathbf{S}} \sum_{\mathbf{m}, \mathbf{h}, \mathbf{p}} \phi_{\mathbf{m}, \mathbf{h}, \mathbf{p}} \sum_{\mathbf{m}', \mathbf{h}' \neq \mathbf{h}} F(\mathbf{m}, \mathbf{h}', \mathbf{S}) F(\mathbf{m}', \mathbf{h}, \mathbf{S}) |\mathbf{m}', \mathbf{h}', \mathbf{p}\rangle \\
 &+ C(\Lambda) \sum_{\mathbf{S}} \sum_{\mathbf{m}, \mathbf{h}, \mathbf{p}} \phi_{\mathbf{m}, \mathbf{h}, \mathbf{p}} \sum_{\mathbf{m}', \mathbf{h}' \neq \mathbf{h}} F(\mathbf{m}, \mathbf{h}', \mathbf{S}) F(\mathbf{m}', \mathbf{h}', \mathbf{S}) |\mathbf{m}', \mathbf{h}, \mathbf{p}\rangle \\
 &+ C(\Lambda) \sum_{\mathbf{S}} \sum_{\mathbf{m}, \mathbf{h}, \mathbf{p}} \phi_{\mathbf{m}, \mathbf{h}, \mathbf{p}} \sum_{\mathbf{h}' \neq \mathbf{h}, \mathbf{h}_{\downarrow}} F(\mathbf{h}_{\downarrow}, \mathbf{h}', \mathbf{S}) F(\mathbf{h}_{\downarrow}, \mathbf{h}, \mathbf{S}) |\mathbf{m}, \mathbf{h}', \mathbf{p}\rangle \\
 &+ C(\Lambda) \sum_{\mathbf{S}} \sum_{\mathbf{m}, \mathbf{h}, \mathbf{p}} \phi_{\mathbf{m}, \mathbf{h}, \mathbf{p}} \sum_{\mathbf{h}' \neq \mathbf{h}, \mathbf{h}_{\downarrow}} F(\mathbf{h}_{\downarrow}, \mathbf{h}', \mathbf{S}) F(\mathbf{h}_{\downarrow}, \mathbf{h}', \mathbf{S}) |\mathbf{m}, \mathbf{h}, \mathbf{p}\rangle.
 \end{aligned} \tag{5.55}$$

Each of the sums over \mathbf{h}' , \mathbf{p}' , and \mathbf{m}' follow the same convention as the sums over \mathbf{h} , \mathbf{p} , and \mathbf{m} , respectively. The sums over \mathbf{h}_{\downarrow} are over $\varepsilon_{\mathbf{h}_{\downarrow}} \leq \varepsilon_{F,\downarrow}$. We

then have

$$\begin{aligned}
 & \langle \psi | V | \psi \rangle \\
 &= C(\Lambda) \sum_{\mathbf{S}} \sum_{\mathbf{h}} F^2(\mathbf{n}_{F+1,\downarrow}, \mathbf{h}, \mathbf{S}) |\phi_0|^2 \\
 &+ C(\Lambda) \sum_{\mathbf{S}} \sum_{\mathbf{m}, \mathbf{h}, \mathbf{p}} F(\mathbf{m}, \mathbf{p}, \mathbf{S}) F(\mathbf{n}_{F+1,\downarrow}, \mathbf{h}, \mathbf{S}) (\phi_0^* \phi_{\mathbf{m}, \mathbf{h}, \mathbf{p}} + \phi_0 \phi_{\mathbf{m}, \mathbf{h}, \mathbf{p}}^*) \\
 &+ C(\Lambda) \sum_{\mathbf{S}} \sum_{\mathbf{h}, \mathbf{h}_\downarrow} F^2(\mathbf{h}_\downarrow, \mathbf{h}, \mathbf{S}) |\phi_0|^2 \\
 &+ C(\Lambda) \sum_{\mathbf{S}} \sum_{\mathbf{m}, \mathbf{h}, \mathbf{p}, \mathbf{m}', \mathbf{p}'} F(\mathbf{m}, \mathbf{p}, \mathbf{S}) F(\mathbf{m}', \mathbf{p}', \mathbf{S}) \phi_{\mathbf{m}', \mathbf{h}, \mathbf{p}'}^* \phi_{\mathbf{m}, \mathbf{h}, \mathbf{p}} \\
 &+ C(\Lambda) \sum_{\mathbf{S}} \sum_{\mathbf{h}, \mathbf{h}_\downarrow} \sum_{\mathbf{p}} F(\mathbf{h}_\downarrow, \mathbf{h}, \mathbf{S}) F(\mathbf{h}_\downarrow, \mathbf{p}, \mathbf{S}) (\phi_0 \phi_{\mathbf{n}_{F+1,\downarrow}, \mathbf{h}, \mathbf{p}}^* + \phi_0^* \phi_{\mathbf{n}_{F+1,\downarrow}, \mathbf{h}, \mathbf{p}}) \\
 &+ C(\Lambda) \sum_{\mathbf{S}} \sum_{\mathbf{m}, \mathbf{h}, \mathbf{p}, \mathbf{p}', \mathbf{h}_\downarrow} F(\mathbf{h}_\downarrow, \mathbf{p}, \mathbf{S}) F(\mathbf{h}_\downarrow, \mathbf{p}', \mathbf{S}) \phi_{\mathbf{m}, \mathbf{h}, \mathbf{p}} \phi_{\mathbf{m}, \mathbf{h}, \mathbf{p}'}^* \\
 &+ C(\Lambda) \sum_{\mathbf{S}} \sum_{\mathbf{m}, \mathbf{h}, \mathbf{p}, \mathbf{m}', \mathbf{h}' \neq \mathbf{h}} F(\mathbf{m}, \mathbf{h}', \mathbf{S}) F(\mathbf{m}', \mathbf{h}, \mathbf{S}) \phi_{\mathbf{m}', \mathbf{h}', \mathbf{p}}^* \phi_{\mathbf{m}, \mathbf{h}, \mathbf{p}} \\
 &+ C(\Lambda) \sum_{\mathbf{S}} \sum_{\mathbf{m}, \mathbf{h}, \mathbf{p}, \mathbf{m}', \mathbf{h}' \neq \mathbf{h}} F(\mathbf{m}, \mathbf{h}', \mathbf{S}) F(\mathbf{m}', \mathbf{h}', \mathbf{S}) \phi_{\mathbf{m}', \mathbf{h}, \mathbf{p}}^* \phi_{\mathbf{m}, \mathbf{h}, \mathbf{p}} \\
 &+ C(\Lambda) \sum_{\mathbf{S}} \sum_{\mathbf{m}, \mathbf{h}, \mathbf{p}} \sum_{\mathbf{h}' \neq \mathbf{h}, \mathbf{h}_\downarrow} F(\mathbf{h}_\downarrow, \mathbf{h}', \mathbf{S}) F(\mathbf{h}_\downarrow, \mathbf{h}, \mathbf{S}) \phi_{\mathbf{m}, \mathbf{h}, \mathbf{p}} \phi_{\mathbf{m}, \mathbf{h}', \mathbf{p}}^* \\
 &+ C(\Lambda) \sum_{\mathbf{S}} \sum_{\mathbf{m}, \mathbf{h}, \mathbf{p}} \sum_{\mathbf{h}' \neq \mathbf{h}, \mathbf{h}_\downarrow} F(\mathbf{h}_\downarrow, \mathbf{h}', \mathbf{S}) F(\mathbf{h}_\downarrow, \mathbf{h}', \mathbf{S}) |\phi_{\mathbf{m}, \mathbf{h}, \mathbf{p}}|^2.
 \end{aligned} \tag{5.56}$$

The cutoff dependence of the sum is cancelled by the coupling constant $C(\Lambda)$. In the limit of large cutoffs, the sums in the last six lines are convergent and when multiplied by $C(\Lambda)$, will give a zero contribution. Therefore, they do not contribute to the energy gain, and will be omitted in the rest of the calculation.

5.2. $N + M$ Body Problem in Traps

Combining Eqs (5.51) and (5.56), the energy to be minimized is

$$\begin{aligned}
\langle H \rangle &= \varepsilon_{F+1,\downarrow} |\phi_0|^2 + \sum_{\mathbf{m},\mathbf{h},\mathbf{p}} |\phi_{\mathbf{m},\mathbf{h},\mathbf{p}}|^2 (\varepsilon_{\mathbf{p}} + \varepsilon_{\mathbf{m}} - \varepsilon_{\mathbf{h}}) \\
&+ C(\Lambda) \sum_{\mathbf{S}} \sum_{\mathbf{h}} F^2(\mathbf{n}_{F+1,\downarrow}, \mathbf{h}, \mathbf{S}) |\phi_0|^2 \\
&+ C(\Lambda) \sum_{\mathbf{S}} \sum_{\mathbf{m},\mathbf{h},\mathbf{p}} F(\mathbf{m}, \mathbf{p}, \mathbf{S}) F(\mathbf{n}_{F+1,\downarrow}, \mathbf{h}, \mathbf{S}) (\phi_0^* \phi_{\mathbf{m},\mathbf{h},\mathbf{p}} + \phi_0 \phi_{\mathbf{m},\mathbf{h},\mathbf{p}}^*) \\
&+ C(\Lambda) \sum_{\mathbf{S}} \sum_{\mathbf{h},\mathbf{h}_\downarrow} F^2(\mathbf{h}_\downarrow, \mathbf{h}, \mathbf{S}) |\phi_0|^2 \\
&+ C(\Lambda) \sum_{\mathbf{S}} \sum_{\mathbf{m},\mathbf{h},\mathbf{p},\mathbf{m}',\mathbf{p}'} F(\mathbf{m}, \mathbf{p}, \mathbf{S}) F(\mathbf{m}', \mathbf{p}', \mathbf{S}) \phi_{\mathbf{m}',\mathbf{h},\mathbf{p}'}^* \phi_{\mathbf{m},\mathbf{h},\mathbf{p}}.
\end{aligned} \tag{5.57}$$

Minimizing $\langle \psi | H | \psi \rangle$ with respect to ϕ_0 and $\phi_{\mathbf{m},\mathbf{h},\mathbf{p}}$ yields the following set of equations

$$\begin{aligned}
(E - \varepsilon_{F+1,\downarrow}) \phi_0 &= \\
C(\Lambda) \sum_{\mathbf{S}} \sum_{\mathbf{h}} F(\mathbf{n}_{F+1,\downarrow}, \mathbf{h}, \mathbf{S}) &\left[F(\mathbf{n}_{F+1,\downarrow}, \mathbf{h}, \mathbf{S}) \phi_0 + \sum_{\mathbf{m},\mathbf{p}} F(\mathbf{m}, \mathbf{p}, \mathbf{S}) \phi_{\mathbf{m},\mathbf{h},\mathbf{p}} \right] \\
+C(\Lambda) \sum_{\mathbf{S},\mathbf{h},\mathbf{h}_\downarrow} F(\mathbf{h}_\downarrow, \mathbf{h}, \mathbf{S}) &F(\mathbf{h}_\downarrow, \mathbf{h}, \mathbf{S}) \phi_0,
\end{aligned} \tag{5.58}$$

$$\begin{aligned}
(E - \varepsilon_{\mathbf{p}} - \varepsilon_{\mathbf{m}} + \varepsilon_{\mathbf{h}}) \phi_{\mathbf{m},\mathbf{h},\mathbf{p}} &= \\
C(\Lambda) \sum_{\mathbf{S}} F(\mathbf{m}, \mathbf{p}, \mathbf{S}) &\left[F(\mathbf{n}_{F+1,\downarrow}, \mathbf{h}, \mathbf{S}) \phi_0 + \sum_{\mathbf{m}',\mathbf{p}'} F(\mathbf{m}', \mathbf{p}', \mathbf{S}) \phi_{\mathbf{m}',\mathbf{h},\mathbf{p}'} \right].
\end{aligned} \tag{5.59}$$

To simplify the equations, we define

$$\chi(\mathbf{h}, \mathbf{S}) = F(\mathbf{n}_{F+1,\downarrow}, \mathbf{h}, \mathbf{S}) \phi_0 + \sum_{\mathbf{m}',\mathbf{p}'} F(\mathbf{m}', \mathbf{p}', \mathbf{S}) \phi_{\mathbf{m}',\mathbf{h},\mathbf{p}'}, \tag{5.60}$$

and also

$$G = C(\Lambda) \sum_{\mathbf{S}} \sum_{\mathbf{h},\mathbf{h}_\downarrow} F^2(\mathbf{h}, \mathbf{h}_\downarrow, \mathbf{S}). \tag{5.61}$$

5.2. $N + M$ Body Problem in Traps

Then Eq. (5.58) and (5.59) can be written as

$$\phi_0 = \frac{C(\Lambda)}{E - \varepsilon_{F+1,\downarrow} - G} \sum_{\mathbf{h}} \sum_{\mathbf{S}} F(\mathbf{n}_{F+1,\downarrow}, \mathbf{h}, \mathbf{S}) \chi(\mathbf{h}, \mathbf{S}), \quad (5.62)$$

$$\phi_{\mathbf{m},\mathbf{h},\mathbf{p}} = \frac{C(\Lambda)}{E - (\varepsilon_{\mathbf{p}} + \varepsilon_{\mathbf{m}} - \varepsilon_{\mathbf{h}})} \sum_{\mathbf{S}} F(\mathbf{m}, \mathbf{p}, \mathbf{S}) \chi(\mathbf{h}, \mathbf{S}). \quad (5.63)$$

Substituting Eq. (5.63) into Eq. (5.60) yields

$$\begin{aligned} \chi(\mathbf{h}, \mathbf{S}) &= F(\mathbf{n}_{F+1,\downarrow}, \mathbf{h}, \mathbf{S}) \phi_0 \\ &+ C(\Lambda) \sum_{\mathbf{S}'} \sum_{\mathbf{m},\mathbf{p}} \frac{F(\mathbf{m}, \mathbf{p}, \mathbf{S}) F(\mathbf{m}, \mathbf{p}, \mathbf{S}')}{E - (\varepsilon_{\mathbf{p}} + \varepsilon_{\mathbf{m}} - \varepsilon_{\mathbf{h}})} \chi(\mathbf{h}, \mathbf{S}'). \end{aligned} \quad (5.64)$$

This equation can be written in the form of a matrix equation

$$\chi(\mathbf{h}, \mathbf{S}) = F(\mathbf{n}_{F+1,\downarrow}, \mathbf{h}, \mathbf{S}) \phi_0 + \sum_{\mathbf{L}} A_{\mathbf{S},\mathbf{L}} \chi(\mathbf{h}, \mathbf{L}), \quad (5.65)$$

where the matrix $A_{\mathbf{S},\mathbf{L}}$ is given by

$$A_{\mathbf{S},\mathbf{L}} = \sum_{\mathbf{m},\mathbf{p}} \frac{C(\Lambda)}{E + \varepsilon_{\mathbf{h}} - \varepsilon_{\mathbf{p}} - \varepsilon_{\mathbf{m}}} F(\mathbf{m}, \mathbf{p}, \mathbf{S}) F(\mathbf{m}, \mathbf{p}, \mathbf{L}). \quad (5.66)$$

Then, the solution to $\chi(\mathbf{h}, \mathbf{S})$ is straightforward:

$$\chi(\mathbf{h}, \mathbf{S}) = \sum_{\mathbf{L}} [(1 - A)^{-1}]_{\mathbf{S},\mathbf{L}} F(\mathbf{n}_{F+1,\downarrow}, \mathbf{h}, \mathbf{L}) \phi_0. \quad (5.67)$$

Substituting this into Eq. (5.62), yields the following equation

$$E - \varepsilon_{F+1,\downarrow} - G = C(\Lambda) \sum_{\mathbf{h}} \sum_{\mathbf{S},\mathbf{L}} F(\mathbf{n}_{F+1,\downarrow}, \mathbf{h}, \mathbf{S}) (1 - A)_{\mathbf{S},\mathbf{L}}^{-1} F(\mathbf{n}_{F+1,\downarrow}, \mathbf{h}, \mathbf{L}). \quad (5.68)$$

For large cutoffs, the coupling constant vanishes, and therefore $G \rightarrow 0$. We then arrive at the equation for the $N + M$ body energy gain E in anisotropic traps,

$$\begin{aligned} &E - \varepsilon_{F+1,\downarrow} \\ &= \sum_{\mathbf{h}} \sum_{\mathbf{S},\mathbf{L}} F(\mathbf{n}_{F+1,\downarrow}, \mathbf{h}, \mathbf{S}) [M^{-1}(\varepsilon_{F,\uparrow}, \varepsilon_{F,\downarrow}, E + \varepsilon_{\mathbf{h}})]_{\mathbf{S},\mathbf{L}} F(\mathbf{n}_{F+1,\downarrow}, \mathbf{h}, \mathbf{L}), \end{aligned} \quad (5.69)$$

5.3. Outlook

where E is measured from the energy of the non-interacting ground state, in weak coupling $E \approx \varepsilon_{F+1,\downarrow}$, and the matrix M is given by

$$\begin{aligned}
M(\varepsilon_{F,\uparrow}, \varepsilon_{F,\downarrow}, E + \varepsilon_{\mathbf{h}})_{\mathbf{S},\mathbf{L}} &= \frac{\delta_{\mathbf{S},\mathbf{L}}}{C(\Lambda)} - M_u(\alpha, E + \varepsilon_{\mathbf{h}})_{\mathbf{S},\mathbf{L}} \\
&+ \sum_{\varepsilon_{\mathbf{p}} \leq \varepsilon_{F,\uparrow}} \sum_{\mathbf{m}} \frac{F(\mathbf{m}, \mathbf{p}, \mathbf{S})F(\mathbf{m}, \mathbf{p}, \mathbf{L})}{E + \varepsilon_{\mathbf{h}} - \varepsilon_{\mathbf{m}} - \varepsilon_{\mathbf{p}}} \\
&+ \sum_{\varepsilon_{\mathbf{p}} \leq \varepsilon_{F,\downarrow}} \sum_{\mathbf{m}} \frac{F(\mathbf{m}, \mathbf{p}, \mathbf{S})F(\mathbf{m}, \mathbf{p}, \mathbf{L})}{E + \varepsilon_{\mathbf{h}} - \varepsilon_{\mathbf{m}} - \varepsilon_{\mathbf{p}}} \\
&- \sum_{\varepsilon_{\mathbf{p}} \leq \varepsilon_{F,\downarrow}} \sum_{\varepsilon_{\mathbf{m}} \leq \varepsilon_{F,\uparrow}} \frac{F(\mathbf{m}, \mathbf{p}, \mathbf{S})F(\mathbf{m}, \mathbf{p}, \mathbf{L})}{E + \varepsilon_{\mathbf{h}} - \varepsilon_{\mathbf{m}} - \varepsilon_{\mathbf{p}}},
\end{aligned} \tag{5.70}$$

where $M_u(\alpha, E + \varepsilon_{\mathbf{h}})_{\mathbf{S},\mathbf{L}}$ is identical to the other sums in Eq. (5.70) with unrestricted sum over \mathbf{p} and \mathbf{m} , and has the analytic form $M_u(\alpha, E + \varepsilon_{\mathbf{h}})_{\mathbf{S},\mathbf{L}} = D(\alpha, \Delta\tilde{E})\delta_{\mathbf{S},\mathbf{L}}$, where $D(\alpha, \Delta\tilde{E})$ is given by Eqs. (4.56) and (4.57), and $\Delta\tilde{E} = \alpha(S_x + S_y + 2) + S_z + 1 - (E + \varepsilon_{\mathbf{h}})/\omega$.

5.3 Outlook

Eq. (5.69) yields the $N + M$ body energy gain E in anisotropic traps. The next step is to evaluate Eq. (5.69) for different particle numbers $N = N_{\uparrow}$, $M = N_{\downarrow}$, and aspect ratio α . The results for E can be used to compute the critical concentration $x_c(\alpha, N, M)$ and critical polarization $P_c(\alpha, N, M)$ in the Local Density Approximation. For further improvement, a full density-functional calculation with surface tension [24] or gradient terms is needed. The resulting critical polarization will provide prediction that can be compared with experimental data, and may shed light for a better understanding of the MIT-Rice differences.

Chapter 6

Summary and Outlook

In summary, we studied the properties of strongly-interacting Fermi gases with population imbalance. We first investigated finite-size and confinement effects in trapped Fermi gases by studying the polaron energy in traps, $\eta(\alpha, N)$. The polaron energy provides the leading contributions to the energy of the polarized normal Fermi liquid phase for large asymmetries. We calculated the polaron energy variationally using a trial wavefunction including one-particle-one-hole excitations. For small particle numbers and isotropic traps, the variational $\eta(1, N)$ agrees well with the Monte Carlo results of Ref. [5]. The polaron energy was computed for $\alpha = 1, 3, 9, 15, 35$ and for particle numbers up to $N \lesssim 10^5$. Based on the results for $\eta(\alpha, N)$, we computed the critical concentration $x_c(\alpha, N)$ and the critical polarization $P_c(\alpha, N)$ in traps. For lower particle numbers and more elongated traps, the change in polaron energy increases the energy of the normal Fermi liquid, and the superfluid extends to larger population imbalances. Finite-size effects are stronger in highly-elongated systems as the dimensionality of the problem is continuously reduced with increasing aspect ratio. This provides a microscopic understanding of the MIT-Rice differences due to the dependence of the polaron energy on the particle number and the trap geometry.

For general asymmetries, we studied the $N + M$ body problem in the uniform system. We evaluated the energy of adding an impurity to an imbalanced Fermi gas variationally. Based on the variational $N + M$ body energy, we constructed the equation of state of the partially-polarized normal Fermi liquid. With the Local Density Approximation (LDA), we applied the results for the equation of state to traps with large particle numbers and computed the critical concentration $x_c(\xi)$ and critical polarization $P_c(\xi)$ as a function of the superfluid energy ξ . Finally, we studied the $N + M$ body problem in traps, and obtained the self-consistent equation for the energy E , Eq. (5.69).

For future investigation, the next step is to evaluate Eq. (5.69) and obtain the $N + M$ body energy for different particle numbers $N = N_\uparrow$, $M = N_\downarrow$ and aspect ratio α . With the LDA, the results for the energy can be used to compute the critical concentration $x_c(\alpha, N, M)$ and the critical polarization

$P_c(\alpha, N, M)$ for different particle numbers N , M , and trap aspect ratio α . Experimentally, the aspect ratio α can be varied, and it is possible to obtain data for the critical polarization P_c as a function of α and particle numbers. The calculated $x_c(\alpha, N, M)$ and $P_c(\alpha, N, M)$ provide predictions that can be compared with experimental data. For further improvement, the effects from a full density-functional calculation, combined with surface tension [24] or gradient terms, needs to be studied. These studies will enable a better quantitative understanding of the phase structure and the MIT-Rice differences. The goal is to fully elucidate the mechanism behind the experimental differences. In the future, one may be able to study finite-size and confinement effects in other strongly-interacting asymmetric systems, such as nuclei and condensed matter systems in lower dimensions, and explore the rich properties of unitary asymmetric Fermi gases, which is highly relevant to many fields of physics.

Bibliography

- [1] M. H. Anderson, J. R. Ensher, M. R. Matthews, C. E. Wieman, and E. A. Cornell. Observation of Bose-Einstein condensation in a dilute atomic vapor. *Science*, 269(5221):198, 1995.
- [2] J. Bardeen, L. N. Cooper, and J. R. Schrieffer. Theory of superconductivity. *Phys. Rev.*, 108(5):1175, 1957.
- [3] M. Bartenstein, A. Altmeyer, S. Riedl, S. Jochim, R. Geursen, C. Chin, J. Hecker Denschlag, and R. Grimm. Exploring the BEC-BCS crossover with an ultracold gas of ^6Li atoms. In *Atomic Physics 19: XIX International Conference on Atomic Physics. AIP Conference Proceedings*, volume 770, page 278. Eds. L. G. Marcassa, V. S. Bagnato, and K. Helmerson. AIP, Melville, NY, 2005.
- [4] G. F. Bertsch. "Many-Body X Challenge Problem". G. F. Bertsch posed the properties of Fermi gases in this limit as a many-body theory challenge problem at MBX, 2001. The first studies were reported by G. A. Baker, *Int. J. Mod. Phys. B*, 13(10):1314, 2001; H. Heiselberg, *Phys. Rev. A*, 63(4):043606, 2001.
- [5] D. Blume. Trapped polarized Fermi gas at unitarity. *Phys. Rev. A*, 78(1):013635, 2008.
- [6] T. Bourdel, J. Cubizolles, L. Khaykovich, K. M. F. Magalhães, S. J. J. M. F. Kokkelmans, G. V. Shlyapnikov, and C. Salomon. Measurement of the interaction energy near a Feshbach resonance in a ^6Li Fermi gas. *Phys. Rev. Lett.*, 91(2):020402, 2003.
- [7] BPA/DEPS. *Scientific Opportunities with a Rare-Isotope Facility in the United States*. The National Academies Press, Washington, D.C., 2007.
- [8] C. C. Bradley, C. A. Sackett, J. J. Tollett, and R. G. Hulet. Evidence of Bose-Einstein condensation in an atomic gas with attractive interactions. *Phys. Rev. Lett.*, 75(9):1687, 1995.

- [9] A. Bulgac and M. M. Forbes. Zero-temperature thermodynamics of asymmetric Fermi gases at unitarity. *Phys. Rev. A*, 75(3):031605, 2007.
- [10] A. Bulgac and M. M. Forbes. Unitary Fermi supersolid: The Larkin-Ovchinnikov phase. *Phys. Rev. Lett.*, 101(21):215301, 2008.
- [11] A. Bulgac, M. M. Forbes, and A. Schwenk. Induced P -wave superfluidity in asymmetric Fermi gases. *Phys. Rev. Lett.*, 97:020402, 2006.
- [12] T. Busch, B. G. Englert, K. Rzażewski, and M. Wilkens. Two cold atoms in a harmonic trap. *Found. Phys.*, 28(4):549, 1998.
- [13] J. Carlson and S. Reddy. Asymmetric two-component Fermion systems in strong coupling. *Phys. Rev. Lett.*, 95(6):060401, 2005.
- [14] J. Carlson and S. Reddy. Superfluid pairing gap in strong coupling. *Phys. Rev. Lett.*, 100(15):150403, 2008.
- [15] R. Casalbuoni and G. Nardulli. Inhomogeneous superconductivity in condensed matter and QCD. *Rev. Mod. Phys.*, 76(1):263, 2004.
- [16] B. S. Chandrasekhar. A note on the maximum critical field of high-field superconductors. *Appl. Phys. Lett.*, 1(1):7, 1962.
- [17] F. Chevy. Universal phase diagram of a strongly interacting Fermi gas with unbalanced spin populations. *Phys. Rev. A*, 74(6):063628, 2006.
- [18] F. Chevy. Unitary polarized Fermi gases. In *Ultra-Cold Fermi Gases, Proceedings of the International School of Physics "Enrico Fermi" Course CLXIV*, page 607. Eds. M. Inguscio, W. Ketterle, C. Salomon. IOS Press, Amsterdam, 2007.
- [19] A. M. Clogston. Upper limit for the critical field in hard superconductors. *Phys. Rev. Lett.*, 9(6):266, 1962.
- [20] T. D. Cohen. Phase separation and an upper bound for a generalized superfluid gap for cold Fermi fluids in the unitary regime. *Phys. Rev. Lett.*, 95(12):120403, 2005.
- [21] R. Combescot and S. Giraud. Normal state of highly polarized Fermi gases: Full many-body treatment. *Phys. Rev. Lett.*, 101(5):050404, 2008.

- [22] R. Combescot, A. Recati, C. Lobo, and F. Chevy. Normal state of highly polarized Fermi gases: Simple many-body approaches. *Phys. Rev. Lett.*, 98(18):180402, 2007.
- [23] K. B. Davis, M.-O. Mewes, M. R. Andrews, N. J. van Druten, D. S. Durfee, D. M. Kurn, and W. Ketterle. Bose-Einstein condensation in a gas of sodium atoms. *Phys. Rev. Lett.*, 75(22):3969, 1995.
- [24] T. N. De Silva and E. J. Mueller. Surface tension in unitary Fermi gases with population imbalance. *Phys. Rev. Lett.*, 97(7):070402, 2006.
- [25] B. DeMarco and D. S. Jin. Onset of Fermi degeneracy in a trapped atomic gas. *Science*, 285(5434):1703, 1999.
- [26] U. Fano. Effects of configuration interaction on intensities and phase shifts. *Phys. Rev.*, 124(6):1866, 1961.
- [27] H. Feshbach. Unified theory of nuclear reactions. *Ann. Phys. (N. Y.)*, 5(4):357, 1958; Unified theory of nuclear reactions II. *Ann. Phys. (N. Y.)*, 19(2):287, 1962.
- [28] P. Fulde and R. A. Ferrell. Superconductivity in a strong spin-exchange field. *Phys. Rev.*, 135(3A):A550, 1964.
- [29] S. Giorgini, L. P. Pitaevskii, and S. Stringari. Theory of ultracold atomic Fermi gases. *Rev. Mod. Phys.*, 80(4):1215, 2008.
- [30] L. P. Gor'kov and T. K. Melik-Barkhudarov. Contribution to the theory of superfluidity in an imperfect Fermi gas. *Zh. Eksp. Teor. Fiz.*, 40:1452, 1961. [Sov. Phys. JETP 13(5):1018, 1961].
- [31] I. S. Gradshteyn and I. M. Ryzhik. *Table of Integrals, Series, and Products*. Academic Press, New York and London, fourth edition, 1965.
- [32] M. Greiner, C. A. Regal, and D. S. Jin. Fermionic condensates. In *Atomic Physics 19: XIX International Conference on Atomic Physics. AIP Conference Proceedings*, volume 770. Eds. L. G. Marcassa, V. S. Bagnato, and K. Helmerson. AIP, Melville, NY, 2005.
- [33] J. Kinast, A. Turlapov, J. E. Thomas, Q. Chen, J. Stajic, and K. Levin. Heat capacity of a strongly interacting Fermi gas. *Science*, 307(5713):1296, 2005.

- [34] M. Ku, J. Braun, and A. Schwenk. Finite-size and confinement effects in spin-polarized trapped Fermi gases. *Phys. Rev. Lett.*, 102(25):255301, 2009.
- [35] L. D. Landau and E. M. Lifshitz. *Quantum Mechanics: Non-relativistic theory*, volume 3 of *Course of Theoretical Physics*. Pergamon Press, Oxford; New York, third edition, 1989.
- [36] A. I. Larkin and Y. N. Ovchinnikov. Inhomogeneous state of superconductors. *Zh. Eksp. Teor. Fiz.*, 47:1136, 1964. [Sov. Phys. JETP 20:762, 1965].
- [37] W. V. Liu and F. Wilczek. Interior gap superfluidity. *Phys. Rev. Lett.*, 90(4):047002, 2003.
- [38] C. Lobo, A. Recati, S. Giorgini, and S. Stringari. Normal state of a polarized Fermi gas at unitarity. *Phys. Rev. Lett.*, 97(20):200403, 2006.
- [39] P. A. Martin and F. Rothen. *Many-Body Problems and Quantum Field Theory: An Introduction*. Theoretical and Mathematical Physics. Springer, New York, second edition, 2004.
- [40] G. B. Partridge, W. Li, R. I. Kamar, Y. A. Liao, and R. G. Hulet. Pairing and phase separation in a polarized Fermi gas. *Science*, 311(5760):503, 2006.
- [41] G. B. Partridge, W. Li, Y. A. Liao, R. G. Hulet, M. Haque, and H. T. C. Stoof. Deformation of a trapped Fermi gas with unequal spin populations. *Phys. Rev. Lett.*, 97(19):190407, 2006.
- [42] C. J. Pethick and H. Smith. *Bose-Einstein Condensation in Dilute Gases*. Cambridge University Press, Cambridge, 2002.
- [43] S. Pilati and S. Giorgini. Phase separation in a polarized Fermi gas at zero temperature. *Phys. Rev. Lett.*, 100(3):030401, 2008.
- [44] L. Pricoupenko and Y. Castin. One particle in a box: The simplest model for a Fermi gas in the unitary limit. *Phys. Rev. A*, 69(5):051601, 2004.
- [45] N. Prokof'ev and B. Svistunov. Fermi-polaron problem: Diagrammatic Monte Carlo method for divergent sign-alternating series. *Phys. Rev. B*, 77(2):020408, 2008.

- [46] N. V. Prokof'ev and B. V. Svistunov. Bold diagrammatic Monte Carlo: A generic sign-problem tolerant technique for polaron models and possibly interacting many-body problems. *Phys. Rev. B*, 77(12):125101, 2008.
- [47] A. Recati, C. Lobo, and S. Stringari. Role of interactions in spin-polarized atomic Fermi gases at unitarity. *Phys. Rev. A*, 78(2):023633, 2008.
- [48] C. A. Regal and D. S. Jin. Measurement of positive and negative scattering lengths in a Fermi gas of atoms. *Phys. Rev. Lett.*, 90(23):230404, 2003.
- [49] J. J. Sakurai. *Modern Quantum Mechanics*. Addison Wesley, revised edition, 1994.
- [50] G. Sarma. On the influence of a uniform exchange field acting on the spins of the conduction electrons in a superconductor. *J. Phys. Chem. Solids*, 24(8):1029, 1963.
- [51] A. Schirotzek, C. H. Wu, A. Sommer, and M. W. Zwierlein. Observation of Fermi polarons in a tunable Fermi liquid of ultracold atoms. *Phys. Rev. Lett.*, 102(23):230402, 2009.
- [52] C. H. Schunck, Y. Shin, A. Schirotzek, M. W. Zwierlein, and W. Ketterle. Pairing without superfluidity: The ground state of an imbalanced Fermi mixture. *Science*, 316(5826):867, 2007.
- [53] A. Sedrakian, J. Mur-Petit, A. Polls, and H. Müther. Pairing in a two-component ultracold Fermi gas: Phases with broken-space symmetries. *Phys. Rev. A*, 72(1):013613, 2005.
- [54] Y. Shin, M. W. Zwierlein, C. H. Schunck, A. Schirotzek, and W. Ketterle. Observation of phase separation in a strongly interacting imbalanced Fermi gas. *Phys. Rev. Lett.*, 97(3):030401, 2006.
- [55] Y.-i. Shin, C. H. Schunck, A. Schirotzek, and W. Ketterle. Phase diagram of a two-component Fermi gas with resonant interactions. *Nature*, 451:689, 2008.
- [56] J. T. Stewart, J. P. Gaebler, C. A. Regal, and D. S. Jin. Potential energy of a ^{40}K Fermi gas in the BCS-BEC crossover. *Phys. Rev. Lett.*, 97(22):220406, 2006.

- [57] L. Tarruell, M. Teichmann, J. McKeever, T. Bourdel, J. Cubizolles, L. Khaykovich, J. Zhang, N. Navon, F. Chevy, and C. Salomon. Expansion of an ultra-cold lithium gas in the BEC-BCS crossover. In *Ultracold Fermi Gases, Proceedings of the International School of Physics "Enrico Fermi" Course CLXIV*, page 845. Eds. M. Inguscio, W. Ketterle, C. Salomon. IOS Press, Amsterdam, 2007.
- [58] M. W. Zwierlein, A. Schirotzek, C. H. Schunck, and W. Ketterle. Fermionic superfluidity with imbalanced spin populations. *Science*, 311(5760):492, 2006.
- [59] M. W. Zwierlein, C. H. Schunck, A. Schirotzek, and W. Ketterle. Direct observation of the superfluid phase transition in ultracold Fermi gases. *Nature*, 442:54, 2006.

Appendix A

1 + 1 Body Problem in Harmonic-Oscillator Traps

The two-body problem of strongly-interacting fermions is solved in Ref. [12]. In this appendix, we derive the exact ground state energy of two cold atoms in a harmonic trap with a variational calculation. We generalize the first term in Eq. (4.22) to include a sum over the spin-down particle in level \mathbf{n} , $\sum_{\mathbf{n}} \phi_{\mathbf{n}}$. The complete-basis variational Ansatz for the two-body problem is then given by

$$|\psi\rangle = \sum_{\mathbf{m}, \mathbf{p}} \phi_{\mathbf{m}, \mathbf{p}} |\mathbf{m}, \mathbf{p}\rangle, \quad (\text{A.1})$$

where $|\mathbf{m}, \mathbf{p}\rangle$ consists of a spin-down particle in the state \mathbf{m} , and a spin-up particle in the state \mathbf{p} . Both quantum numbers run over all levels. Because this Ansatz includes all possible particle-hole excitations, it gives the exact ground state energy. We evaluate $\langle H \rangle$, with H given by Eq. (4.1) and the interaction matrix given by Eq. (4.12). Minimizing the expectation value yields the following equation,

$$E\phi_{\mathbf{m}, \mathbf{p}} = (\varepsilon_{\mathbf{p}} + \varepsilon_{\mathbf{m}})\phi_{\mathbf{m}, \mathbf{p}} + C(\Lambda) \sum_{\mathbf{S}, \mathbf{m}', \mathbf{p}'} F(\mathbf{m}, \mathbf{p}, \mathbf{S})F(\mathbf{m}', \mathbf{p}', \mathbf{S})\phi_{\mathbf{m}', \mathbf{p}'}, \quad (\text{A.2})$$

where E is the total energy of the 1 + 1 body system. We define

$$\chi(\mathbf{S}) = \sum_{\mathbf{m}, \mathbf{p}} F(\mathbf{m}, \mathbf{p}, \mathbf{S})\phi_{\mathbf{m}, \mathbf{p}}, \quad (\text{A.3})$$

and solve for $\phi_{\mathbf{m}, \mathbf{p}}$ in Eq. (A.2) to obtain

$$\phi_{\mathbf{m}, \mathbf{p}} = \frac{C(\Lambda)}{E - (\varepsilon_{\mathbf{p}} + \varepsilon_{\mathbf{m}})} \sum_{\mathbf{S}} F(\mathbf{m}, \mathbf{p}, \mathbf{S})\chi(\mathbf{S}). \quad (\text{A.4})$$

Substituting this into Eq. (A.3) yields

$$\chi(\mathbf{S}) = C(\Lambda) \sum_{\mathbf{m}, \mathbf{p}, \mathbf{L}} \frac{F(\mathbf{m}, \mathbf{p}, \mathbf{S})F(\mathbf{m}, \mathbf{p}, \mathbf{L})}{E - (\varepsilon_{\mathbf{p}} + \varepsilon_{\mathbf{m}})} \chi(\mathbf{L}). \quad (\text{A.5})$$

We can rewrite this equation in matrix form,

$$\chi(\mathbf{S}) = C(\Lambda) \sum_{\mathbf{L}} M_u(1, E)_{\mathbf{S}, \mathbf{L}} \chi(\mathbf{L}), \quad (\text{A.6})$$

with $M_u(\alpha, E)_{\mathbf{S}, \mathbf{L}}$ defined in Eq. (4.47). It has the analytic form $M_u(\alpha, E)_{\mathbf{S}, \mathbf{L}} = D(\alpha, \Delta\tilde{E})\delta_{\mathbf{S}, \mathbf{L}}$ given by Eq. (4.53).

Eq. (A.6) leads to $\delta_{\mathbf{S}, \mathbf{L}}/C(\Lambda) = M_u(1, E)_{\mathbf{S}, \mathbf{L}}$, and in the unitary regime $1/a = 0$, it is equivalent to $D(1, \Delta\tilde{E}) = 0$, with $D(1, \Delta\tilde{E})$ given by Eq. (4.58), and $\Delta\tilde{E} = S_x + S_y + S_z + 3 - E/\omega$. Then the solution to Eq. (A.6) is given by

$$0 = \frac{\Gamma((S + 3 - E/\omega)/2)}{\Gamma((S + 2 - E/\omega)/2)}, \quad (\text{A.7})$$

whose root is given by

$$E = \omega(2 + S + 2n), \quad (\text{A.8})$$

where S and n are integers. Therefore, we find the ground state energy is $E = 2\omega$, which corresponds to the exact ground state energy for the relative motion $E_{\text{rel}} = \omega/2$, in agreement with the exact solution of Ref. [12].